21

Semiannual Status Report No. 8 on

PROPAGATION AND DISPERSION OF HYDROMAGNETIC AND ION CYCLOTRON WAVES IN PLASMAS IMMERSED IN MAGNETIC FIELDS

January 15, 1967

Period Covered: July 15, 1966 through January 14, 1967

Research Grant NsG-353
Office of Grants and Research Contracts
Code SC
National Aeronautics and Space Administration
Washington, D. C. 20546

PLASMA DYNAMICS RESEARCH LABORATORY
DEPARTMENT OF ELECTRICAL ENGINEERING
THE UNIVERSITY OF TEXAS
AUSTIN, TEXAS 78712

N67-28838

FACILITY FORM 602

(ACCESSION NUMBER)	(THRU)
96	1
(PAGES)	(CODE)
CR-84833	25
(NASA CR OR TMX OR AD NUMBER)	(CATEGORY)

Semiannual Status Report No. 8 on

PROPAGATION AND DISPERSION OF HYDROMAGNETIC AND ION CYCLOTRON WAVES IN PLASMAS IMMERSED IN MAGNETIC FIELDS

January 15, 1967

Period Covered: July 15, 1966 through January 14, 1967

Electrophysics Research Division
Attn: Dr. Harry Harrison, Chief and Dr. Karlheinz Thom
Research Grant NsG-353
Office of Grants and Research Contracts, Code SC
National Aeronautics and Space Administration
Washington, D. C. 20546

PLASMA DYNAMICS RESEARCH LABORATORY
DEPARTMENT OF ELECTRICAL ENGINEERING
THE UNIVERSITY OF TEXAS
AUSTIN, TEXAS 78712

Faculty Member Initiator and Principal Investigator:
Dr. Arwin A. Dougal
Professor of Electrical Engineering

TABLE OF CONTENTS

		Page
	Abstract	iii
	Faculty and Staff	v
	Communications and Coordination of Research with National Aeronautics and Space Administration Research Centers	vi
	Papers Presented, Lectures, and Publications by Faculty and Staff	vii
	Illustrations	x
	List of Tables	xii
I.	Introduction	1
II.	Experimental Investigation of Harmonic Ion Cyclotron Wave Propagation and Attenuation	4
III.	Theoretical Investigations of Quasi-Static Ion Waves and Wave Energy Densities	34
IV.	Experimental Facilities	51
V.	Experimental Investigation of Non-Linear Plasma Phenomena	66
	References	82

ABSTRACT

New wave phenomena are described which have been observed in the course of an experimental investigation of ion cyclotron resonance heating of hydrogen and deuterium plasmas in strong magnetic fields. It was found that waves can propagate for frequencies larger than the ion cyclotron frequency f_c, and attenuate at harmonics of f_c with resulting increase in the transverse temperature-density product $n\beta T_\perp$. The harmonic number at which the waves attenuate increases with increasing gas pressure. Attenuation at harmonics up to the 8th was observed. The plasma density is typically $6 \times 10^{17} m^{-3}$, the transverse plasma temperature $(T_{e\perp} + T_{i\perp}) \leq 50$ eV equivalent, and the magnetic field 1-9 kG. A magnetic beach geometry is employed and the waves are excited by a Faraday-shielded Stix coil from a 30 kW, 5.8 MHz driver. Harmonic cyclotron heating is related to large transverse wave numbers which are shown to exist in this experiment.

Additional theoretical investigations consider the quasistatic approximation of the dispersion relation for a hot, homogeneous, infinite plasma in a magnetic field. For several simplifying approximations, dispersion curves are derived for ion acoustic waves, electrostatic and quasistatic ion cyclotron waves, and ion "Bernstein modes". The wave energy densities for ion cyclotron waves and for electrostatic ion cyclotron waves are calculated and found to be comparable in magnitude.

Improvements in the experimental facilities are described. The improvements include the addition of an 8-mm microwave interferometer, construction of a screen room, addition of remote control of the probe drive and the magnet system, the construction of an improved Faraday-shielded Stix coil, the addition of spectrum analysis equipment, and the design of a P.I.G. discharge preionizer.

The observation of three new plasma phenomena is reported. Investigations were conducted with a spectrum analyzer to measure the frequency spectrum of magnetic probe signals from the plasma. Three effects were observed: (1) frequency mixing of two waves in the general neighborhood of the ion cyclotron frequency to produce sum and difference frequencies, (2) harmonic frequency generation from a propagating wave undergoing harmonic ion cyclotron resonance

absorption in the magnetic beach, and (3) dense spectra of frequencies generated in the plasma which appear to be distinct from the harmonic and the sum and difference effects above. The effects appear to be due to nonlinear reactions in the plasma.

FACULTY AND STAFF

The following individuals contributed to one or more areas of the research in progress at various times during the period July 15, 1966, to January 14, 1967.

1. Dr. Arwin A. Dougal; Professor of Electrical Engineering, and Principal Investigator.

2. Magne Kristiansen; Doctoral Candidate, and Research Engineering Assistant III.

3. Jimmy Gary Melton: Graduate Student, and Research Engineer Assistant III.

4. Nathan B. Dodge; Graduate Student, and Research Engineer Assistant II.

5. Franklin Creswell Harris; Graduate Student and Research Engineer Assistant I.

6. Glenn C. Andrew; Undergraduate and Laboratory Research Assistant I.

7. Miss Nancy Louise Bagley; Senior Secretary

COMMUNICATIONS AND COORDINATION OF RESEARCH WITH NATIONAL AERONAUTICS AND SPACE ADMINISTRATION RESEARCH CENTERS

1. October 31--November 1, 1966, Austin, Texas: Mr. I. R. Schwartz reviewed research in progress on NASA Grant NsG-353, and future plans with Professor Arwin A. Dougal and other staff members at the Plasma Dynamics Research Laboratory, The University of Texas.

PAPERS PRESENTED, LECTURES, AND PUBLICATIONS BY FACULTY AND STAFF*

A. Papers Presented:

1. Arwin A. Dougal, "Coupled Infrared Maser Resonators and Faraday Rotation for Diagnostics of Fusion Plasmas," Aerospace Research Laboratories, Wright-Patterson Air Force Base, Dayton, Ohio, August 4, 1966.

2. David K. Ferry, Robert W. Young, and Arwin A. Dougal, "Microwave Emission from InSb and InAs," 1966 Summer Meeting of the American Physical Society, Mexico City, Mexico, August 29-31, 1966.

3. Otto M. Friedrich, Jr., Dennis H. Gill, and Arwin A. Dougal, "Shock Dynamics of Laser-Induced Plasmas in High Pressure Gases," 1966 Summer Meeting of American Physical Society, Mexico City, Mexico, August 29-31, 1966.

4. M. Kristiansen and Arwin A. Dougal, "Waves Propagating above the Ion Cyclotron Frequency (f_c) and Attenuating near Harmonics of f_c," 1966 Summer Meeting of the American Physical Society, Mexico City, Mexico, August 29-31, 1966.

5. Marion O. Hagler, Howard N. Roberts, and Arwin A. Dougal, "Infrared-Maser Diagnostics of a Dynamical Deuterium Plasma Produced in a 30-KJ θ-Pinch," 1966 Summer Meeting of the American Physical Society, Mexico City, Mexico, August 29-31, 1966.

6. Otto M. Friedrich, Frederic Weigl, and Arwin A. Dougal, "Strong Blast Waves Produced in Laser Induced Plasmas in Atmospheric and High Pressure Gases," Eighth Annual Meeting, Div. of Plasma Physics, American Physical Society, Boston, Massachusetts, November 2-5, 1966.

7. M. Kristiansen and Arwin A. Dougal, "Wave Propagation and Plasma Heating Near Harmonics of the Ion Cyclotron Frequency," Eighth Annual Meeting, Div. of Plasma Physics, American Physical Society, Boston, Massachusetts, November 2-5, 1966.

8. Arwin A. Dougal, "Two-Fluid Hydromagnetic Analysis and Experimental Space-Time Resolved Properties of a Dynamical Theta Pinch," Second Texas Symposium on Controlled Thermonuclear Research, December 8-9, 1966.

---

*Consolidates all papers presented, lectures, and publications by faculty and staff.

9. Arwin A. Dougal, "Plasma Heating and Wave Propagation near the Fundamental and Harmonics of the Ion Cyclotron Frequency," Second Texas Symposium on Controlled Thermonuclear Research, December 8-9, 1966.

B. Publications:

1. R. F. Gribble, J. P. Craig, O. M. Friedrich, Jr., and A. A. Dougal, "Infrared Maser Coupled Resonator and Faraday Rotation Techniques for Experimental Ionized Gas Diagnostics," Proceedings of the Seventh International Conference on Phenomena in Ionized Gases," Gradevinska Knjiga Publishing House, Beograd, Yugoslavia, VII, pages 205-208, July, 1966.

2. R. B. Allen, R. B. Starnes, and A. A. Dougal, "A New Pulsed Ion Laser Transition in Nitrogen at 3995 Å," Institute of Electrical and Electronics Engineers Journal of Quantum Electronics, QE-2, page 334, August, 1966.

3. D. K. Ferry and A. A. Dougal, "Input Power Induced Thermal Effects Related to Transition Time Between Avalanche and Second Breakdown in p-n Silicon Junctions," Institute of Electrical and Electronics Engineers Transactions on Electron Devices, ED, August-September, 1966.

4. Otto M. Friedrich, Jr. and Arwin A. Dougal, "Shock Dynamics of Laser-Induced Plasmas in High-Pressure Gases," Bulletin of the American Physical Society, 11, 1966, p. 731 (ABSTRACT).

5. Otto M. Friedrich, Jr. and Arwin A. Dougal, "Space-Time Resolved Plasma Properties of a Dynamical Theta Pinch," Bulletin of the American Physical Society, II-11, p. 579, 1966 (ABSTRACT).

6. Otto M. Friedrich, Jr., Dennis H. Gill, and Arwin A. Dougal, "Shock Dynamics of Laser-Induced Plasmas in High-Pressure Gases," Bulletin of the American Physical Society, II-11, page 731, 1966.

7. Marion O. Hagler, Howard N. Roberts, and Arwin A. Dougal, "Infrared-Maser Diagnostics of a Dynamical Deuterium Plasma Produced in a 30-kJ θ Pinch," Bulletin of the American Physical Society, II-11, page 731, 1966 (ABSTRACT).

8. Magne Kristiansen and Arwin A. Dougal, "Waves Propagating above the Ion Cyclotron Frequency (f_c) and Attenuating near Harmonics of f_c," Bulletin of the American Physical Society, II-11, page 716, 1966 (ABSTRACT).

9. David K. Ferry, Robert W. Young, and Arwin A. Dougal, "Microwave Emission from InSb and InAs," Bulletin of the American Physical Society, II-11, page 754, 1966 (ABSTRACT).

10. Otto M. Friedrich, Jr. and Arwin A. Dougal, "Comparison of Numerical Calculations and Measured Space-Time Resolved Plasma Properties of a Dynamical Theta Pinch," AIAA Journal, 12, pages 2159-2165, December 1966.

11. Nathan B. Dodge, Magne Kristiansen, and Arwin A. Dougal, "Evaluation of Faraday Shielded Stix Coils for Ion Cyclotron Resonance Heating of Plasma," Review of Scientific Instruments, 37, page 1455, 1966.

12. Magne Kristiansen and Arwin A. Dougal, "Experimental Investigation of Harmonic Ion Cyclotron Wave Propagation and Attenuation," (accepted for publication in Physics of Fluids).

13. Arwin A. Dougal, "Plasma Heating and Wave Propagation near the Fundamental and Harmonics of the Ion Cyclotron Frequency," Proceedings of Second Texas Symposium on Controlled Thermonuclear Research, Austin, Texas, December 8-9, 1966 (ABSTRACT).

14. Arwin A. Dougal, "Two-Fluid Hydromagnetic Analysis and Experimental Space-Time Resolved Properties of a Dynamical Theta Pinch," Proceedings of Second Texas Symposium on Controlled Thermonuclear Research, Austin, Texas, December 8-9, 1966 (ABSTRACT).

ILLUSTRATIONS

II. EXPERIMENTAL INVESTIGATION OF HARMONIC ION CYCLOTRON WAVE PROPAGATION AND ATTENUATION

Fig. No.		Page
II-1	Block Diagram of ICRH Experiment	5
II-2	Magnetic Field Configuration	7
II-3	Diamagnetic and Magnetic Probe Signals	8
II-4	Magnetic Probe Construction	9
II-5	Wave Magnetic Field ($\dot{b}_z$) Variation in Beach Region	11
II-6	Wave Attenuation at the 8th Harmonic of the Ion Cyclotron Frequency	13
II-7	Magnetic Probe Signal ($\dot{b}_z$) vs Magnetic Field	15
II-8	Radial Variation in Wave Magnetic Probe Signals	16
II-9	Electron Density vs Magnetic Field	17
II-10	Diamagnetic Probe Signal vs Magnetic Field	20
II-11	Axial Variation in Diamagnetic Probe Signal Near B_c/G	21
II-12	Cold Plasma Dispersion Relation	27
II-13	Single Particle Acceleration at the 2nd Harmonic of f_c	30
II-14	Single Particle Acceleration -- Definition of Symbols	32

III. THEORETICAL INVESTIGATIONS OF QUASI-STATIC ION WAVES AND WAVE ENERGY DENSITIES

III-1	Ion Acoustic and Electrostatic Ion Cyclotron Modes ($\Omega_i < \omega_{pi}$)	40
III-2	Ion Acoustic and Electrostatic Ion Cyclotron Modes ($\Omega_i > \omega_{pi}$)	40

Fig. No.		Page
III-3	Electrostatic "Bernstein" Ion Cyclotron Modes	43
III-4	Quasistatic Ion Cyclotron Modes	44

IV. EXPERIMENTAL FACILITIES

IV-1	Photograph of Experimental Facilities	52
IV-2	Drawing of P.I.G. Discharge Assembly	54
IV-3	Block Diagram of 8-mm Microwave Interferometer	56
IV-4	Photographs of 8-mm Microwave Interferometer	57
IV-5	Photograph of New Wave Coupler	59
IV-6	Photograph of New Wave Coupler	59
IV-7	Photograph of Assembled Wave Coupler and Test Facilities	60
IV-8	Schematic Diagram of Probe Position Indicator	61
IV-9	Photograph of Probe Carriage	63
IV-10	Photograph of Experimental Facilities and Screen Room	65

V. EXPERIMENTAL INVESTIGATION OF NON-LINEAR PLASMA PHENOMENA

V-1	Schematic of Spectrum Analysis Equipment	70
V-2	Frequency Spectrum: Sum Signal	72
V-3	Frequency Spectrum: No gas in system	73
V-4	Frequency Spectrum: Showing frequency harmonics	73
V-5	Frequency Spectrum: Showing families of lines	76
V-6	Frequency Spectrum: In near field of Stix Coil, no gas	78
V-7	Frequency Spectrum: Showing dense spectral display	78

LIST OF TABLES

Page

Table I Hot plasma Theory Expansion Parameter, λ . 29

PROPAGATION AND DISPERSION OF HYDROMAGNETIC AND ION CYCLOTRON WAVES IN PLASMAS IMMERSED IN MAGNETIC FIELDS

Magne Kristiansen, Jimmy G. Melton, Nathan B. Dodge (Prof. Arwin A. Dougal)

I. INTRODUCTION

The primary objective of the studies undertaken during the period covered by this report has been to compare ion cyclotron waves and harmonic ion cyclotron waves with regard to how effectively they can be used to heat a plasma. In the course of this research, extensive experimental investigations were conducted into the basic characteristics of harmonic ion cyclotron waves. It is the purpose of this report to describe the experimental results, to present the theoretical investigations which have been undertaken in support of the experiment, and to report on the experimental observation of several nonlinear plasma phenomena that have been observed to occur.

It has been previously reported[1,2,3,4,5] that plasma waves have been observed in our experiment which propagate above the ion cyclotron frequency and attenuate at harmonics of the ion cyclotron frequency. It was further observed that when these harmonic ion cyclotron waves damp in a magnetic beach, the transverse energy-density product of the plasma is substantially increased, in a manner similar to the way ion cyclotron waves damp in a magnetic beach at the ion cyclotron fundamental frequency.[6] These waves are being investigated experimentally and theoretically to determine how efficiently they can be used to heat a plasma, to determine whether they can be used for effective heating under conditions in which the ion cyclotron wave cannot be used effectively, and to determine, so far as it is possible on this experiment, whether there exist physical limitations which will limit the plasma temperatures which can be achieved by this method.

The problem of comparing ion cyclotron and harmonic ion cyclotron waves is divided into three phases: (1) to determine the mechanism and efficiency of coupling the waves from an external power source to the plasma column; (2) to determine the wave energy density and wave energy flux associated with the waves, or stated in practical terms, to determine how the energy which is to heat the plasma is carried through the plasma by the waves; and (3) to determine the efficiency of thermalizing

the wave energy by the ion cyclotron damping process.

There are three principal energy loss mechanisms which affect the efficiency of plasma heating by ion cyclotron waves. One is the energy lost due to plasma instabilities. Another is energy loss due to the escape of particles from the experimental environment; notably, the anomalous diffusion of particles across the confining magnetic field. A third is the energy loss due to waves which propagate through the experimental environment without heating the plasma. The third of these mechanisms is currently under investigation, due to the bearing it has on the wave damping and energy conversion which occurs in the magnetic beach.

The experimental observations of harmonic ion cyclotron wave propagation and damping are presented in Sec. II of this report. The experimental results were obtained from magnetic probes as the initial gas pressure, confining magnetic field, and probe positions were varied. The results are explained qualitatively in terms of the hot plasma conditions which exist for large $\lambda = \frac{1}{2} k_\perp^2 \rho_L^2$, shown to exist in the plasma.

Section III presents results from a theoretical investigation directed toward (1) firmly identifying the waves present in the plasma, and (2) determining the energy carried by the waves. The quasistatic approximation of the dispersion relation is investigated for several approximate cases, and dispersion curves are obtained for ion-acoustic waves, electrostatic and quasistatic[7,8] ion cyclotron waves, and for the "Bernstein modes" near ion cyclotron resonance conditions. A generalization of Poynting's Theorem for an anisotropic, dispersive medium is discussed, which permits analysis of the wave energy density and flux in a hot, homogeneous plasma in a magnetic field. The results are applied to the simple case of a cold plasma to obtain a comparison of the wave energy densities of ion cyclotron and electrostatic ion cyclotron waves.

The improvements which have been made to the experimental facilities since the last semiannual status report are described in Sec. IV. These improvements include the addition of an 8-mm microwave interferometer for density measurements, the construction of an rf-shielded room, addition of remote controls for the probe drive and the magnet power supply, the construction of an improved Stix-type wave

coupler, the addition of a spectrum analyzer, and the design of a P.I.G. discharge preionizer.

Section V reports the experimental observation of three new and unique non-linear plasma phenomena. These phenomena, which were observed via a spectrum analyzer, are: (1) Frequency mixing of one wave near the ion cyclotron frequency or its harmonics with a second higher frequency to produce sum and difference frequencies, (2) Harmonic frequency generation from a propagating wave undergoing harmonic ion cyclotron resonance absorption in the magnetic beach, and (3) Dense spectra of frequencies distinct from the harmonic and sum and difference effects above.

II. EXPERIMENTAL INVESTIGATION OF HARMONIC ION CYCLOTRON WAVE PROPAGATION AND ATTENUATION,* Magne Kristiansen and Arwin A. Dougal

A. Introduction

It has been observed[2,5] that for certain experimental conditions the ion cyclotron waves propagate for frequencies above the ion cyclotron frequency f_c. The harmonic number G at which the waves attenuate is found to be pressure dependent such that G increases for increasing gas pressure. Both hydrogen and deuterium plasmas were investigated. Attenuation at harmonics up to the 8th was observed. Spatial measurements of the wave magnetic fields were made with magnetic probes for several plasma densities and confining magnetic fields in a "magnetic beach"[3] geometry. Axial measurements of the wave magnetic fields demonstrate the wave propagation and wave damping. Radial measurements of the wave magnetic fields indicate a higher order transverse mode structure. Diamagnetic probe measurements show that enhanced plasma heating occurs whenever the wave fields attenuate at harmonics of f_c.

A qualitative discussion of the observed phenomena is presented. It is shown that a higher order transverse mode structure may be expected under experimental conditions similar to those reported here. Particle acceleration at harmonics of the cyclotron frequency for the case of higher order transverse modes and finite Larmor radii is briefly described. Finite temperature plasma theory, where harmonic effects are inherent, is shown to apply for even moderately hot plasmas provided the radial wave number is large.

B. Experimental Arrangement

A block diagram of the experimental arrangement is shown in Fig. II-1. The plasma tube is made of Pyrex and has a 6 cm diameter. Sorption and ion pumps provide a clean evacuated system. The vacuum is better than 10^{-8} torr. Hydrogen

---

*Preprint of paper submitted for publication on August 29, 1966 and accepted for publication in Physics of Fluids, scheduled to appear in Vol. 10, pp. 596-604, March, 1967 issue.

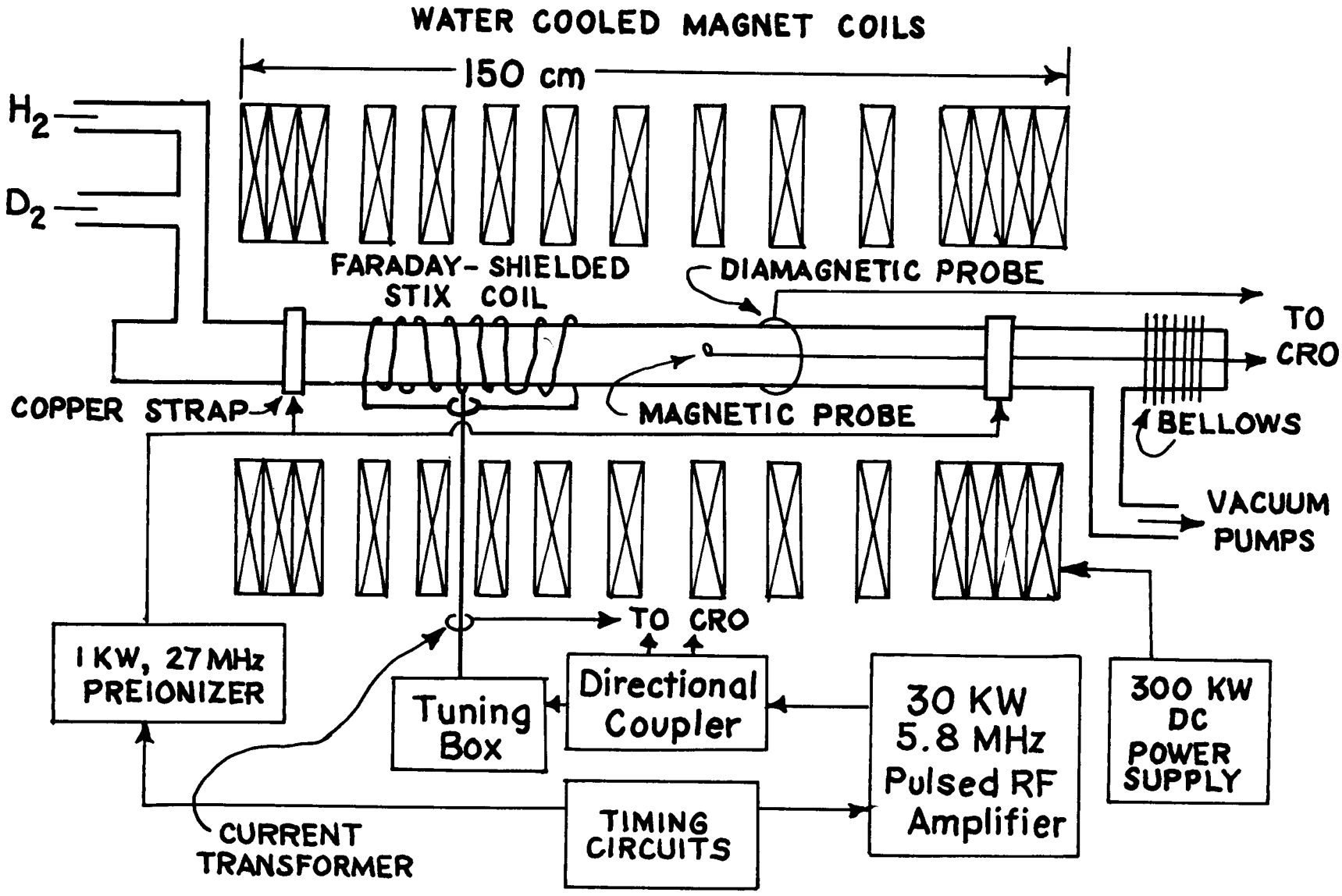

Fig. II-1. Block Diagram of ICRH Experiment

and/or deuterium can be leaked into the system. The vacuum gauges used for $p > 10^{-4}$ torr are calibrated against a McLeod gauge, but the uncertainty in pressure reading for 10^{-4} torr $< p < 10^{-3}$ torr is at least a factor of two. The solenoidal air core magnetic field system has an overall length of 150 cm and an inside diameter of 18 cm. Rf power is coupled into the plasma through a Stix coil[9] located in a uniform (±1/3%) magnetic field region with a maximum of 10.6 kG. The center fed Stix coil is a 4-section coil with 4 turns per section and a periodicity (wavelength) of 16 cm. A Faraday shield is used to shield the E_z field component underneath the Stix coil. The shield is not grounded. A shielding efficiency of approximately 75% is obtained.[10] A 43 cm long, slowly decreasing magnetic field region (magnetic beach) is used for wave propagation studies. The field at the end of the beach is 83.5% of the field in the Stix coil region. At each end of the magnetic field system there is a small magnetic mirror as shown in Fig. II-2. The plasma is preionized with a 27.12 MHz, 1 kW, rf preionizer. The preionizing power is capacitively coupled into the plasma through two copper straps located near the mirror peaks, approximately 123 cm apart. The rf preionizer is on for 1-6 msec and is turned off 10 μsec before the onset of the main rf pulse, which lasts 100-600 μsec. Maximum incident power in the main rf pulse is over 30 kW. The incident and reflected rf power are measured with adjustable, calibrated directional couplers. Net rf power absorbed by the plasma and the tuning system is typically 12-24 kW when ion cyclotron waves are generated. The main rf driver is crystal controlled at 5.8 MHz. (Fig. IV-1, Experimental facilities section)

A diamagnetic probe[11] can be moved along the outside of the Pyrex tube. The signal from this probe is integrated with a Tektronix type O operational amplifier and displayed on a Tektronix type 555 oscilloscope. The integrated signal is proportional to $n\beta(T_{e\perp} + T_{i\perp})$, where n is the electron density, β is Boltzmann's constant and $T_{e\perp}$ and $T_{i\perp}$ are the transverse electron and ion temperatures respectively. The integrated signal is shown in Fig. II-3. A movable magnetic probe, shown in Fig. II-4, is used to measure the wave magnetic fields. The probe is oriented to detect one of the r, θ, or z components of the wave magnetic field. The probe is coated with a colloidal graphite solution ("Aquadag") and surrounded by an axially slit copper cylinder to minimize the electrostatic

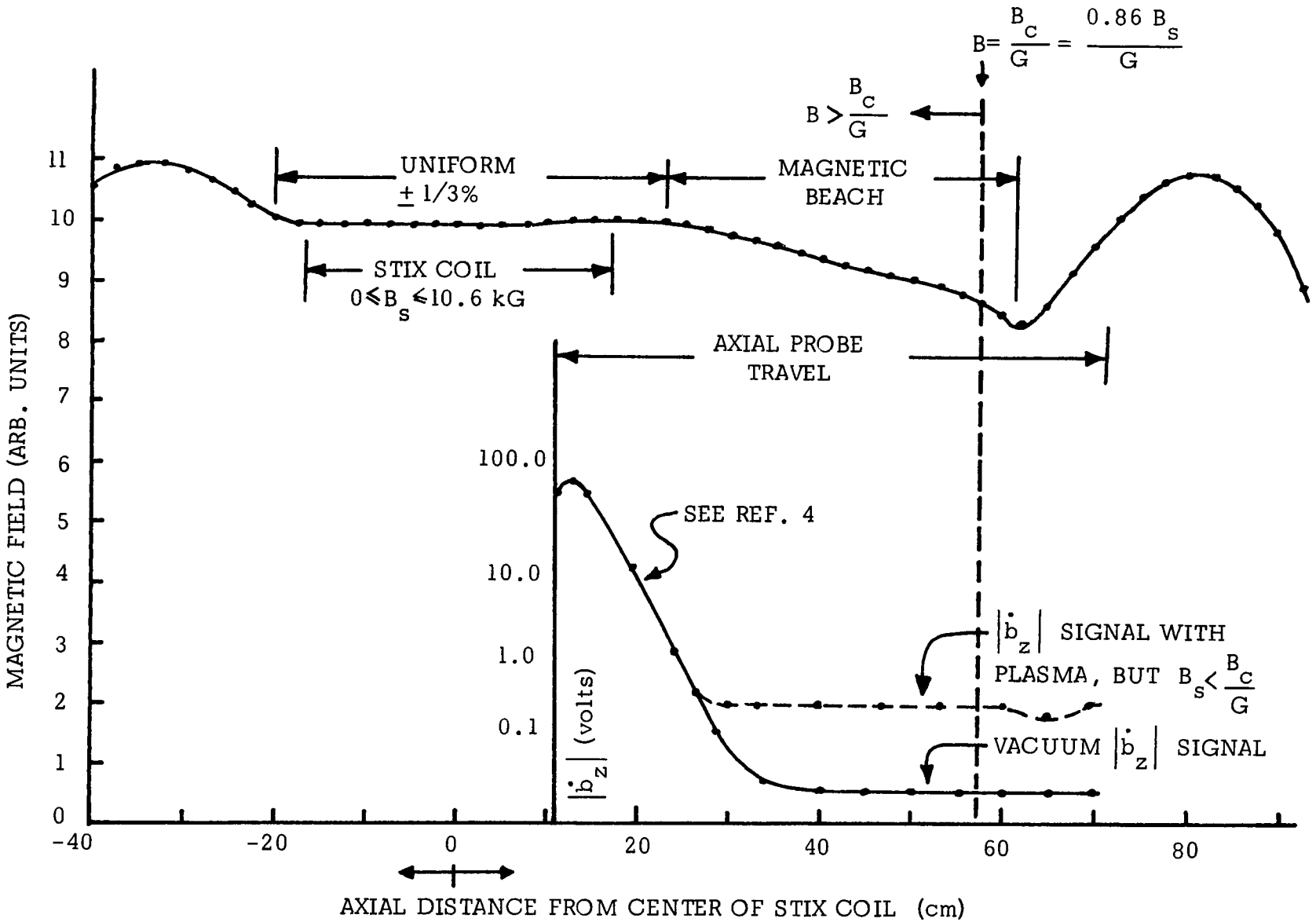

Fig. II-2. Magnetic Field Configuration.

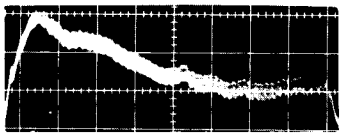

INTEGRATED DIAMAGNETIC SIGNAL, B_s = 3000 G,

p = 0.2 millitorr
Deuterium Gas
$\sim$10 ev/cm, 20 μs/cm

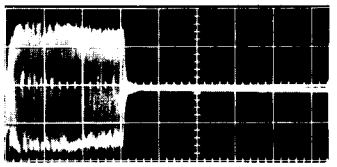

MAGNETIC PROBE SIGNAL ($\dot{b}_z$)

B_s = 4350 G
p = 0.2 millitorr
Deuterium Gas
370 mv/cm, 200 μs/cm

Fig. II-3. Diamagnetic and Magnetic Probe Signals.

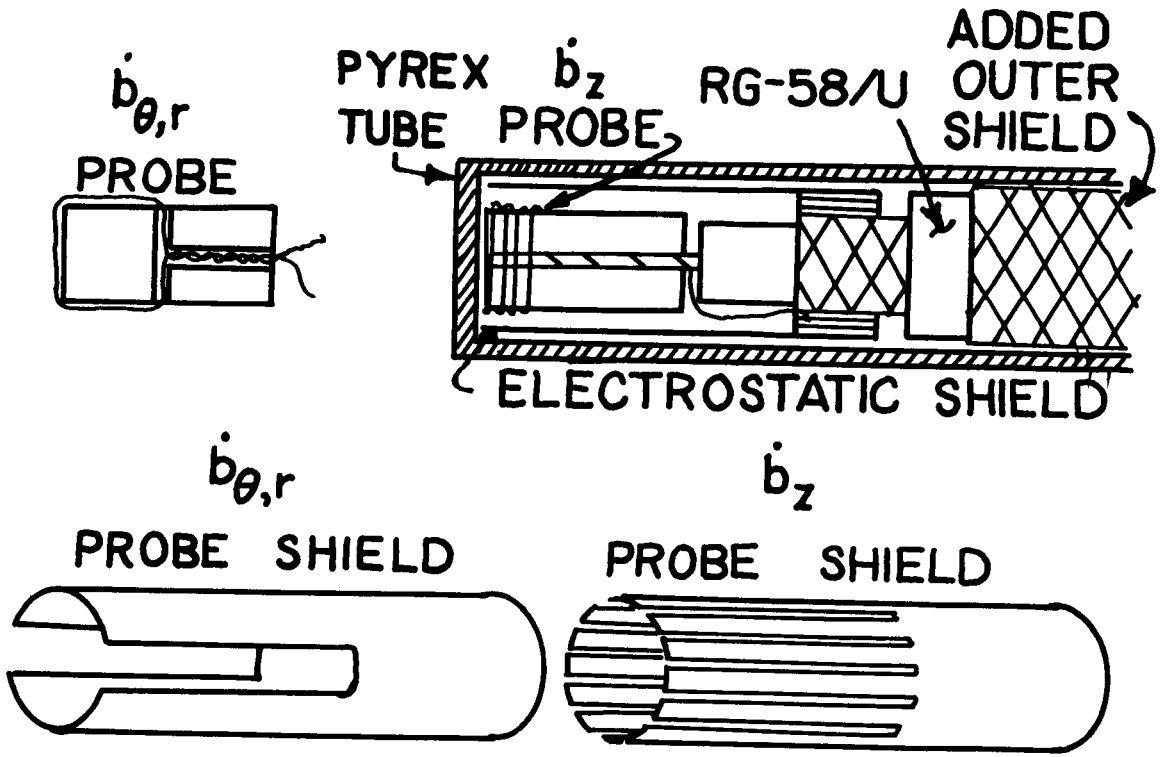

Fig. II-4. Magnetic Probe Construction

pickup. A double shielded coaxial cable transmits the signal to the oscilloscope which is housed in a screen room. The probe assembly is housed in a re-entry Pyrex tube which is attached through a glass-Kovar seal to a stainless steel bellows drive assembly. The probe assembly can be moved across the plasma tube, from wall to wall, for radial wave magnetic field plots. Maximum axial travel is 61 cm. Most of the wave field measurements were made on the z component of the time varying wave magnetic field $\dot{b}_z$. The $\dot{b}_\theta$ and $\dot{b}_r$ probes are more critical to align to only one field component and their signal amplitudes are usually less. A typical signal for the $\dot{b}_z$ probe is shown in Fig. II-3. The vacuum rf field, i.e., the rf field from the Stix coil with no plasma in the tube, was measured with the $\dot{b}_z$ probe for various axial positions in the system. The measured amplitude is plotted in Fig. II-2. The peak in $\dot{b}_z$ at z = 12 cm occurs exactly as expected[10] since the Stix coil has a periodicity of 16 cm which should give peaks in $|\dot{b}_z|$ at z = -12,-4,4,12 cm.

A typical $\dot{b}_z$ magnetic probe signal is 0.6-1.2 volts when a wave is propagating in the plasma. With plasma, but under conditions for no propagation, the $\dot{b}_z$ signal is typically 0.1-0.3 volts. The axial variation of the $\dot{b}_z$ signal for the nonpropagating case is plotted in Figs. II-2 and II-5.

C. Measurements of $\dot{b}$ and $n\beta T_\perp$

In this experimental investigation the frequency of the driver is a constant and the other parameters, like gas pressure p and magnetic field strength B, are varied. The magnetic probes were translated from 30-70 cm from the center of the Stix coil.

For low hydrogen pressure, $p < 2$ millitorr, an ion cyclotron wave was observed to propagate for $B > B_c$, where $B_c = \omega m_i/q_i$ and to attenuate quite sharply near $B = B_c$ as would be generally expected. However, as the gas pressure was increased, it was found that a wave propagates for $B < B_c$, which was unexpected. Closer investigation revealed that the wave attenuates near B_c/G, where G is an integer. This means that the wave propagates for $f > f_c$ and attenuates at a harmonic of f_c. The value of G was found to depend upon the gas pressure such that G increased for higher pressures.

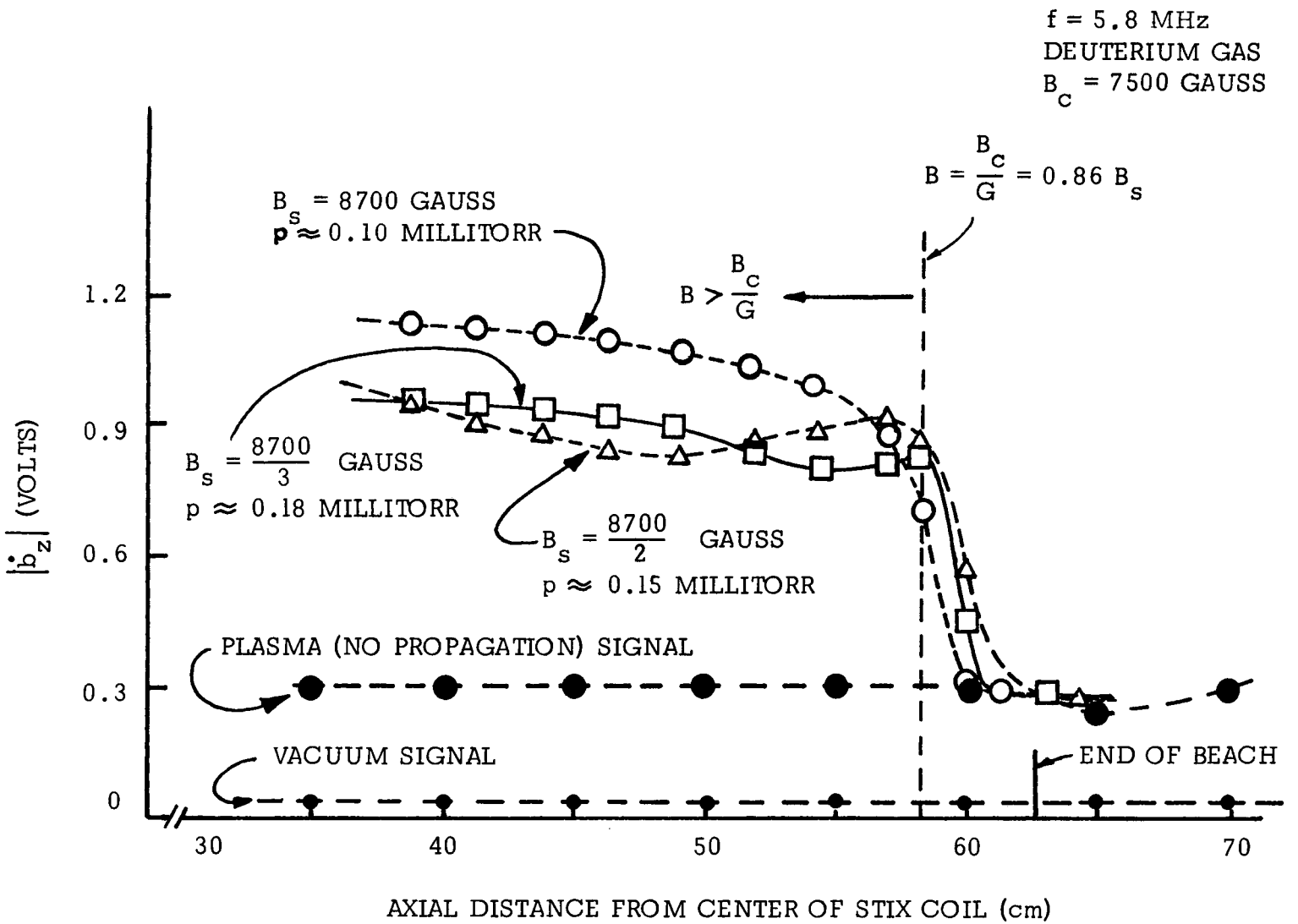

Fig. II-5. Wave Magnetic Field ($\dot{b}_z$) Variation in Beach Retion

The same wave effects were found for deuterium plasmas. They were actually more evident, since the separations between the various B_c/G are larger due to the larger ion mass. Fig. II-5 shows measurements in a deuterium plasma. The wave is seen to propagate , at p = 0.10 millitorr, for $B > B_c$ and then attenuate quite abruptly near the place in the beach where $B = B_c$. The wave will then not propagate at all if the magnetic field is lowered such that $B_s < B_c$, in agreement with theory.[12] When the magnetic field underneath the Stix coil B_s is lowered such that $B_s \gtrsim B_c/2$, the wave again propagates if the pressure is increased slightly to about 0.15 millitorr. The wave now attenuates in the beach where $B = B_c/2$. Similarly the wave can be made to propagate near successively higher harmonics of f_c by lowering the magnetic field and increasing the pressure. The wave then propagates for $B > B_c/G$ and attenuates at $B = B_c/G$. Propagation and attenuation were observed at harmonics up to the 8th, when p = 0.26 millitorr. The measurements at these low magnetic fields are, however, complicated by the fact that there now may be more than one critical field B_c/G in the beach at one time since the difference between the various B_c/G becomes sufficiently small. An added complication is that for $G > 8$ the fast wave may also propagate and its amplitude is larger than that of the harmonic ion cyclotron wave.

The amplitudes of the various harmonic waves do not vary greatly. The first three or four harmonics are almost equal in amplitude as are shown in Fig. II-5. The higher harmonics have only slightly lower amplitudes as seen in the plot of $\dot{b}_z$ for the 8th harmonic in Fig. II-6.

The $\dot{b}_z$ signal is small and almost constant along the beach region when B and p are adjusted for no wave propagation. The amplitude is shown in Figs. II-2 and II-5. For $z < 30$ cm, the amplitude is characteristic of the induction field of the Stix coil.

Keeping the magnetic probe at a fixed axial position and sweeping the magnetic field past the critical field B_c/G verifies that the observed phenomena are functions of the magnetic field and not of some perculiarity of the magnetic beach at the probe position. An example is shown in Fig. II-7 for the fundamental wave. It is seen that the wave increases considerably when the magnetic field at the

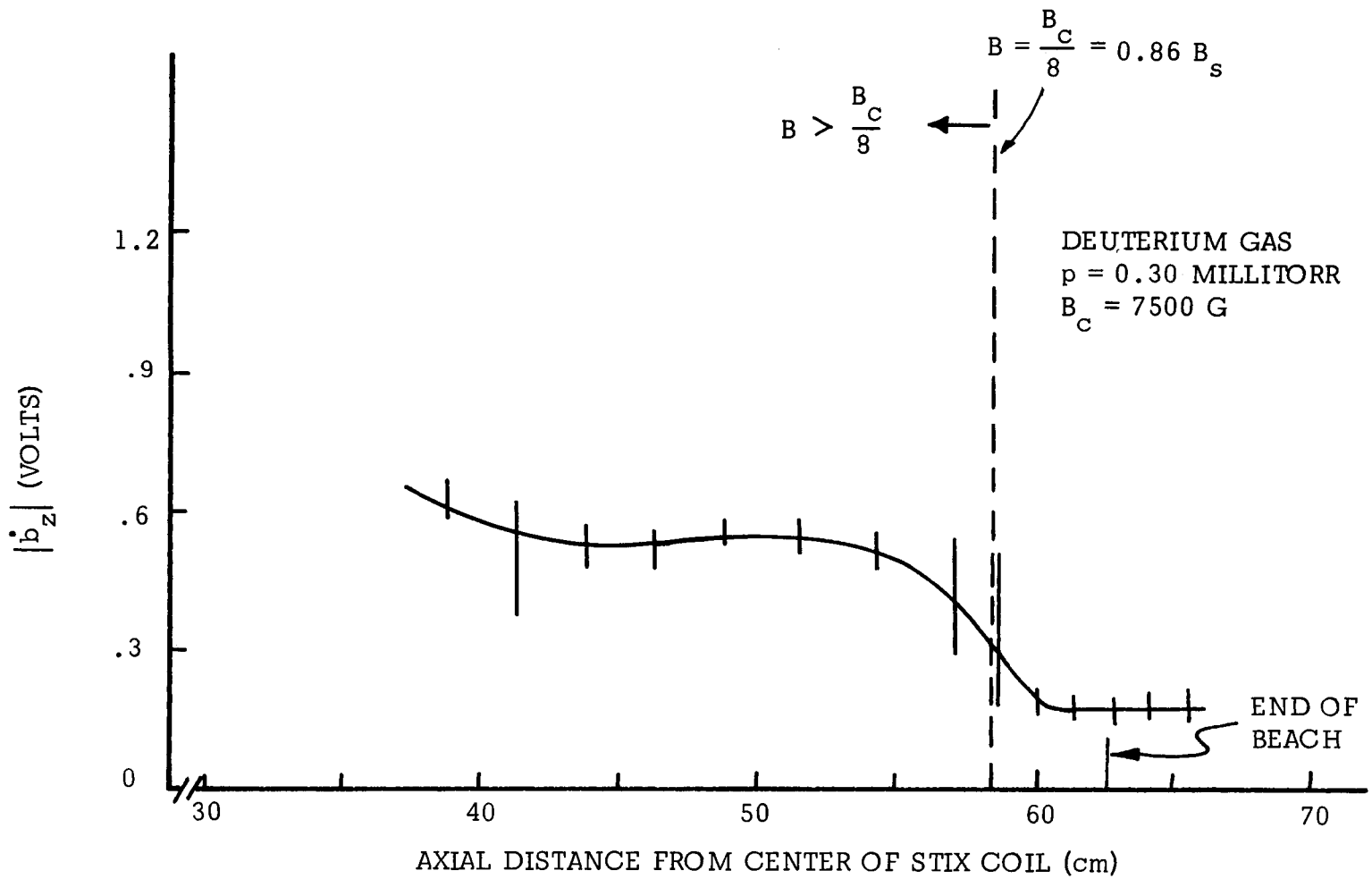

Fig. II-6. Wave Attenuation at the 8th Harmonic of the Ion Cyclotron Frequency.

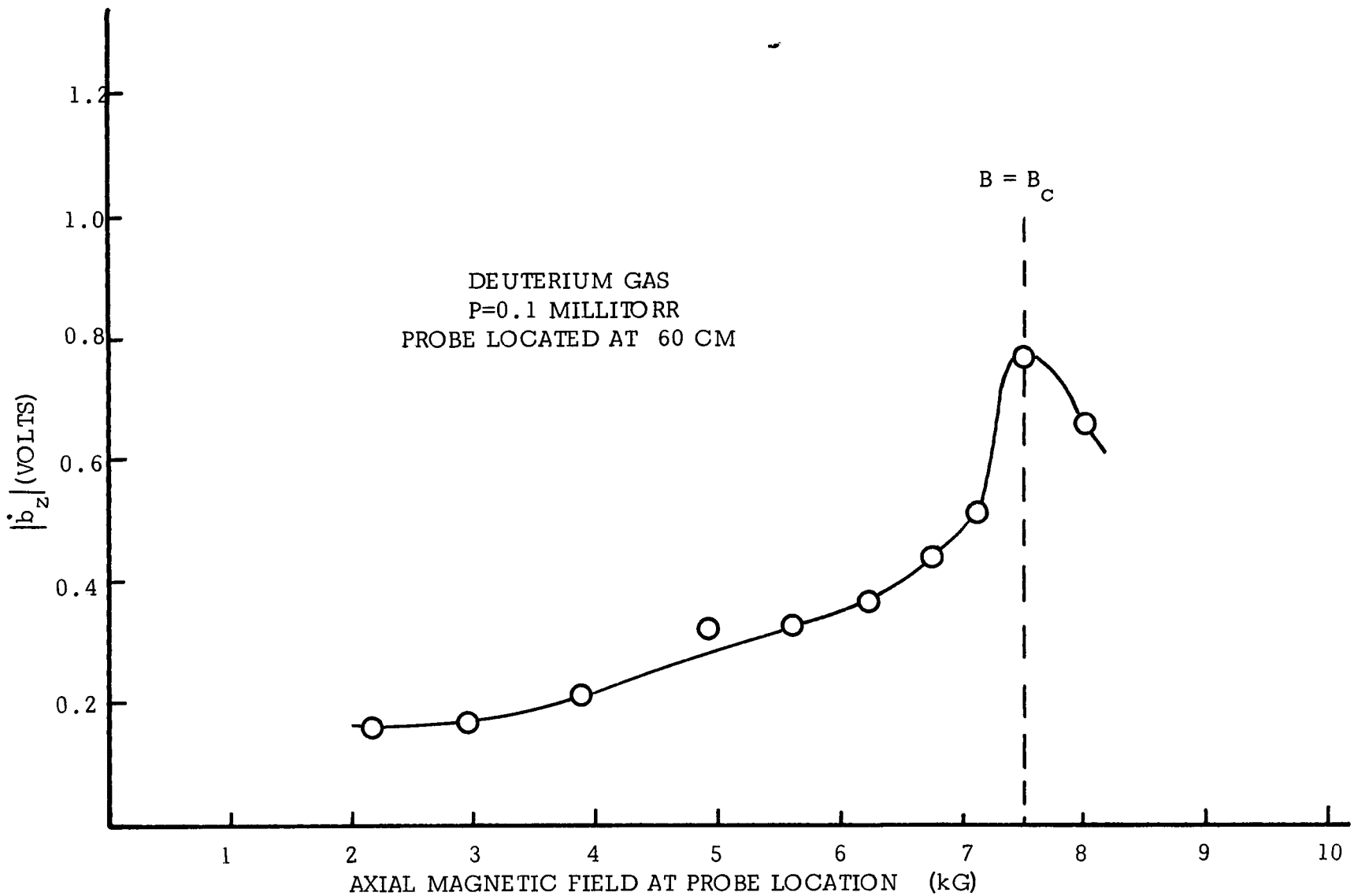

Fig. II-7. Magnetic Probe Signal ($\dot{b}_z$) vs Magnetic Field

probe position $B_p = B_c$. The plasma and tuning conditions do, however, change somewhat as the B field is varied. It is therefore in general easier and more reliable to interpret the measurements made by moving the probe in the magnetic beach region and keeping the magnetic field constant.

For the second and third harmonics, $\dot{b}_z$ increases somewhat in the region $B \gtrsim B_c/G$. This increase near $B = B_c/G$ has also been observed for $G = 1$ in hydrogen plasma, but not in deuterium plasma. The amplitude increase is not unexpected since the wavelength will decrease as the waves propagate along the magnetic beach. For low dissipation the energy content per wavelength may decrease slower than the wavelength such that the net result is an increase in wave amplitude. This is in contrast to the signal amplitude not increasing for the fundamental wave in deuterium plasma.

Fig. II-8 shows radial plots of $\dot{b}_z$, $\dot{b}_r$, and $\dot{b}_\theta$ for a given set of experimental conditions. One would expect a pronounced minimum in $\dot{b}_\theta$ and $\dot{b}_r$ at $r = 0$, as explained in Sec. II-D. The absence of such a pronounced minimum is taken to be indicative of a higher order radial mode structure. The magnetic probes have a resolution of approximately 9 mm, and for a transverse mode number higher than the 5th one would then not expect to be able to measure any pronounced wave field minima.

The electron density of the deuterium plasma was measured with a 70 GHz microwave interferometer. Earlier it was assumed from coupling resonance and fast wave cut-off measurements that $n > 10^{18}\ m^{-3}$. The measurements indicate, however, that $n < 10^{18}\ m^{-3}$. This density is somewhat low for the millimeter wave frequency so the resolution was not optimum. The density as a function of the magnetic field is shown in Fig. II-9 for two different gas pressures. Measurements at other pressures show that the plasma density increases with pressure up to about 0.8 millitorr. For high pressures the density gradually decreased. A typical density for this experiment is thus $6 \times 10^{17}\ m^{-3}$.

The 70 GHz frequency of this interferometer gives a cutoff density of approximately $6.1 \times 10^{19}\ m^{-3}$. The plasma path length is about 5 cm and the density should be larger than $6 \times 10^{17}\ m^{-3}$ in order to get good resolution. The measurements were made by balancing the interferometer with no plasma in the system and

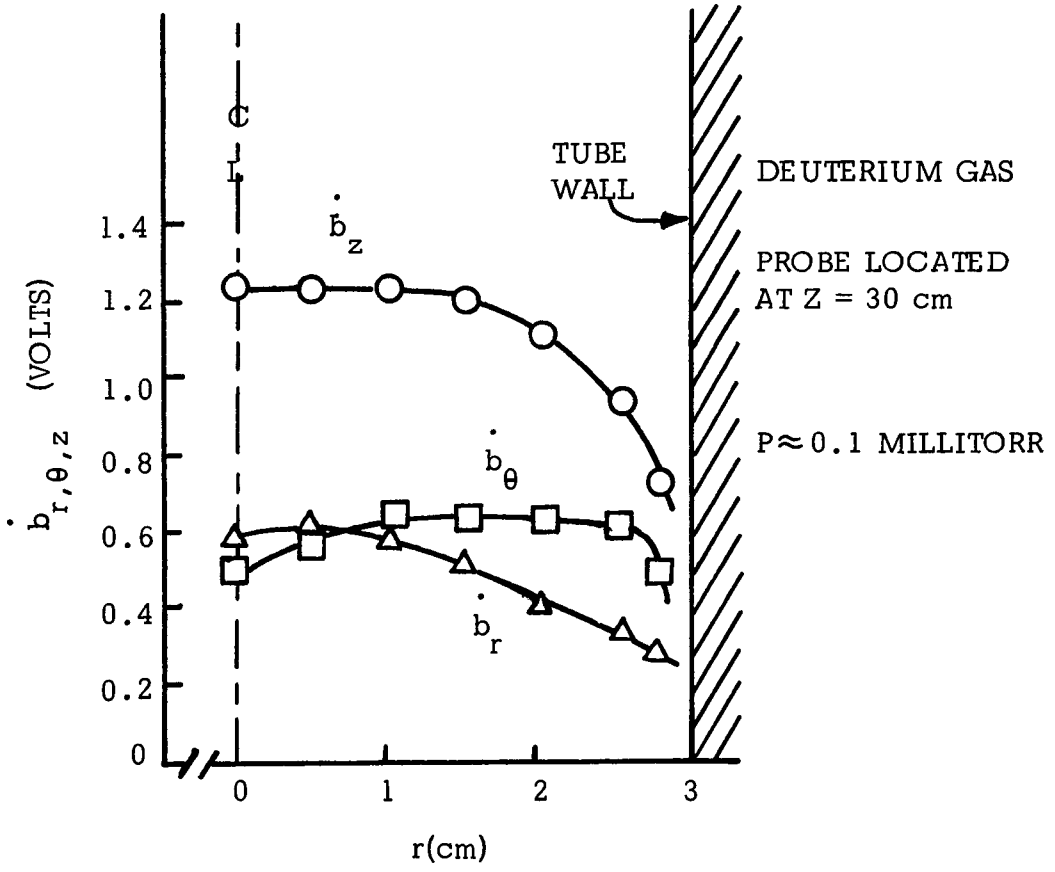

Fig. II-8. Radial Variation in Wave Magnetic Probe Signals.

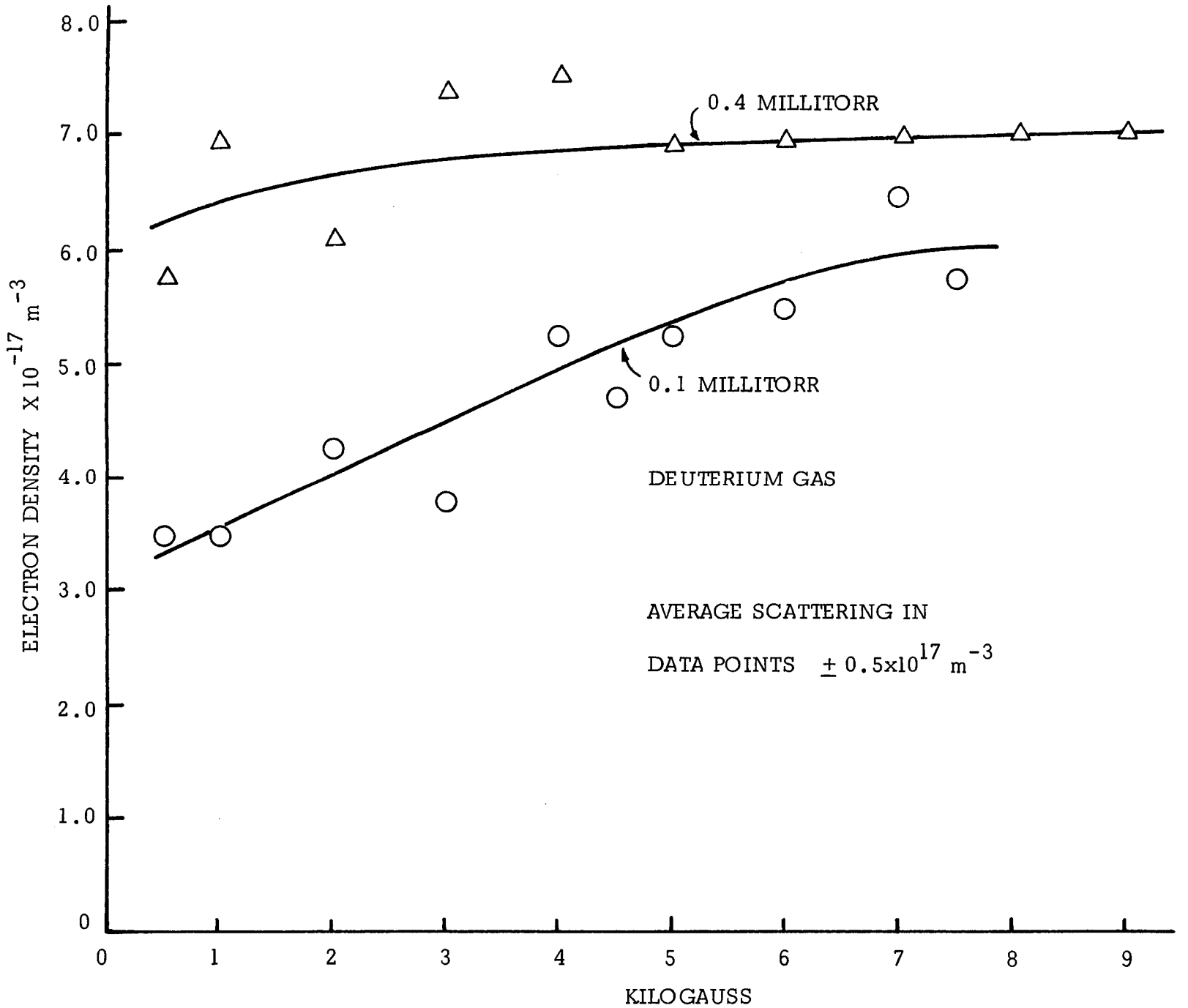

Fig. II-9. Electron Density vs Magnetic Field.

then measuring the signal amplitude when the plasma was pulsed. The signal amplitude was interpreted in degrees by comparing it with the signal amplitude caused by inserting a known phase shift from a calibrated phaseshifter. The hybrid ring detectors give two outputs, proportional to the square of respectively the sum and the difference of the signals through the two arms of the interferometer. Either one of these two outputs can be used to measure the phaseshift, provided the attenuation through the plasma is small. If the plasma attenuation is large, then both signals must be recorded and used to compute the phaseshift $\Delta\chi$. In this experiment it was experimentally verified that the plasma attenuation is small, such that only one signal was recorded. This was usually the sum signal, $A_1^2 + A_2^2 + 2A_1A_2 \cos\chi$.

A cosinusoidal density distribution was assumed and the density calculated from the equation

$$n \approx 1.1 \times f \times (\Delta\chi/d) \times 10^6 m^{-3}, \qquad \text{(II-1)}$$

which is valid for n much less than the cut-off density for the microwave signal. The microwave frequency f is in Hz, the phase shift $\Delta\chi$ in degrees, and the plasma diameter d in cm.

The density was measured at the middle of the main rf pulse. The density varied approximately $\pm 5\%$ from this measured value during the rf pulse and was usually maximum near the beginning of the pulse. The plasma decayed with an e-folding time of typically 50 μsec. The preionization is turned off approximately 10 μsec before the main rf is turned on, and the rise and fall times of both preionizer and main rf pulses are less than 10 μsec. The density measurements were made 40 cm from the center of the Stix coil, in the magnetic beach where the wave propagation measurements were made.

It should be noted that recent calculations[13] show that a significant amount of power may be coupled into the ion cyclotron waves even if the natural and forced plasma modes are not very well matched. This is due to a beat phenomenon between the forced and the natural plasma modes which leads to two off resonant maxima on the high field side in the power absorption vs magnetic field plots. These off resonant maxima have significant amplitudes and can lead to quite efficient

power transfer even at off resonant conditions. It is also pointed out that the true coupling resonance has such a small half width that it may be difficult to observe experimentally. The first off resonant maximum, which is the highest and narrowest, may be mistaken for the true coupling resonance. Density estimates based on coupling resonance measurements may thus be too high by almost a factor of two.

Diamagnetic probe measurements verify that the waves are actually damped and transfer their energy to the plasma particles. Fig. II-10 shows a plot of $n \beta T_{\perp}$ vs B for pressure conditions which give attenuation at B_c and $B_c/2$. The magnetic probe was retracted during this series of experiments in order not to disturb or cool the plasma. For the condition of damping at the fundamental frequency, the transverse temperature-density product increases near $B = B_c$. For the condition of damping at the second harmonic, the diamagnetic signal increases near $B = B_c/2$.

The diamagnetic signal was also measured by moving the diamagnetic loop along the discharge tube in the region where the waves were made to damp. Fig. II-11 shows the axial variation in the diamagnetic signal at the end of the beach where the natural local B-field minimum is purposely deepened. The diamagnetic signal is seen to increase in this region when the waves attenuate there. The magnetic probe was retracted here such that it did not cool or disturb the plasma in any way. The diamagnetic signal is seen to be very small when the magnetic field is adjusted such that the wave does not damp anywhere in the beach.

Reducing the preionization power does not change the basic phenomena, but the wave amplitude decreases and the attenuation regions become wider. For lower preionization power, the various harmonic attenuations also occur at higher gas pressures. This indicates that the phenomena are more electron density dependent than neutral gas pressure dependent. The broadening of the attenuation regions for higher gas pressures is attributed to ion-neutral collisional effects, while the lower wave field amplitude is attributed to the lower electron temperature. It was shown in this work, using a 40 kW rf preionizer, that increasing the preionization and electron temperature caused almost order of magnitude increases in the wave fields.

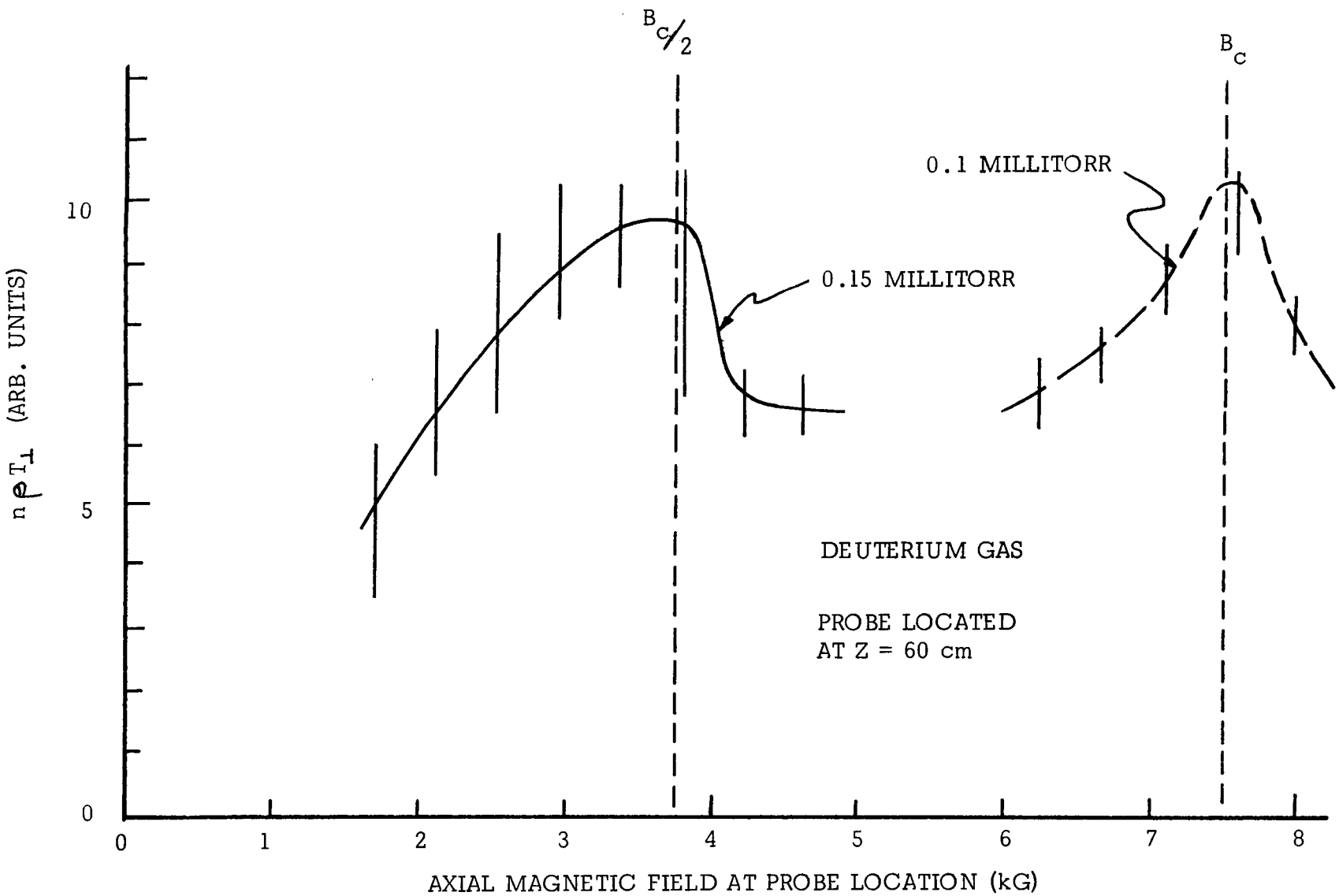

Fig. II-10. Diamagnetic Probe Signal vs Magnetic Field

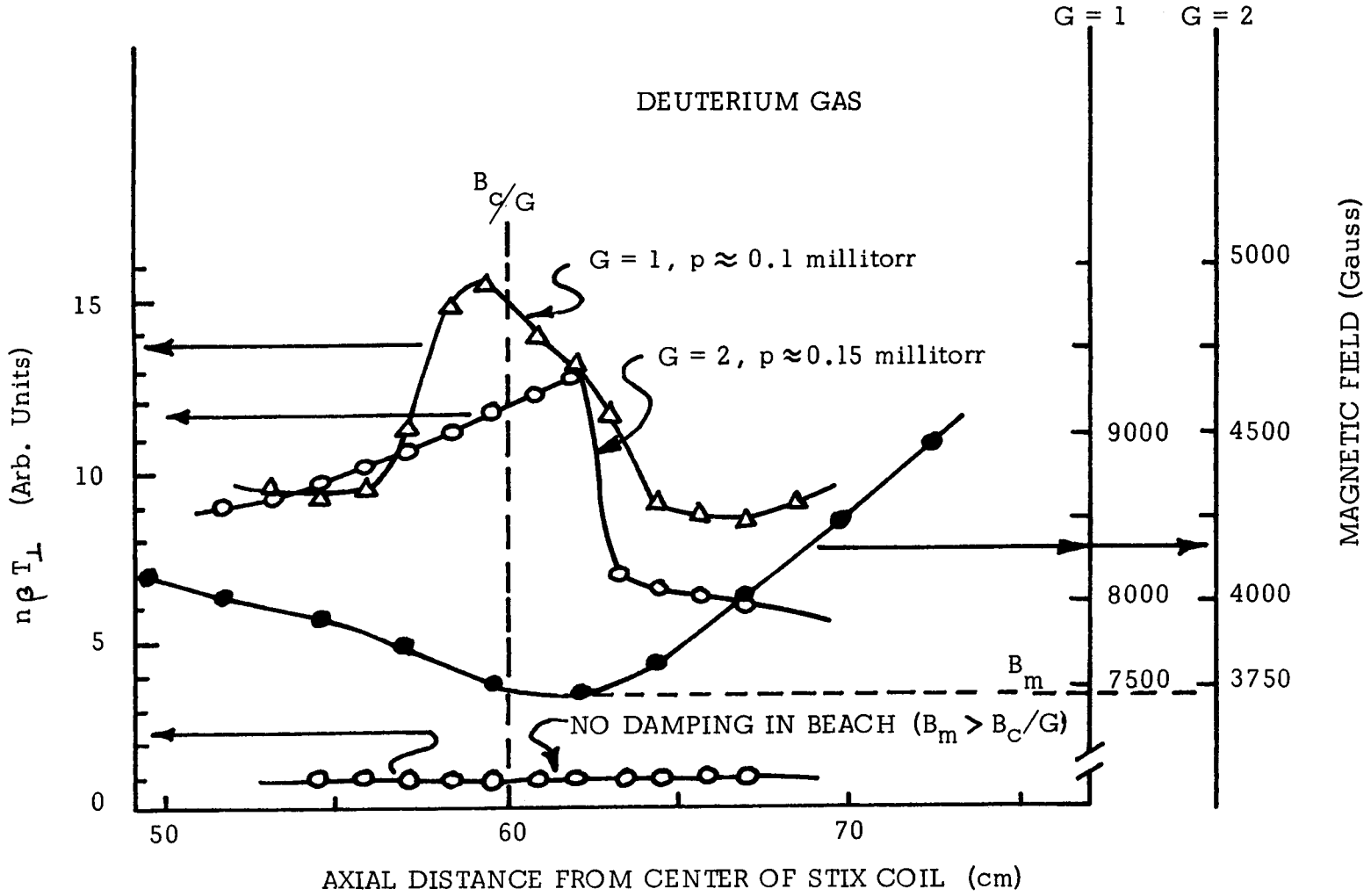

Fig. II-11. Axial Variation in Diamagnetic Probe Signal Near B_c/G.

D. Theoretical Considerations

There has been considerable interest in cyclotron harmonic resonance phenomena in plasmas in the last few years. Most of the experimental and theoretical investigations, however, were concerned with electron cyclotron harmonic resonance. Emission up to very high harmonic numbers was observed.[14] Absorption[15] and transmission[16] perpendicular to the magnetic field at electron cyclotron harmonics were also demonstrated.

Experimental evidence of ion cyclotron harmonic resonance phenomena are much more sparse. Ion cyclotron harmonic emission was observed from some of the larger plasma devices like OGRA.[17] Transmission of harmonic ion cyclotron waves has been reported in two instances.[18,19] It is significant that both of these describe propagation along the magnetic field. No report has been found of direct evidence for transmission along the magnetic field at electron cyclotron harmonics. From considerations given by Stix[12] it is expected that waves propagating along the magnetic field near electron or ion cyclotron harmonics may be heavily Landau damped. Yoshikawa, Rothman, and Sinclair,[18] however, report heating in a magnetic beach at harmonics of f_c up to the fifth. Kristiansen and Dougal[1,4] have reported measurements of wave magnetic fields for waves propagating at $f > f_c$ and attenuating at harmonics of f_c. Stix[19] has made theoretical calculations pertaining to ion cyclotron harmonic resonance and propagation transverse to the magnetic field, but no experimental confirmation has yet been reported.

The experimental findings reported here indicate the presence of higher order transverse modes. Most theoretical calculations based on the cold plasma theory consider only the lowest order modes. For this case, it can easily be shown how the components of the wave magnetic fields are related to the aximuthal electric field E_θ. If the field quantities are assumed to vary as $\exp i[\omega t - k_0 z]$, then

$$|\dot{b}_z| \approx \left|\frac{1}{r}\frac{\partial}{\partial r}(rE_\theta)\right| = |k_\perp J_0(k_\perp r)| \tag{II-2a}$$

$$|\dot{b}_r| \approx |k_0 E_\theta| \tag{II-2b}$$

$$|\dot{b}_\theta| \approx |k_0 E_r| \tag{II-2c}$$

$$E_r = \frac{-i\mu q_i^2 n \omega^3 E_\theta}{\omega^2(\mu q_i^2 n \Omega_i + k_o^2 m_i \Omega_i) - k_o^2 m_i \Omega_i^3} \tag{II-3}$$

$$E_\theta = A J_1(k_\perp r) \tag{II-4}$$

$J_o(x)$ and $J_1(x)$ are Bessel functions in the notation of Watson,[20] μ is the permeability of the medium, q_i is the charge of the ion, m_i is the mass of the ion, n is the particle density, Ω_i is the angular ion cyclotron frequency, $k_\perp$ is the transverse wave number, and k_o is the lowest order parallel wave number, corresponding to the fundamental wave number of the Stix coil. It would, from Eqs. (II-2) - (II-4), be expected that experimental plots of $\dot{b}_\theta$ and $\dot{b}_r$ versus r would have pronounced minima, or ideally a zero, at the center of the plasma tube. Possible errors in probe and plasma tube alignment, as well as the finite resolution of the probe, could prevent measuring actual zero field magnitude at the tube center. For higher order transverse modes it becomes, for the same reasons, even more difficult to detect field minima. For sufficiently higher order modes (approximately 5 in this case) the mode spacing becomes even smaller than the size of the magnetic probe. Then it is not possible to measure any pronounced minima in the $\dot{b}_\theta$ and $\dot{b}_r$ amplitudes across the plasma column.

The waves are excited by a Stix coil of length 2a. Since the coil is of finite length, each Fourier component of the coil current can be decomposed into its Fourier spectrum such that the total azimuthal driving current can be expressed as

$$\vec{J}_c = \vec{\theta} \sum_\nu J_\nu \int_{-\infty}^{\infty} \frac{\sin(k_\parallel - \nu k_o)a}{\pi(k_\parallel - \nu k_o)} \exp i(\omega t - k_\parallel z)\, dk_\parallel \tag{II-5}$$

where $k_\parallel$ is the parallel wave number. J_c is proportional to the electric field E_θ. From this an expression can be derived (Ref. 12, Ch. 5) for the power transferred to the m'th plasma mode for a given Fourier component, averaged from z = -a to z = +a. Each Fourier component (ν) can thus couple power into some plasma mode m. The amount of power coupled into the plasma depends not only upon the coefficient of the Fourier component but also upon how well it is matched to a natural plasma mode. Woollett[13] has, as mentioned earlier, shown that

significant amounts of power can be coupled into the plasma even at off resonant conditions because of a beat phenomena between the forced and the natural plasma modes.

The conditions for natural modes of a plasma cylinder surrounded by vacuum are found by determining the conditions under which E_θ is finite when $J_c = 0$. This leads to

$$\frac{k_\perp r_p J_1'(k_\perp r_p)}{J_1(k_\perp r_p)} = \frac{k_\parallel r_p K_1'(k_\parallel r_p)}{K_1(k_\parallel r_p)} \qquad \text{(II-6)}$$

where $K_1(x)$ is a Bessel function in the notation of Watson,[20] primes indicate derivatives with respect to the argument, and r_p is the plasma radius. This relation can also be termed the "boundary conditions" for the vacuum boundary case. Simultaneous solution of Eq. (II-6) and the dispersion relation, which is given below, gives the values of $k_\perp$ and $k_\parallel$ for the m'th natural plasma mode at a given plasma density, magnetic field and frequency.

Only the first few Fourier components in the coil current distribution are of any appreciable magnitude. The fundamental component is almost four times as large as the next largest component. The Stix coil impresses upon the plasma column waves with a relatively fixed $k_\parallel$. It is commonly assumed that $k_\parallel = k_0$, but it is then also possible to excite waves with $k_\parallel = \nu k_0$ where ν is the index of the Fourier components of the coil current. For large integer ν the excitation will, however, be very inefficient, but it should be noted that the finite length of the Stix coil also introduces a spatial subharmonic which may couple quite efficiently to the plasma at low densities.[21]

Now consider the cold plasma dispersion relation

$$\begin{aligned}\eta^4 (K_{xx} \sin^2\varphi + K_{zz} \cos^2\varphi) - \eta^2 (K_{xx} K_{yy} \sin^2\varphi + K_{xx} K_{zz} \\ + K_{yy} K_{zz} \cos^2\varphi - K_{xy} K_{yx} \sin^2\varphi) \\ + (K_{xx} K_{yy} K_{zz} - K_{xy} K_{yx} K_{zz}) = 0,\end{aligned} \qquad \text{(II-7)}$$

where $\vec{\eta} = \frac{c\vec{k}}{\omega}$, $k^2 = k_\perp^2 + k_\parallel^2$, $\varphi = \measuredangle(\vec{k}, \vec{B}_0)$

$$K_{xx} = K_{yy} = 1 + \Pi_i^2/(\Omega_i^2 - \omega^2) + \Pi_e^2/(\Omega_e^2 - \omega^2),$$

$$K_{xy} = -K_{yx} = i\left[\frac{\Pi_i^2 \Omega_i/\omega}{\Omega_i^2 - \omega^2} - \frac{\Pi_e^2 \Omega_e/\omega}{\Omega_e^2 - \omega^2}\right],$$

$$K_{zz} = 1 - (\Pi_e^2 + \Pi_i^2)/\omega^2 ,$$

c = velocity of light,

Ω_k = angular cyclotron frequency of k'th plasma species,

Π_k = plasma frequency of k'th plasma species.

For the case of $\omega \approx \Omega_i$, it is customary to neglect certain terms on the basis of m_e/m_i size arguments and assuming lower order modes. The dispersion relation then becomes

$$c^2 k_\perp^2 = \frac{-c^4 k_\parallel^4 (\Omega_i^2 - \omega^2) + \omega^2 c^2 k_\parallel^2 2\Pi_i^2 - \omega^4 \Pi_i^4/\Omega_i^2}{c^2 k_\parallel^2 (\Omega_i^2 - \omega^2) - \omega^2 \Pi_i^2} \qquad \text{(II-8)}$$

This relation shows that $k_\perp$ must increase with the plasma density n if $k_\parallel$ is considered fixed by the Stix coil and all other parameters are kept constant. It is, however, seen that $k_\perp$ is an exceedingly sensitive function of n. A change in density by a factor of two implies a change in $k_\perp$ from zero to infinity.

Now admit, instead, the possibility of higher order radial wave numbers, i.e., $k_\perp \gg k_\parallel$. Electron inertia terms must then be included in the dispersion relation, but some minor algebraic simplifications can still be made, assuming only that ω is of the order of Ω_i. The dispersion relation, Eq.(II-7), can then be written

$$c^2 k_\perp^2 = \left(\frac{c^2 k_\parallel^2 (\Omega_i^2 - \omega^2)\Pi_e^2}{2\Pi_i^2 \omega^2} - \frac{\Pi_e^2}{2}\right) \pm \left[\left(\frac{c^2 k_\parallel^2 (\Omega_i^2 - \omega^2)\Pi_e^2}{2\Pi_i^2 \omega^2} - \frac{\Pi_e^2}{2}\right)^2 + c^4 k_\parallel^4 \frac{(\Omega_i^2 - \omega^2)\Pi_e^2}{\Pi_i^2 \omega^2} - c^2 k_\parallel^2 2\Pi_e^2 + \frac{\Pi_i^2 \omega^2 \Pi_e^2}{\Omega_i^2}\right]^{1/2} \qquad \text{(II-9)}$$

This relation is double valued and leads to different conclusions than Eqs. (II-8). Fig. II-12 shows both forms of the dispersion relation, Eqs. (II-8) and (II-9), plotted for a given set of plasma parameters. The axial wavelength, frequency and magnetic fields are assumed to be constant and $k_\perp^2$ is plotted as a function of density. It is seen that for low densities Eq. (II-8) indicates that the only solution is $k_\perp^2 < 0$, while Eq. (II-9) indicates that there is also a solution $k_\perp^2 \gg 0$. For low densities, such as in this experiment, the only possible real value of k is then indeed $k_\perp \gg k_\parallel$. Fig. II-12 also shows the dispersion relation, Eq. (II-9), for another set of parameters pertaining to measurements reported in this paper. The lower branch of the dispersion relation is, for these parameters, not real at any of the densities of interest here.

The radial wave number must also satisfy the boundary conditions, Eq. (II-6), which imposes a discreteness on $k_\perp$ such that $k_\perp = k_{\perp m}$, where m is the mode number. For densities measured in this experiment ($3\text{-}8 \times 10^{17}\ m^{-3}$), an axial wavelength corresponding to the fundamental wavelength of the Stix coil ($k_\parallel = 39.2 m^{-1}$), a plasma radius of 2.5 cm, and a magnetic field such that $\frac{\Omega_i}{\omega} = 1.19$ ($B = B_c$ at z = 58 cm) it is found that $m \approx 12$. It is also possible for the spatial subharmonic ($k_\parallel = \frac{39.2}{2} m^{-1}$) caused by the finite coil length to couple quite efficiently into the waves.[21] This would for $\Omega_i/\omega = 1.19$ lead to $m \approx 6$. In either case, the radial wave number is large enough to explain the lack of any observed minimum in the radial plots of $\dot{b}_\theta$ and $\dot{b}_r$ shown in Fig. II-8.

The observed propagation and damping of waves near harmonics of the ion cyclotron frequency were found to be very pressure dependent. Fig. II-9 showed that, for a given neutral gas pressure, the electron density decreases with decreasing magnetic field in the range of interest for this experiment. The harmonic phenomena were observed by decreasing the magnetic field and increasing the pressure slightly. Within the experimental errors it therefore appears that the electron density in fact is very nearly the same for all cases where wave propagation and damping are observed. It thus appears from this experimental evidence that there is a critical density $n_c \approx 6 \times 10^{17}\ m^{-3}$ above which these waves can propagate. This would be the density which satisfied the appropriate dispersion relation along with the vacuum boundary conditions.

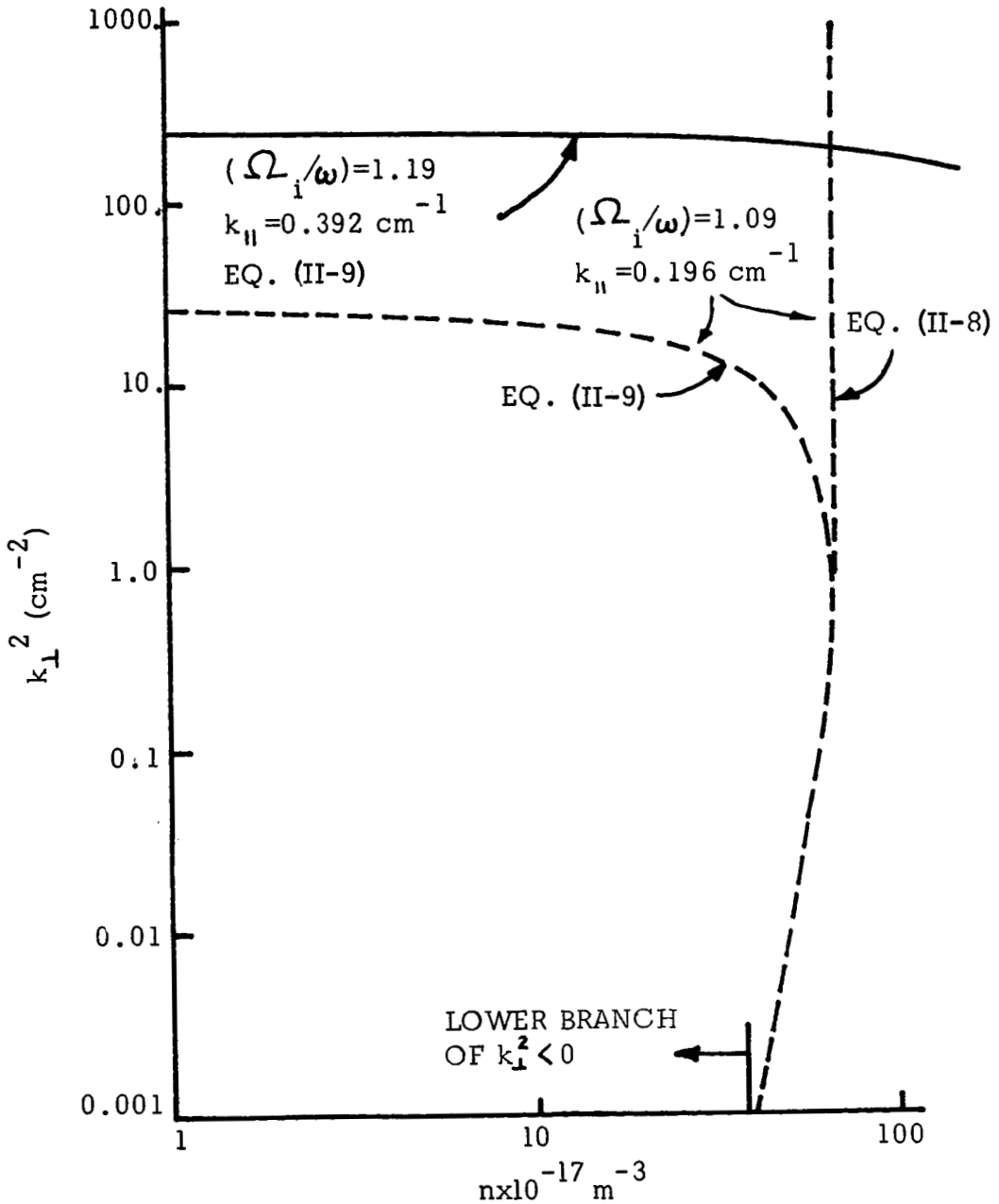

Fig. II-12. Cold Plasma Dispersion Relation.

The possible existence of cyclotron harmonics is well known in the hot plasma theory (Ref. 12, Chs. 8 and 9). The transverse temperature ($T_{e\perp} + T_{i\perp}$) of the plasma described in this paper is less than 50 eV equivalent, but the large radial wave numbers can still make the hot plasma theory very pertinent to this case. Consider the finite temperature plasma theory expansion parameter[12]

$$\lambda \equiv k_\perp^2 \frac{\beta T_\perp}{\Omega_k^2 m_k} \tag{II-10}$$

where β is Boltzmann's constant. Table I lists values of λ calculated for some parameters of interest. For values of λ near one the hot plasma theory definitely becomes pertinent and thus applies to the conditions of this experimental investigation. Indeed, further analysis to be presented elsewhere by the authors shows that the finite Larmor radii effects are prominent and that propagation at harmonics of the ion cyclotron frequency is permitted for certain density ranges.

The higher order transverse mode structure can also explain the wave damping at harmonics of the ion cyclotron frequency. It is quite easy to show that single particles can be accelerated at harmonics of f_c provided there is a radial variation in E_θ. Fig. II-13 gives a simplified description of the particle acceleration for the case of an electric field which varies as exp $i(2\Omega_i t - k_\perp \cdot r)$. Consider that the particle is at location A at t = 0. The particle will then be accelerated along A - B, whereupon the field reverses. The particle is decelerated along B - C, accelerated along C - D and decelerated along D - A. The accelerations along A - B and C - D are obviously much larger than the decelerations along B - C and D - A because of the angle between the particle path and the accelerating field. The particle can thus gain energy per orbit from an E_θ field which varies at twice the cyclotron frequency. Different orbit center positions and random phase angles will influence the net energy gain per particle but it can be shown that, as in regular cyclotron heating, there is an average energy gain.

Ignore the curvature of the E_θ field across the particle orbit and assume that

$$E_\theta(r,t) = \mathcal{E} \sin(k_\perp r) \sin(G\Omega_i t) = \mathcal{E} \sin k_\perp (r_c + r_0 \sin\alpha) \sin(G\Omega_i t) \tag{II-11}$$

Table I - Hot Plasma Theory Expansion Parameter, λ .

(Deuterium Gas)

$n(m^{-3})$	$T_{\perp}$ (eV)	$k_{\parallel}$ (cm^{-1})	Ω_i/ω	$k_{\perp}^2$ (cm^{-2})	λ
6×10^{17}	50	0.392	1.19	233	4.2
6×10^{17}	50	0.392	1.09	104	1.9
6×10^{17}	50	0.392	1.05	55.9	1.0
6×10^{17}	50	0.392	1.01	9.3	0.17
6×10^{17}	50	0.196	1.19	56.6	1.0

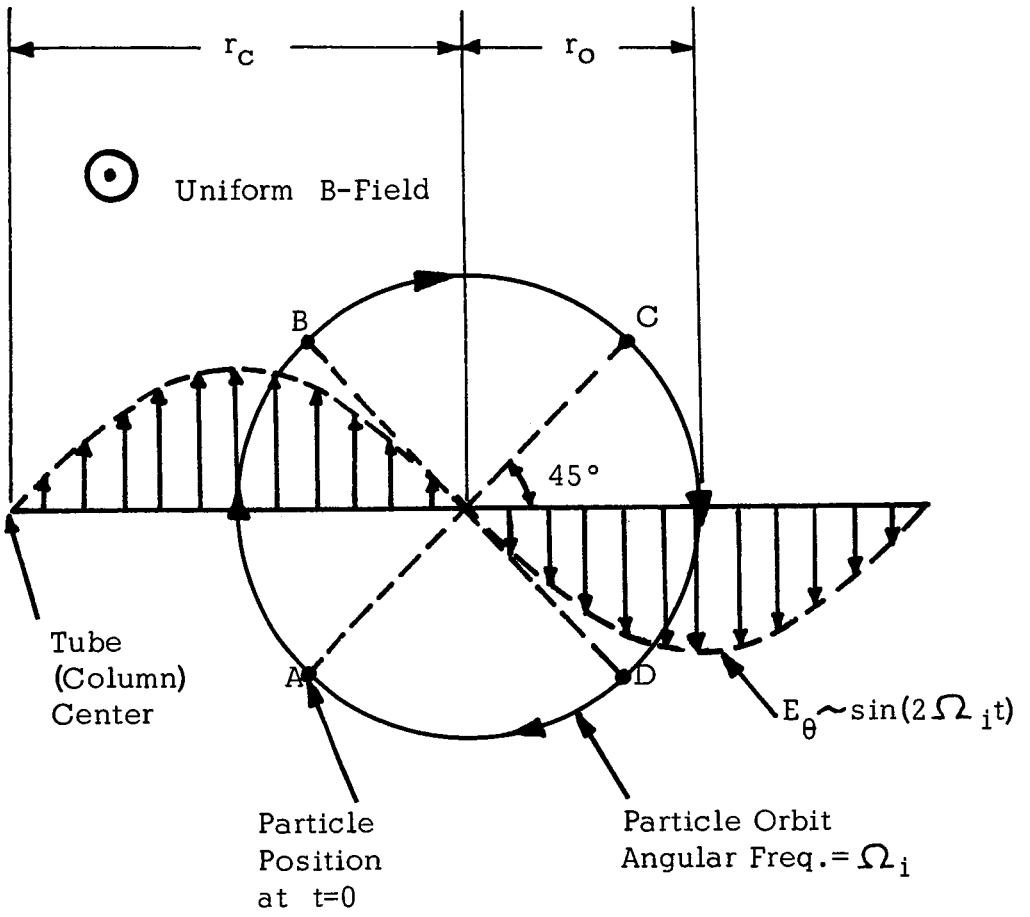

Fig. II-13. Single Particle Acceleration at the 2nd Harmonic of f_c.

The energy gain per orbit of the particle is

$$\Delta W = q_i \oint \vec{E} \cdot d\vec{s}$$

$$\approx q_i r_o \mathcal{E} \oint \sin[k_\perp(r_c + r_o \sin\alpha)] \sin G\alpha \sin[\alpha + \delta + \pi(G-1)/2G]\, d\alpha \qquad \text{(II-12)}$$

See Fig. II-14 for definition of the symbols. One has the relation

$$e^{-ix\sin\beta} = \sum_{n=-\infty}^{\infty} e^{-in\beta} J_n(x) \qquad \text{(II-13)}$$

The trigonometric functions in Eq.(II-12) can be expressed in exponential form and Eq.(II-13) substituted into Eq.(II-12). Upon performing the indicated integration, it is found that the energy gain per particle per orbit at the G'th harmonic of Ω_i is

$$\Delta W_{G(odd)} = q_i r_o \mathcal{E} \pi \sin(k_\perp r_c) \cos[\delta + \pi(G-1)/2G][J_{G-1}(k_\perp r_o) - J_{G+1}(k_\perp r_o)] \qquad \text{(II-14a)}$$

$$\Delta W_{G(even)} = q_i r_o \mathcal{E} \pi \cos(k_\perp r_c) \sin[\delta + \pi(G-1)/2G][J_{G-1}(k_\perp r_o) + J_{G+1}(k_\perp r_o)] \qquad \text{(II-14b)}$$

The error introduced by ignoring the field curvature is very apparent in Eq.(II-14b) which indicates that for even harmonics it should be possible to accelerate particles whose orbit center coincides with the plasma tube center. Eq.(II-14) is, however, only valid for $r_c > r_o$. For $r_c < r_o$ one should use the equation

$$\Delta W = q_i \mathcal{E} \oint r(\alpha) \sin[k_\perp(r_c + r_o(\alpha)\sin\alpha)] \sin G\alpha$$
$$\times \sin\left[\alpha + \delta + \pi(G-1)/2G + \arctan\frac{r_o(\alpha)\cos\alpha}{r_c + r_o(\alpha)\sin\alpha}\right] d\alpha \qquad \text{(II-15)}$$

The arctan term accounts for the field curvature and the indicated angular dependence of r_o shows that r_o should be continuously reevaluated as α changes. Eq.(II-15) has been evaluated on a digital computer for various typical parameter values and agrees quite well with Eq.(II-14) for $r_c > r_o$. ΔW is proportional to to $r_o(\alpha)$ and a random phase angle averaging will therefore show an average energy gain since an "in phase" particle will gain more energy per orbit than an

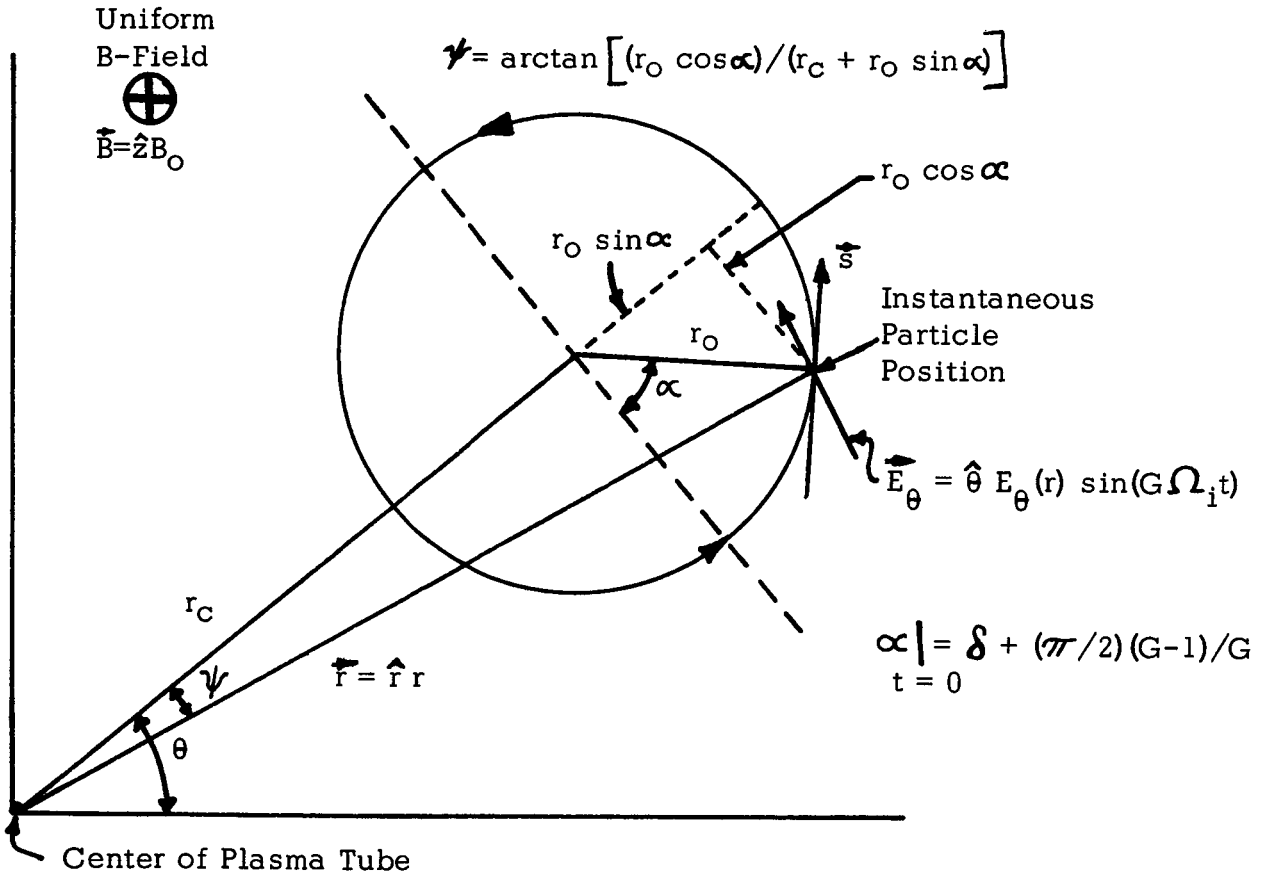

Fig. II-14. Single Particle Acceleration--Definition of Symbols.

"out of phase" particle will lose.

E. Conclusion

It has been shown experimentally that waves can propagate along the magnetic field near harmonics of the ion cyclotron frequency. These waves are shown to damp in a "magnetic beach" when $B \rightarrow B_c/G$. The wave damping leads to an enhanced transverse temperature-density product. Experimental and theoretical investigations indicate the existence of higher order transverse modes in this experimental arrangement. The observed phenomena are qualitatively explained in terms of finite Larmor radii, higher order transverse modes and finite temperature plasma theory.

III. THEORETICAL INVESTIGATIONS OF QUASI-STATIC ION WAVES AND WAVE ENERGY DENSITIES, Jimmy G. Melton and Professor Arwin A. Dougal

Theoretical investigations have been directed to two goals. The first is the development of a more complete picture of the types of quasistatic waves which could be present in the experimental plasma. This is necessary in order to positively identify the waves which have been observed experimentally. The second goal is to establish the theoretical basis necessary for an experimental measurement of the energy being carried by plasma waves. The experimental goal toward which this work is directed is a quantitative comparison of the plasma heating efficiencies of ion cyclotron waves and quasistatic ion cyclotron waves.

In Section III-A the class of quasistatic waves is investigated for frequencies in the region of the ion cyclotron frequency. The plasma considered is the hot, homogeneous, infinite plasma in a magnetic field, and has an isotropic Maxwellian velocity distribution. Special limiting cases are examined and the similarities and differences of these limiting cases are discussed.

In Section III-B a mathematical formalism for treating the energy flux and energy density of waves in a plasma is presented. The results were applied to the two waves of primary interest in order to obtain estimates of energy densities. The energy densities were found to be similar in magnitude and form, within the limits of the analysis.

A. Quasistatic Plasma Waves

If one considers only electrostatic type waves, i.e. waves with electric field $\vec{E}$ approximately parallel to the propagation vector $\vec{k}$, it is possible to greatly simplify the more general plasma dispersion relation. In general, electrostatic waves are those whose electric field can be derived from a scalar potential,

$$\vec{E} = -\nabla\phi = -i\vec{k}\phi \tag{III-1}$$

Thus $\vec{E}$ is parallel to $\vec{k}$ and the wave is longitudinal. To the extent that a wave is truly electrostatic, it has no associated magnetic field, or more exactly, no time-varying magnetic field. That this is the case may been seen immediately from

the more generally valid formulas,

$$\vec{E} = -\nabla\phi - \frac{1}{c}\frac{\partial\vec{A}}{\partial t}$$
$$\vec{B} = \nabla\times\vec{A} \qquad \text{(III-2)}$$

where $\vec{A}$ is the magnetic vector potential. Thus $\frac{\partial\vec{B}}{\partial t}$ for the wave is zero, and for many purposes $\vec{B}$ itself is zero. (CGS units are used throughout Sec. III.)

Before considering the quasistatic dispersion relation, we wish to determine conditions for which the quasistatic approximation may be used.[12] In general $\vec{E}$ can be decomposed into components parallel and perpendicular to the direction of propagation.

$$\vec{E} = \vec{E}_\perp + \vec{E}_\parallel$$
$$\vec{E}_\perp = -\frac{\vec{k}\times(\vec{k}\times\vec{E})}{k^2} \qquad \text{(III-3)}$$
$$\vec{E}_\parallel = \frac{\vec{k}(\vec{k}\cdot\vec{E})}{k^2}$$

The general dispersion relation for a wave in a plasma may be written as

$$\vec{k}\times(\vec{k}\times\vec{E}) + \frac{\omega^2}{c^2}\overleftrightarrow{K}\cdot\vec{E} = 0 \qquad \text{(III-4)}$$

where all information concerning the plasma appears in the dielectric tensor $\overleftrightarrow{K}$. Upon dotting with $\vec{k}$, the dispersion relation becomes

$$\frac{\omega^2}{c^2}\vec{k}\cdot\overleftrightarrow{K}\cdot\vec{E} = \frac{\omega^2}{c^2}\vec{k}\cdot\overleftrightarrow{K}\cdot(\vec{E}_\parallel + \vec{E}_\perp) = 0 \qquad \text{(III-5)}$$

If $\vec{E}$ is longitudinal and we have a longitudinal wave, i.e. $\vec{E}_\perp = 0$, then

$$\vec{k}\cdot\overleftrightarrow{K}\cdot\vec{k} = 0 \qquad \text{(III-6)}$$

which is the electrostatic dispersion relation.

If we now allow $\vec{E}$ to be approximately longitudinal, with

$$|\vec{E}_\parallel| \gg |\vec{E}_\perp| , \qquad \text{(III-7)}$$

we can derive a sufficiency condition. Write (III-4) in the form

$$\left[\frac{c^2}{\omega^2}k^2 - \overleftrightarrow{K}\cdot\right]\vec{E}_\perp = \overleftrightarrow{K}\cdot\vec{E}_\parallel \qquad \text{(III-8)}$$

and it is easy to see that

$$|k^2| \gg \frac{\omega^2}{c^2}\,|K_{ij}| \qquad \text{for all } i,j \qquad \text{(III-9}$$

is a sufficient condition for using the electrostatic relation. Eq.(III-9)is not a necessary condition, but if

$$\frac{\omega^2}{c^2}|K_{ij}| \gg k^2 \qquad \text{(III-10)}$$

then condition(III-7) is violated, and one may not consider the wave to be essentially electrostatic.

Using a quasistatic approximation, one may show that the small-signal dispersion relation for a hot, homogeneous, infinite, plasma in a magnetic field with an isotropic Maxwellian velocity distribution is [12]

$$k_\perp^2 + k_\parallel^2 + \sum_j \sum_{n=-\infty}^{+\infty} \frac{\omega_{pj}^2 m_j e^{-\lambda_j} I_n(\lambda_j)}{\kappa T_j}\left[1 + \frac{\omega}{k_\parallel v_j} Z\left(\frac{\omega + n\Omega_j}{k_\parallel v_j}\right)\right] = 0 \qquad \text{(III-11)}$$

where $k_\perp$ = propagation vector perpendicular to the static magnetic field B_o

$k_\parallel$ = parallel propagation vector

ω_{pj} = plasma frequency of jth plasma species

$= \dfrac{4\pi n_j Z^2 e^2}{m_j}$

λ_j = hot plasma expansion parameter for j^{th} species,

$= k_\perp^2 \kappa T_j / \Omega_j^2 m_j$

κ = Boltzmann's constant, 1.38×10^{-16} erg deg^{-1}

v_j = thermal velocity of jth species

$$= (2\,\kappa\, T_j/m_j)^{1/2}$$

Ω_j = cyclotron frequency of jth species

$$= \left| \frac{Z e B_o}{m_j c} \right|$$

$I_n(\lambda_j)$ is the modified Bessel function of complex argument. In the notation of G.N. Watson,[20] $Z(\zeta_n)$ is the plasma dispersion function tabulated by Fried and Conte,[23] and

$$\zeta_n = \frac{\omega + n\Omega_j}{k_\parallel v_j}$$

It should be noted that the dispersion relation contains terms $k_\perp^{\ 2}$ hidden in the λ's in the summation terms.

One may proceed by considering special cases of Eq.(III-11). For the n = 0 terms in the sum, use the identity

$$1 + \zeta_o Z(\zeta_o) = -\frac{1}{2} Z'(\zeta_o) \tag{III-12}$$

to obtain

$$1 + \frac{\omega}{k_\parallel v_j} Z\left(\frac{\omega}{k_\parallel v_j}\right) = -\frac{1}{2} Z'\left(\frac{\omega}{k_\parallel v_j}\right). \tag{III-13}$$

For large arguments, the $Z(\zeta_n)$ may be approximated by

$$Z(\zeta_n) \approx i\pi^{1/2}\sigma \exp(-\zeta_n^2) - \zeta_n^{-1}\left[1 + \frac{1}{2\zeta_n^2} + \cdots\cdots\right]$$

$$\sigma = \left\{\begin{array}{ll} 0 & \text{if } \mathrm{Im}\{\zeta_n\} > 0 \text{ (growing wave)} \\ 1 & \text{if } \mathrm{Im}\{\zeta_n\} = 0 \\ 2 & \text{if } \mathrm{Im}\{\zeta_n\} < 0 \text{ (damping wave)} \end{array}\right\} \zeta_n \text{ large.} \tag{III-14}$$

For small arguments, $Z(\zeta_n)$ is given by

$$Z(\zeta_n) = i\pi^{1/2}\exp(-\zeta_n^2) - 2\zeta_n\left[1 - \frac{2\zeta_n^2}{3} + \cdots\right] \qquad \text{(III-15)}$$

The special cases to be considered are those which are easily accessible via the asymptotic and power series expansions. One can thus derive a number of waves which are enough alike with regard to the conditions for propagation that one might expect to see any or all of these waves for a given small range of experimental conditions. By means of such analysis, one can hope to establish means of experimentally resolving two or more wave modes. Damping effects will be neglected for simplicity.

1. Ion Acoustic and Electrostatic Ion Cyclotron Waves

The assumptions appropriate to these waves are that the electron and ion temperatures are different and that the wave phase velocity parallel to the field is greater than the ion thermal velocity but less than the electron thermal velocity. Under these assumptions, the power series for the n = 0 ion Z-function are the appropriate approximations. By neglecting the effects of cyclotron damping, i.e.

$$\left|\frac{\omega + n\Omega_j}{k_{\parallel} v_j}\right| \gg 1 \qquad \text{for } |n| \geq 1$$

the terms for $n \neq 0$ in the summation can be approximated by taking

$$Z(\zeta) \approx -\frac{1}{\zeta}$$

to give

$$1 + \frac{\omega}{k_{\parallel} v_j} Z\left(\frac{\omega + n\Omega_j}{k_{\parallel} v_j}\right) \approx 1 - \frac{\omega}{\omega + n\Omega_j} = \frac{n\Omega_j}{\omega + n\Omega_j}$$

The n = 0 terms are approximated by

$$1 + \frac{\omega}{k_{\parallel} v_j} Z\left(\frac{\omega}{k_{\parallel} v_j}\right) \approx -\frac{1}{2}\left(\frac{k_{\parallel}^2 v_j^2}{\omega^2}\right) \qquad \text{for ions (i.e. } \zeta_0 \text{ large)}$$

$$\approx 1 \qquad \text{for electrons (i.e. } \zeta_0 \text{ small) (damping term neglected).}$$

The dispersion relation reduces to

$$k_\perp^2 + k_\parallel^2\left[1 - \frac{\omega_{pi}^2}{\omega^2} I_0(\lambda_i) e^{-\lambda_i}\right] + \frac{\omega_{pe}^2 m_e}{\kappa T_e} I_0(\lambda_e) e^{-\lambda_e}$$
$$+ \left[\frac{2m_i \omega_{pi}^2}{\kappa T_i} \sum_{n=1}^{\infty} \frac{e^{-\lambda_i} I_n(\lambda_i)}{1 - \left(\frac{\omega}{n\Omega_i}\right)^2} + \frac{2 m_e \omega_{pe}^2}{\kappa T_e} \sum_{n=1}^{\infty} \frac{e^{-\lambda_e} I_n(\lambda_e)}{1 - \left(\frac{\omega}{n\Omega_e}\right)^2}\right] = 0 \qquad \text{(III-16)}$$

where the terms for $\pm$ n have been combined in the series.

By assuming λ small for both ions and electrons, for the sake of further analytical reduction, one may expand

$$e^{-\lambda} I_n(\lambda) \approx \frac{1}{n!}\left(\frac{\lambda}{2}\right)^n + \cdots \quad , \quad \lambda \ll 1$$
$$e^{-\lambda_i} I_0(\lambda_i) \approx 1 + \left(\frac{\lambda}{2}\right)^0 + \cdots \text{ etc.} \qquad \text{(III-17)}$$

With this additional simplification, Eq. III-16 becomes

$$k_\perp^2\left[1 + \frac{\omega_{pi}^2}{\Omega_i^2 - \omega^2} + \frac{\omega_{pe}^2}{\Omega_e^2 - \omega^2}\right] + k_\parallel^2\left[1 - \frac{\omega_{pi}^2}{\omega^2}\right]$$
$$+ \frac{k_\perp^2 \omega_{pi}^2 k_\parallel^2 \bar{V}_i^2}{4\omega^2 \Omega_i^2} + \frac{1}{\lambda_D^2} = 0 \qquad \text{(III-18)}$$

where λ_D is the electron Debye length. This is recognized as the dispersion relation for ion acoustic and electrostatic ion cyclotron waves. The $k_\parallel^2$ terms correspond roughly to ion acoustic propagation, while the $k_\perp^2$ terms correspond to electrostatic ion cyclotron waves.

For fixed angle of propagation with respect to the field, i.e. fixed ratio $k_\parallel^2 : k_\perp^2$, one can plot dispersion curves to describe the waves. This is done in Fig. III-1 for three different angles. Electron cyclotron effects have been neglected and ω_{pi} has been assumed to be greater than Ω_i. The same thing has been plotted in Fig. III-2, but for $\Omega_i > \omega_{pi}$. It should be noted that at each of the resonances the analysis breaks down. The power series expansion for small λ Eq.(III-17) was used to obtain Eq.(III-18). As $k_\perp \to \infty$, this is no longer correct except in the limit of no magnetic field.

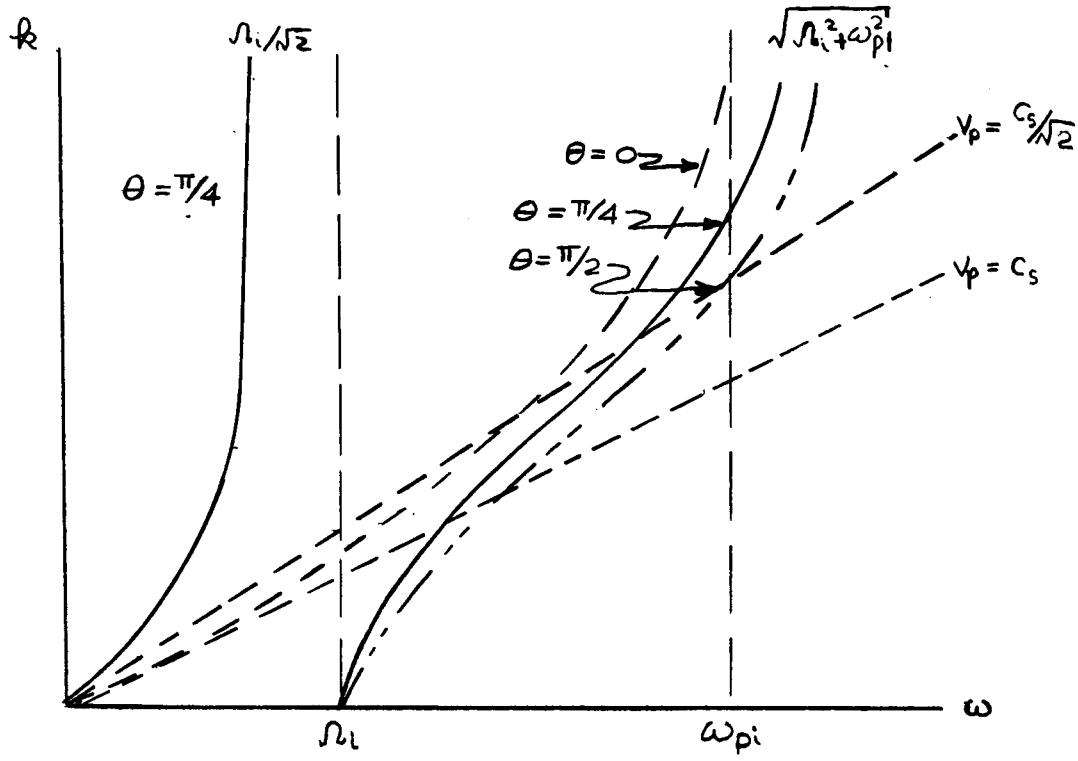

Fig. III-1. Ion Acoustic and Electrostatic Ion Cyclotron Modes for $\Omega_i < \omega_{pi}$

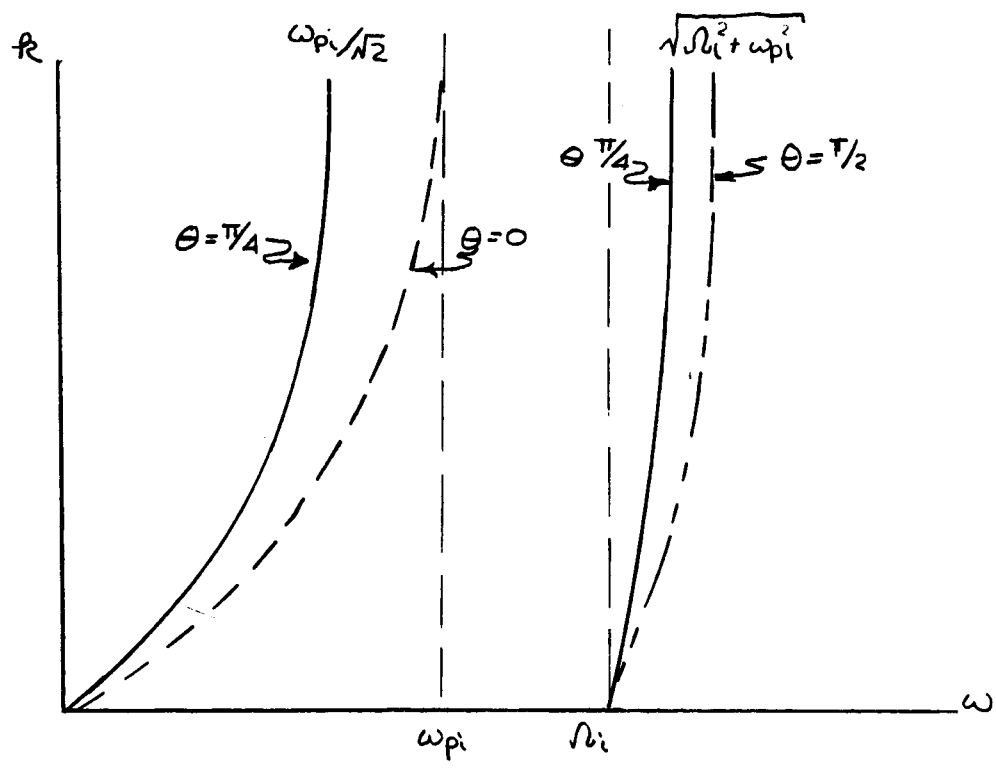

Fig. III-2. Ion Acoustic and Electrostatic Ion Cyclotron Modes for $\omega_{pi} < \Omega_i$

2. Quasistatic Ion Cyclotron Modes and Bernstein Modes for Ions

If the wave phase velocity parallel to the magnetic field is greater than the thermal velocity of both the electrons and the ions, the treatment is the same, until the expansion to obtain Eq.(III-16). Then the n = 0 term for electrons is expanded as an asymptotic series rather than a power series (i.e. large argument expansion is taken rather than small argument.) For this case, the equation corresponding to Eq.(III-16) is

$$k_\perp^2 + k_\parallel^2 \left[1 - \frac{\omega_{pi}^2}{\omega^2} I_0(\lambda_i) e^{-\lambda_i} - \frac{\omega_{pe}^2}{\omega^2}\right]$$

$$+ \left[\frac{2 m_i \omega_{pi}^2}{\kappa T_i} \sum_{n=1}^{\infty} \frac{e^{-\lambda_i} I_n(\lambda_i)}{1 - \left(\frac{\omega}{n\Omega_i}\right)^2} + \frac{2 m_e \omega_{pe}^2}{\kappa T_e} \sum_{n=1}^{\infty} \frac{e^{-\lambda_e} I_n(\lambda_e)}{1 - \left(\frac{\omega}{n\Omega_e}\right)^2}\right] = 0 \qquad \text{(III-19)}$$

Then expanding for λ small results in an equation corresponding to Eq.(III-18)

$$k_\perp^2 \left[1 + \frac{\omega_{pi}^2}{\Omega_i^2 - \omega^2} + \frac{\omega_{pe}^2}{\Omega_e^2 - \omega^2}\right] + k_\parallel^2 \left[1 - \frac{\omega_{pi}^2}{\omega^2} - \frac{\omega_{pe}^2}{\omega^2}\right] = 0 \qquad \text{(III-20)}$$

From Eq.(III-19) several different plasma modes can be deduced. The difference between these modes are to some extent artificial. However, these modes have appeared in the literature and names have been assigned to them, so that we have attempted to label these modes in what follows in keeping with the convention.

If $k_\parallel$ is taken to be zero in Eq.(III-19), one may derive the Bernstein modes,[24]

$$k_\perp^2 = \sum_j \frac{\omega_{pj}^2 m_j}{\kappa T_j} \alpha(q, \lambda)$$

where

$$\alpha(q,\lambda) = -2 \sum_{n=1}^{\infty} e^{-\lambda} I_n(\lambda) \frac{n^2}{n^2 - q^2}, \qquad \text{(III-21)}$$

and

$$q = \omega / \Omega .$$

Solutions for real $k_\perp$ appear whenever $\sum_j \alpha(g,\lambda)$ is positive. By considering frequencies in the neighborhood of one of the cyclotron frequencies, one can plot the appropriate $\alpha(g,\lambda)$, as in Fig. III-3. Thus propagation is allowed on the high side of each $\omega = n\Omega_j$ asymptote, and the various harmonics are separated by stop bands, where propagation cannot occur.

By allowing $k_\parallel \neq 0$, one may deduce the quasistatic ion cyclotron waves investigated by Swanson.[7,8] In the case of $\lambda_e \ll 1$, the relevant approximation is

$$k_\parallel^2 = -\frac{m_e\omega^2}{\kappa T_i}\left[\sum_{n=1}^{\infty} \alpha(g_i, \lambda_i)\right], \tag{III-22}$$

$$= \frac{2m_e\omega^2}{\kappa T_i}\sum_{n=1}^{\infty}\frac{e^{-\lambda_i} I_n(\lambda_i)}{1-\left(\frac{\omega}{n\Omega_i}\right)^2} .$$

These waves are plotted in Fig. III-4. Comparing (III-22) with (III-21) brings out the very similar forms of these two waves. Comparing Figs. III-3 and III-4 shows their apparent differences.

The similarities and differences of these various plasma modes can be easily seen from the figures. Each of the waves exhibits a resonance condition somewhere near the ion cyclotron frequency. Although the curves for the ion acoustic mode (Figs. III-1, III-2), do not show resonances at the harmonics of the ion cyclotron frequency, this is because the series summations were truncated before these terms appear. The terms necessary for harmonic resonances are present in Eq. (III-16) and would have appeared had the next higher order terms in λ been included. Another feature of similarity is that each of the waves exhibits a band gap.

The differences are more important, since they offer means of differentiating between the modes. The ion acoustic modes shows resonant behavior near the ion plasma frequency. Both the ion acoustic and the Bernstein modes are density dependent, whereas the quasistatic ion cyclotron waves are independent of density. The Bernstein modes exhibit perpendicular propagation <u>above</u> the cyclotron harmonics, and the quasistatic ion cyclotron waves exhibit parallel propagation <u>below</u> the cyclotron harmonics.

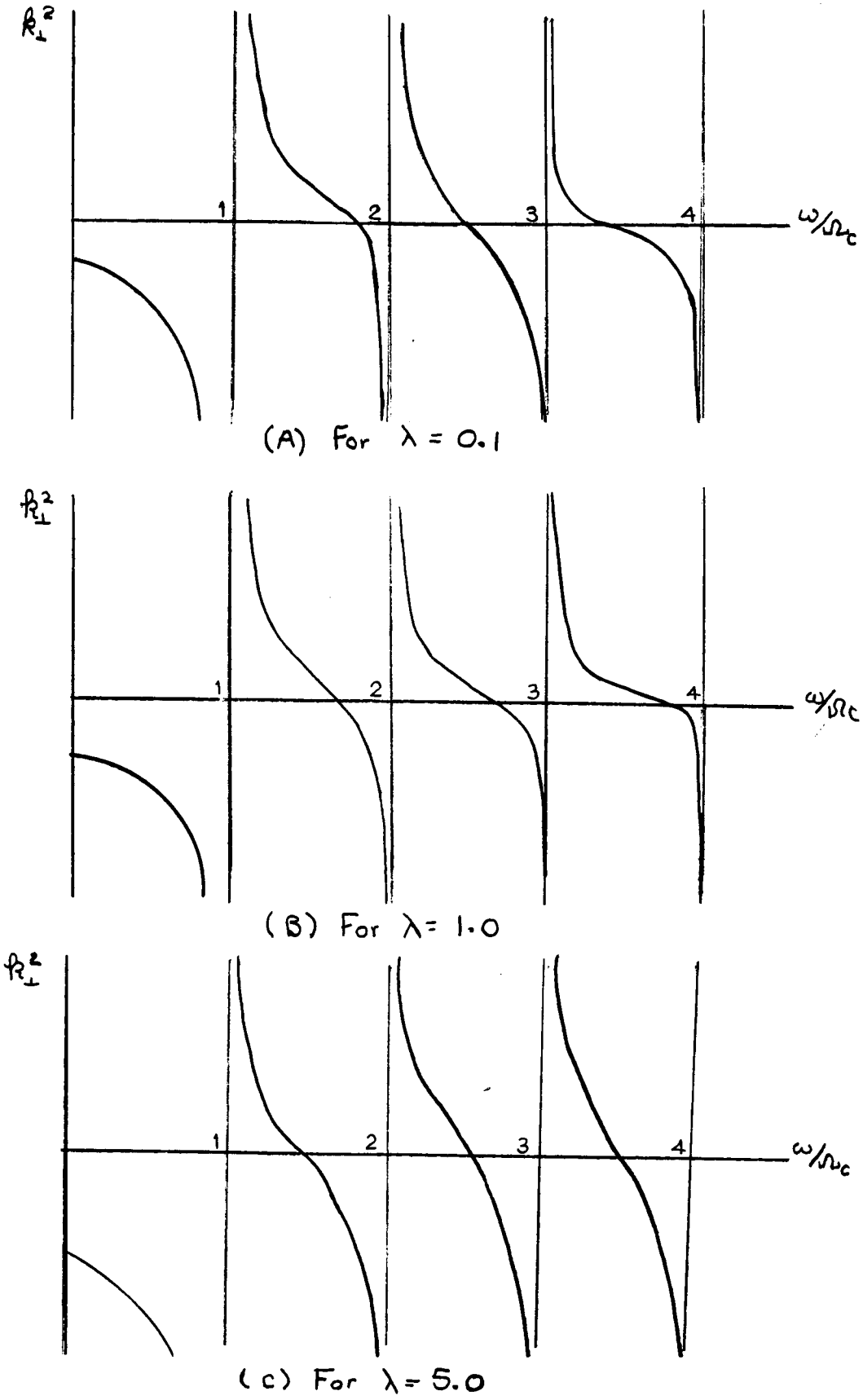

Fig. III-3. Electrostatic "Bernstein" Ion Cyclotron Modes

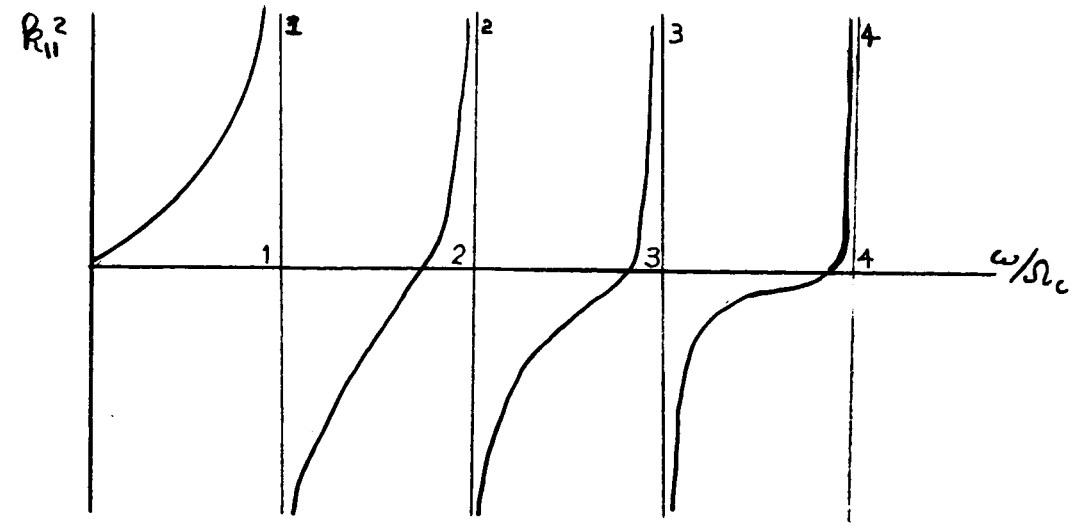

(A) $\lambda = 0.1$

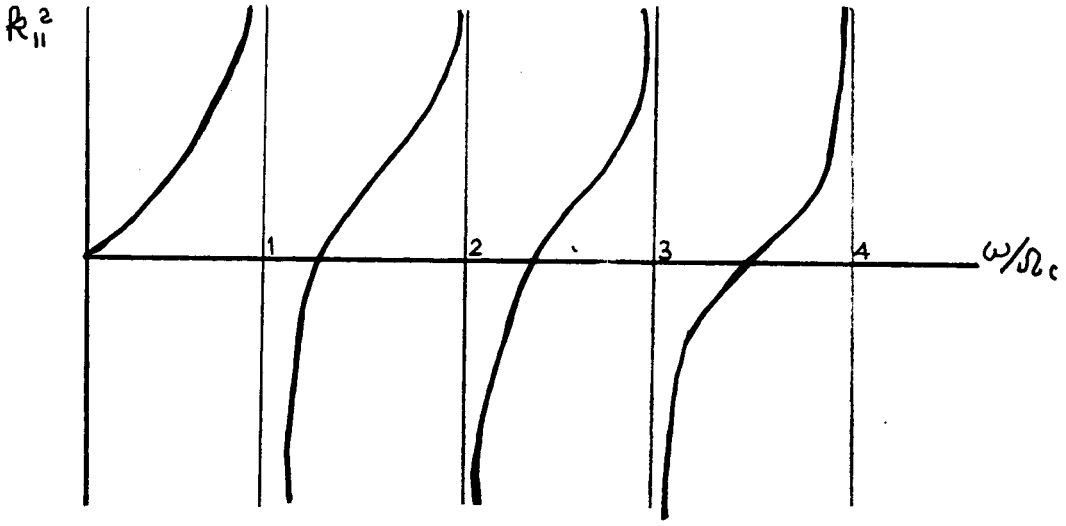

(B) $\lambda = 1.0$

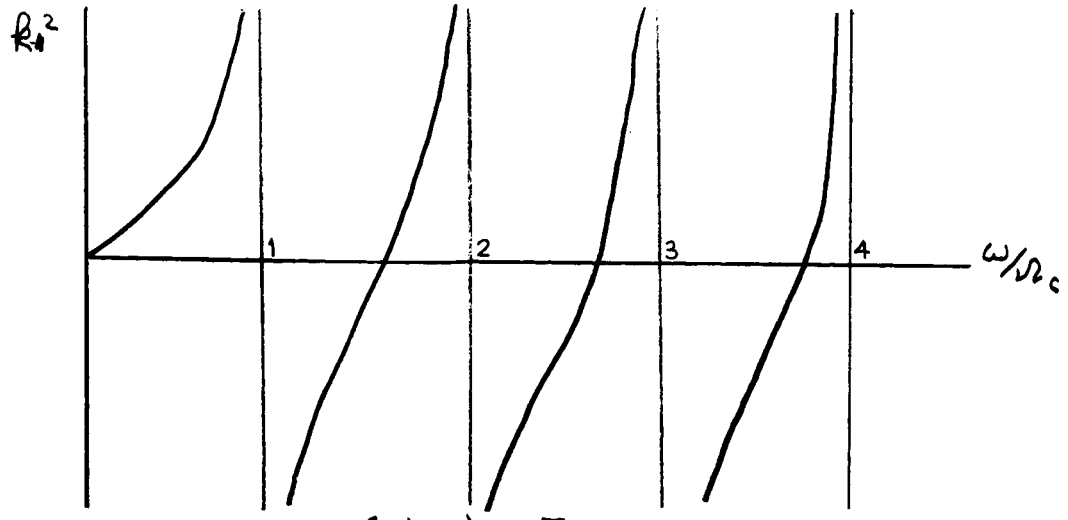

(C) $\lambda = 5.0$

Fig. III-4. Quasistatic Ion Cyclotron Modes

It should be expected that in a physical plasma the distinction between the various modes will not be nearly as distinct as it appears in theory. However, the differences should be sufficient to determine which is the dominant laboratory mode.

B. Energy Content of Waves

1. General Considerations

In order to compare the heating efficiences of ion cyclotron waves and quasi-static ion cyclotron waves, it is desirable to examine theoretically the energy content and transport by the waves. This problem can be approached through Poynting's Theorem which states

$$\nabla \cdot \vec{P} + \frac{\partial W}{\partial t} = 0 \qquad \text{(III-23)}$$

where $\vec{P}$ is Poynting's vector for the wave, representing the flux of energy, and W is the energy density for the wave.

Poynting's Theorem for electromagnetic waves in vacuum can be generalized to a plasma in a magnetic field. Quite general conditions could be considered, such as an inhomogeneous and dissipative plasma which is slowly time-varying. This section will consider only plasmas which are dispersive and anisotropic, but we will include nonelectromagnetic (i.e. kinetic) energy, which is necessary for a hot plasma.

We follow the development of Stix,[12] considering the tensor defined by the relation

$$\overleftrightarrow{G} \cdot \vec{E} = \frac{c^2}{16\pi\omega} \vec{k} \times (\vec{k} \times \vec{E}) + \frac{\omega}{16\pi} \overleftrightarrow{K} \cdot \vec{E} \qquad \text{(III-24)}$$

Equation III-24 is very similar to the wave equation Eq. (III-4), and in fact

$$\overleftrightarrow{G} \cdot \vec{E} = 0 \qquad \text{(III-25)}$$

follows directly from the wave equation. If we allow small changes to occur in the plasma parameters and in ω and $\vec{k}$, a new wave equation may be written

$$\overleftrightarrow{G}_1 \cdot \vec{E}_1 = 0 \tag{III-26}$$

where

$$\overleftrightarrow{G}_1 = \overleftrightarrow{G} + \delta\omega \frac{\partial \overleftrightarrow{G}}{\partial \omega} + \delta\vec{k} \cdot \frac{\partial \overleftrightarrow{G}}{\partial \vec{k}} + \delta\overleftrightarrow{G} . \tag{III-27}$$

For real $\vec{k}$ and ω, $\overleftrightarrow{G}$ is Hermitian, and (III-25) may be written

$$\vec{E}^* \cdot \overleftrightarrow{G}^{+} = \vec{E}^* \cdot \overleftrightarrow{G} = 0 \tag{III-28}$$

Now dotting (III-28) into $\vec{E}$, and $\vec{E}^*$ into (III-26) obtains upon subtraction

$$\vec{E}^* \cdot \left(\delta\omega \frac{\partial \overleftrightarrow{G}}{\partial \omega} + \delta\vec{k} \cdot \frac{\partial \overleftrightarrow{G}}{\partial \vec{k}} + \delta\overleftrightarrow{G} \right) \cdot \vec{E}_1 = 0. \tag{III-29}$$

Evaluating each term in this product leads to

$$\vec{E}^* \cdot \frac{\partial \overleftrightarrow{G}}{\partial \omega} \cdot \vec{E} = \frac{1}{16\pi} \left[\vec{B}^* \cdot \vec{B} + \vec{E}^* \cdot \frac{\partial}{\partial \omega} \left\{ (\omega \overleftrightarrow{K}) \cdot \vec{E} \right\} \right] \tag{III-30}$$

$$\vec{E}^* \cdot \frac{\partial \overleftrightarrow{G}}{\partial \omega} \cdot \vec{E} = -\frac{c}{16\pi} \left(\vec{E}^* \times \vec{B} + \vec{E} \times \vec{B}^* \right) + \frac{\omega}{16\pi} \vec{E}^* \cdot \frac{\partial \overleftrightarrow{K}}{\partial \vec{k}} \cdot \vec{E} \tag{III-31}$$

Equation (III-30) may be written as

$$\vec{E}^* \cdot \frac{\partial \overleftrightarrow{G}}{\partial \omega} \cdot \vec{E} = \frac{1}{16\pi} \left[\vec{E}^* \cdot \overleftrightarrow{K} \cdot E + \vec{B}^* \cdot \vec{B} \right] + \frac{\omega}{16\pi} \vec{E}^* \cdot \frac{\partial \overleftrightarrow{K}}{\partial \omega} \cdot \vec{E} \quad . \tag{III-32}$$

The first term, containing the brackets, is just the sum of electric and magnetic energy densities for a wave in a medium characterized by dielectric tensor $\overleftrightarrow{K}$. The second term is the energy density due to the dispersive nature of the medium. In a plasma, we can associate this term with the density of ordered charged-particle kinetic energy. Consequently we can identify Eq. (III-32) with the total

energy density, that is, wave energy plus ordered particle energy,

$$W = \vec{E}^* \cdot \frac{\partial \overleftrightarrow{G}}{\partial \omega} \cdot \vec{E} \tag{III-33}$$

Similarly, in Eq. (III-31), the first term is just the electromagnetic Poynting vector, and the second term represents the energy flux due to ordered particle motion, such that

$$\vec{P} = \frac{c}{16\pi}\left(\vec{E}^* \times \vec{B} + \vec{E} \times \vec{B}^*\right),$$

$$\vec{T} = -\frac{\omega}{16\pi}\vec{E}^* \cdot \frac{\partial \overleftrightarrow{K}}{\partial \vec{k}} \cdot \vec{E} \quad ,$$

and

$$\vec{P} + \vec{T} = -\vec{E}^* \cdot \frac{\partial \overleftrightarrow{G}}{\partial \vec{k}} \cdot \vec{E} \quad . \tag{III-34}$$

We note that in a cold plasma, the dielectric tensor elements are idependent of $\vec{k}$, so that $\frac{\partial \overleftrightarrow{K}}{\partial \vec{k}} = 0$. That is, in a cold plasma there is no energy flux due to particle motion. However, for the cold plasma $\frac{\partial \overleftrightarrow{K}}{\partial \omega} \neq 0$, such that the wave does contain some energy due to particle motion. Thus the energy of ordered particle motion in a cold plasma does not propagate, and energy transport is due to the electromagnetic waves.

We also note that for the hot plasma, the energy flux due to ordered particle motion must be included to satisfy Poynting's Theorem. In the hot plasma the elements of $\overleftrightarrow{K}$ are not in general independent of $\vec{k}$.

The derivation of Eqs. (III-30) and (III-31) and the association between the various terms and the energies they represent can be performed more rigorously by starting from a study of the particle motions. This is done in Ref. 26.

2. Energy Densities of Ion Cyclotron Waves

Equations (III-30, 32, 33) may be used to calculate the energy density for ion cyclotron and quasistatic ion cyclotron waves. Since the main question is the

ability of these waves to transport energy, the real quantity of interest is the energy flux $\vec{P} + \vec{T}$. However, in the cold plasma, $\vec{T} = 0$, such that there is no particle energy flux, and for the hot plasma, the quantity $\frac{\partial \overleftrightarrow{K}}{\partial \vec{k}}$ must be evaluated, which can be quite complicated. For the purposes of discussion, we will circumvent the second difficulty by calculating the energy density W, and then using the relation

$$\vec{P} + \vec{T} = W \vec{v}_g$$

where $\vec{v}_g$ is the group velocity for the wave, to obtain an estimate of the energy carrying capabilities for the two waves.

For simplicity, only the cold plasma will be considered here. The cold plasma dielectric tensor is given by

$$\overleftrightarrow{K} = \begin{pmatrix} 1-\sum_j \frac{\omega_{pj}^2}{\omega^2-\Omega_j^2} & -i\sum_j \frac{\Omega_j \omega_{pj}^2}{\omega(\omega^2-\Omega_j^2)} & 0 \\ i\sum_j \frac{\Omega_j \omega_{pj}^2}{\omega(\omega^2-\Omega_j^2)} & 1-\sum_j \frac{\omega_{pj}^2}{\omega^2-\Omega_j^2} & 0 \\ 0 & 0 & 1-\sum_j \frac{\omega_{pj}^2}{\omega^2} \end{pmatrix} \qquad \text{(III-35)}$$

The quantities we wish to complete are $\vec{E}^* \cdot \overleftrightarrow{K} \cdot \vec{E}$ and $\vec{E}^* \cdot \left(\omega \frac{\partial \overleftrightarrow{K}}{\partial \omega}\right) \cdot \vec{E}$. For ion cyclotron waves, propagating in the Z-direction along the field, the ratio of the transverse fields is[12]

$$\frac{iE_r}{E_\theta} = \frac{\omega^3/\Omega_i^3}{\frac{k_\parallel^2 c^2}{\omega_{pi}^2}\left(\frac{\omega^2}{\Omega_i^2}-1\right)+\frac{\omega^2}{\Omega_i^2}} \qquad \text{(III-36)}$$

The wave is in general elliptically polarized, but as $\omega \to \Omega_i$, the ratio $\frac{iE_r}{E_\theta} \to 0$, that is the field becomes predominantly azimuthal. So we take

$$\vec{E} = (0, E_\theta, E_z)$$

including E_z just for completeness. Then we have

$$\left[\omega \frac{\partial K}{\partial \omega}\right]_{11} = \left[\omega \frac{\partial K}{\partial \omega}\right]_{22} = \sum_j \frac{2\omega^2 \omega_{pj}^2}{(\omega^2-\Omega_j^2)^2}$$

$$\left[\omega \frac{\partial K}{\partial \omega}\right]_{12} = -\left[\omega \frac{\partial K}{\partial \omega}\right]_{21} = i \sum_j \left\{ \frac{\Omega_j \omega_{pj}^2}{\omega(\omega^2 - \Omega_j^2)} + \frac{2\omega\omega_{pj}^2 \Omega_j}{(\omega^2 - \Omega_j^2)^2} \right\}$$

$$\left[\omega \frac{\partial K}{\partial \omega}\right]_{33} = \sum_j \frac{2\omega_{pj}^2}{\omega^2} \tag{III-37}$$

Now form the dot product in two parts:

$$\vec{E}^* \cdot \overleftrightarrow{K} \cdot \vec{E} = \left(1 - \sum_j \frac{\omega_{pj}^2}{\omega^2 - \Omega_j^2}\right) E_\theta^* E_\theta + \left(1 - \sum_j \frac{\omega_{pj}^2}{\omega^2}\right) E_z^* E_z \,, \tag{III-38}$$

and

$$\vec{E}^* \cdot \left(\omega \frac{\partial \overleftrightarrow{K}}{\partial \omega}\right) \cdot \vec{E} = \left(\sum_j \frac{2\omega^2 \omega_{pj}^2}{(\omega^2 - \Omega_j^2)^2}\right) E_\theta^* E_\theta + \left(\sum_j \frac{2\omega_{pj}^2}{\omega^2}\right) E_z^* E_z \,. \tag{III-39}$$

The first term represents "electrostatic" energy density of the wave. The second term represents the particle motion energy density. Completing the expression, the total energy density is

$$W_1 = \frac{1}{16\pi}\left[\vec{B}^* \cdot \vec{B} + \left(1 + \sum_j \frac{\omega_{pj}^2(\omega^2 + \Omega_j^2)}{(\omega^2 - \Omega_j^2)^2}\right) E_\theta^* E_\theta + \left(1 + \sum_j \frac{\omega_{pj}^2}{\omega^2}\right) E_z^* E_z\right] \tag{III-40}$$

Similarly the energy density for electrostatic ion cyclotron waves may be computed. Assume $E_\theta = 0$, then

$$W_2 = \frac{1}{16\pi}\left[\left(1 + \sum_j \frac{\omega_{pj}^2(\omega^2 + \Omega_j^2)}{(\omega^2 - \Omega_j^2)^2}\right) E_r^* E_r + \left(1 + \sum_j \frac{\omega_{pj}^2}{\omega^2}\right) E_z^* E_z\right] . \tag{III-41}$$

The energy densities for these two waves are just the same, except of course, the electrostatic wave has no magnetic field energy density. However, one thing should be pointed out. In the expression for the quasistatic waves, Eq.(III-22), it is seen that the waves are independent of density. Consequently, at least in theory, quasistatic ion cyclotron waves may be used to heat much denser plasmas than ion cyclotron waves.[7,8] In such a case, there is no factor entering into

Eq. (III-41) which suggests any sort of limit on this increase in performance.

A complete analysis of this point should include the hot plasma effects. Since the "energy content" of the two waves is about the same, the efficiency for heating will be determined by any of three things; (1) the hot plasma propagation, i.e. the group velocities, (2) the efficiency of coupling the waves to the plasma, and (3) the relative efficiencies of the damping mechanisms. Investigations are being continued into this point.

C. Continuation of this Theoretical Work

The results in Sec. III-A for the various quasistatic waves were obtained for the assumption of no damping. The analysis will be expanded to include the effects of damping and to include intermediate values of λ in the series expansions.

The results in Sec. III-B for wave energy density were obtained using the cold plasma dielectric tensor. A similar analysis will be performed using the appropriate hot plasma dielectric tensor elements in order to include the contributions from particle energy to the total energy flux.

It would be desirable to obtain experimental measurements of the energy being transported by the waves. It was mentioned in Sec. III-A that purely electrostatic modes are not accompanied by a changing magnetic field, such that magnetic probes could not be used to study such waves. However, if the waves are only approximately electrostatic, i.e. quasistatic, there is a small associated magnetic field which could be measured and related to wave energy. Analysis of the field components for quasistatic waves is underway in order to establish a theoretical basis for such wave energy measurements.

IV. EXPERIMENTAL FACILITIES, Jimmy G. Melton and Nathan B. Dodge (Professor Arwin A. Dougal)

During the period covered by this report, several additions and improvements have been made to the experimental facilities which were described in Sec. II-B. The improvements include (1) the addition of an 8-mm wave interferometer for electron density measurements; (2) the addition of a screen room for reduced noise pick-up; (3) the addition of remote control facilities for the probe carriage and the magnetic power supply, so that these units can be controlled from within the screen room; (4) the design of a reflex P.I.G discharge assembly, to be investigated for its preionization capabilities; (5) the design and construction of a new shielded-Stix coil arrangement, for better shielding of the wave-field components which are impressed on the plasma column; and (6) the addition of a spectrum analyzer oscilloscope plug-in unit to provide information on the frequency spectrum of the waves in the plasma.

In this chapter the equipment is discussed according to the particular phase of the experiment involved. The Sections are (A) preparation and confinement, including preionization and measurements of plasma density, (B) wave coupling to the plasma column, and (C) propagation and damping of the waves. The spectrum analysis equipment is described in Sec. V-B, along with experimental observations of nonlinear wave phenomena.

A. Preionization Equipment and Microwave Interferometer

The preionization equipment which have been used previously consist of several combinations of rf drivers, oscillators, and amplifiers. The two units usually used are 1) a 40-kw oscillator, at a frequency between 15 and 25 MHz, with a variable plate voltage supply, and 2) a 1-kw, 21.3 MHz driver-amplifier combination. The second unit is most often used.

In addition, a third unit was added to the facilities. This consists of a 250 watt exciter of variable frequency and a 1 - kw linear amplifier with variable plate voltage. Since the characteristics of rf induced plasma discharges depend quite strongly on the frequency and voltage used, this

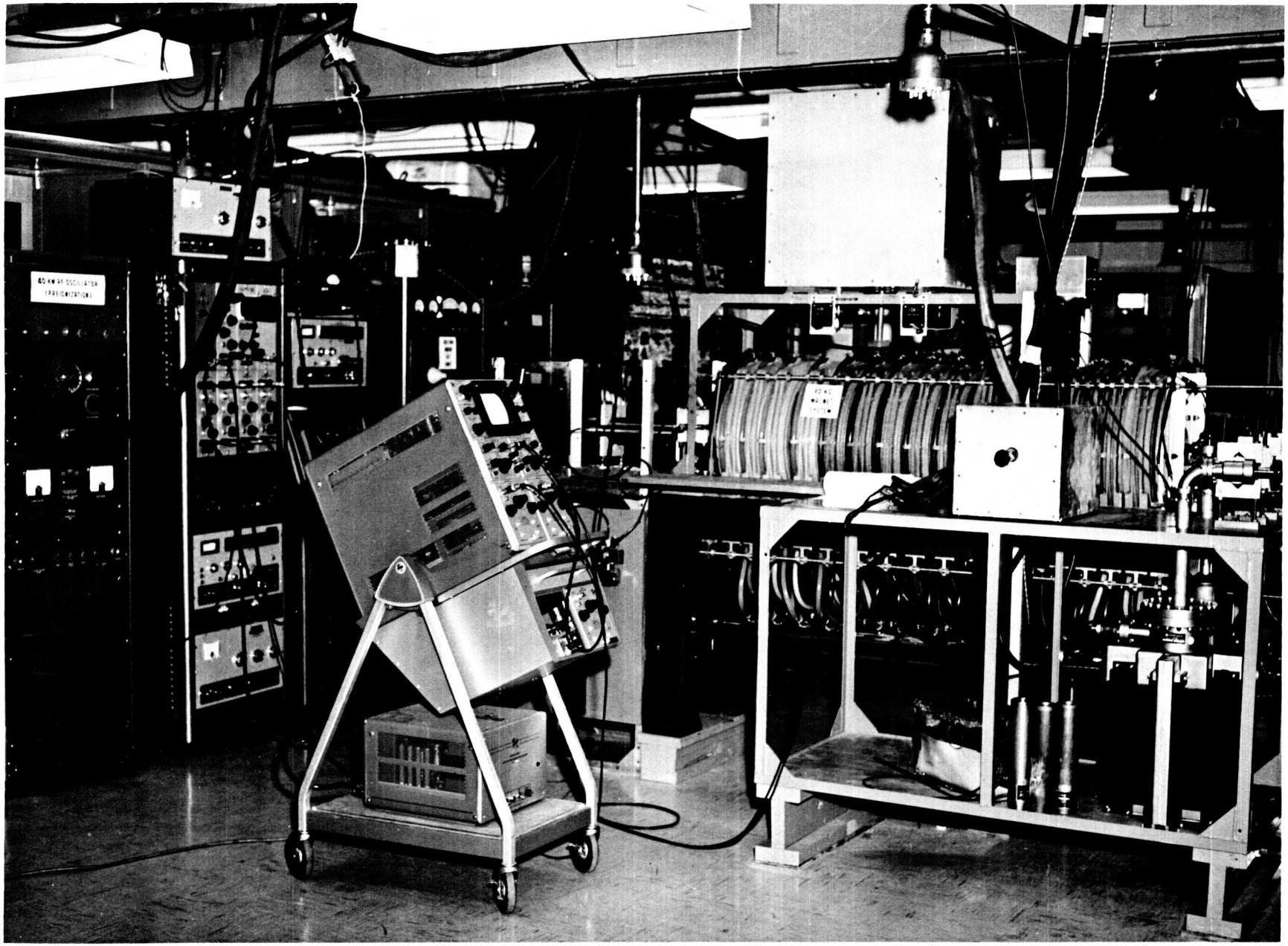

Fig. IV-1. Photograph of Experimental Facilities.

unit can be used to study the rf preionization phase of the experiment, and to determine whether rf preionization is flexible and dependable enough for the studies planned for the future.

In order to have some means of preionization available other than rf discharges, a reflex P.I.G. discharge arrangement[27] was designed for installation on the main experiment. Shown in Fig. IV-2, it consists of an anode-cathode pair at each end of the discharge tube. Both anodes are hollow ring assemblies and are held at ground potential. One cathode is simply a hollow plate, to allow the insertion of probes through one end of the tube. The other cathode is a heated tungsten filament. Both cathodes are pulsed to negative high voltage to establish the discharge.

Similar reflex P.I.G. discharges are known to yield high fractional ionizations in the pressure region of interest.[27] It is expected that the addition of this preionization arrangement will permit a wider range of operation conditions and greater flexibility in choosing plasma parameters.

In Semiannual Status Report No. 7,[4] the plasma density, as measured by a 4-mm microwave interferometer, was reported. The densities measured, typically $7 \times 10^{11} cm^{-3}$, corresponded to phase shifts on the 4-mm interferometer of about 10 degrees. Since phase shifts of this magnitude approach the resolution of the 4-mm instrument, it was decided that an interferometer for permanent installation on the system should be of longer wavelength. At the same time, it should be of short enough wavelength to afford density measurements should it become desirable to investigate higher densities.

The 8-mm interferometer (35 GHz) which is now installed will respond with twice as much phase shift at the lower densities, and will be able to measure densities up to $1.5 \times 10^{13} cm^{-3}$ and beyond. Thus, it affords more sensitivity at lower densities, and will be able to measure densities corresponding to 100% ionization at 0.2 millitorr in hydrogen and deuterium plasmas. It is anticipated that future operations will be within this range.

Figure IV-3 is a block diagram of the interferometer, showing the various 8-mm microwave components. The klystron is a Varian VA-283 with an output of

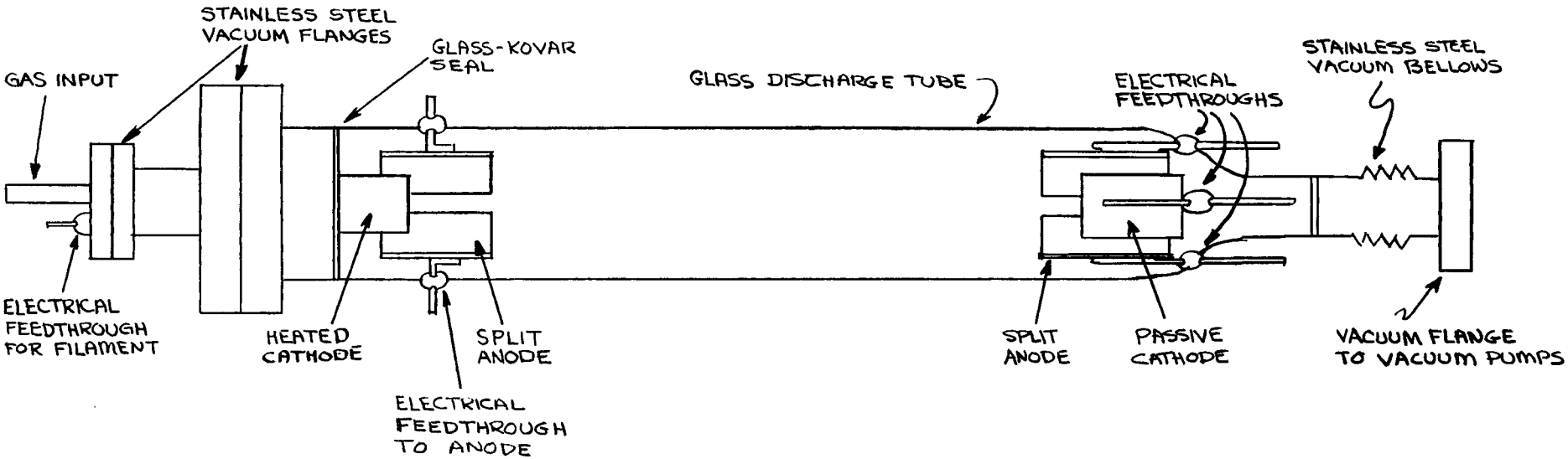

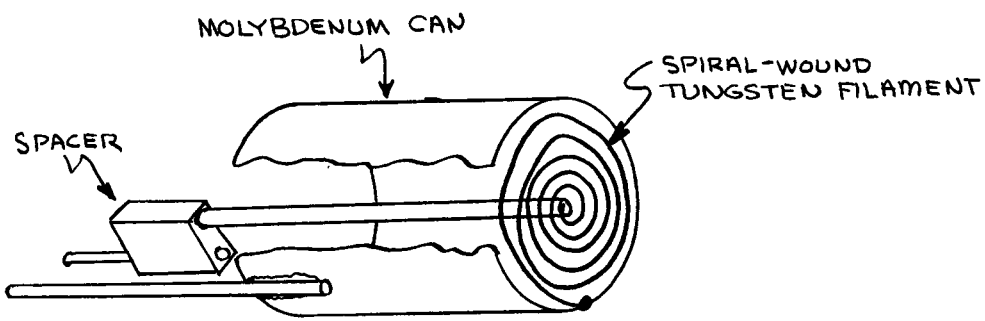

CUT-AWAY VIEW OF HEATED CATHODE

Fig. IV-2. Drawing of P.I.G. Discharge Assembly

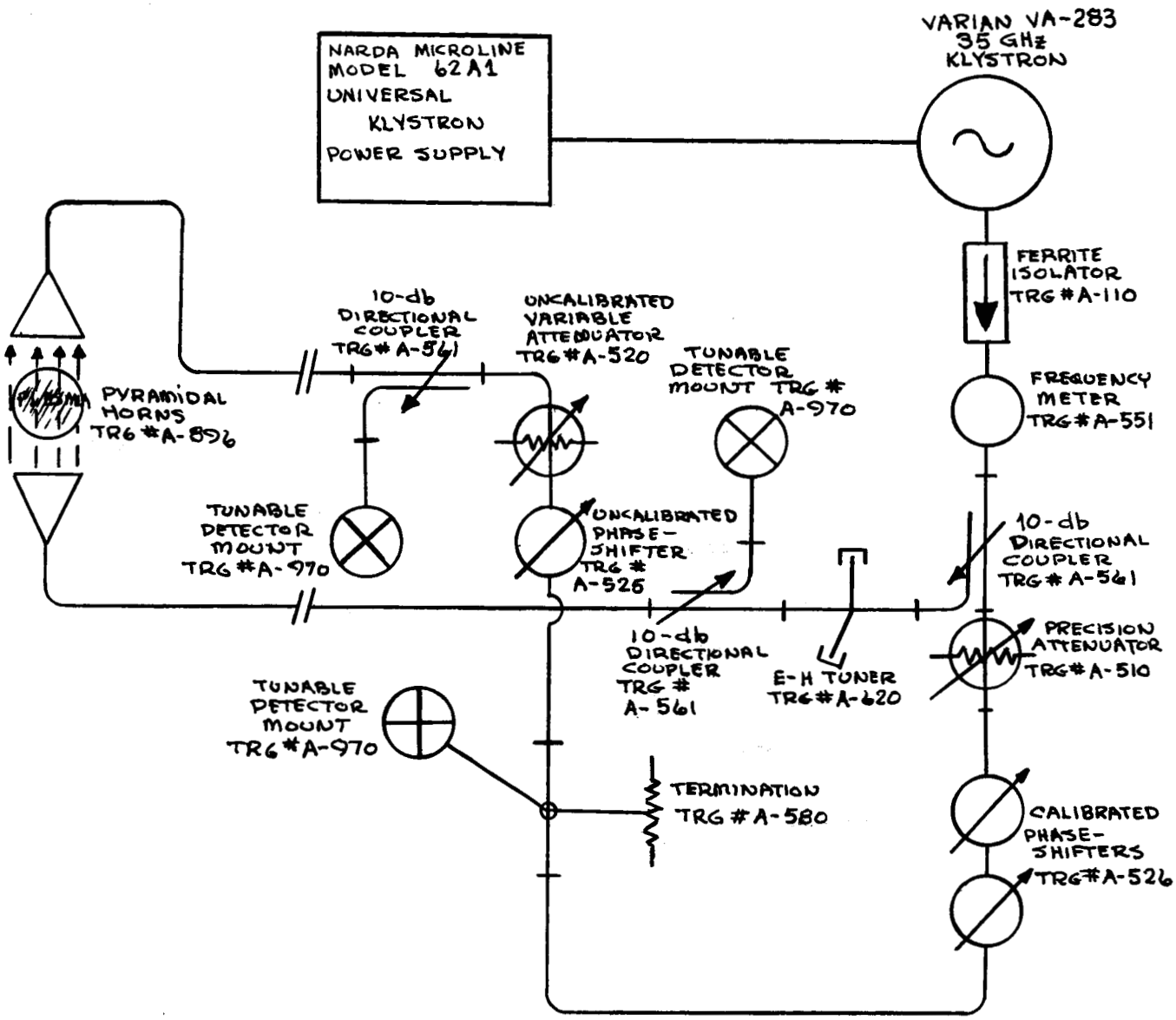

Fig. IV-3. 8-mm Microwave Interferometer

280 milliwatts at 35 GHz. It is mechanically trimmable over 3.5 GHz and electronically tunable over 100 MHz. It is powered by a Narda Microline Model 62A1 Universal Klystron Power Supply. The klystron and microwave components are rack-mounted in a vertical position, as shown in Fig. IV-4. The interferometer can be quickly and easily repositioned, and the waveguide arms to the pyramidal horns can be easily positioned between the magnet coils by means of a positioning bracket. The microwaves are transmitted directly through the pyrex tube. No absorbing coatings or dielectric lenses are used in the present arrangement.

B. New Wave Coupler

Studies have been undertaken at this facility[4,10] leading to the improvement of the "Stix Coil" energy coupler used on the main experiment. The "Stix Coil" couples pulsed 30-Kw 5.8 MHz rf power into the plasma. A fringing E_z field exists between adjacent coil turns and, in the plasma case, causes particle interactions resulting in radial forces which drive the energetic particles into the walls of the plasma container. This field can be shorted out by means of a Faraday shield, consisting generally of a series of longitudinal conductors placed parallel to the coil axis between the inner coil surface and the outer surface of the plasma tube.

It was found [4,10] that significant improvements in coil and shield performance could be achieved through the use of more effective shielding, and careful construction or modification of the standard Stix coil. The more effective shielding was achieved by means of a "squirrel-cage" Faraday shield consisting of parallel longitudinal conductors, placed as described above, but shorted azimuthally at both ends in order to form nodes to the accelerating (E_θ) field. The Stix coil was modified through a variable spacing of coil turns in the four sections, providing a more nearly sinusoidal accelerating field and thereby reducing spatial harmonics. A more nearly sinusoidal E_θ waveform and a 75% reduction in E_z was achieved in this way.

Further improvements are now reported. The "squirrel-cage" shield itself produces a fringing E_z field along the edges of the azimuthal shorting straps. Although this fringing field is small compared to the unshielded E_z, its reduction

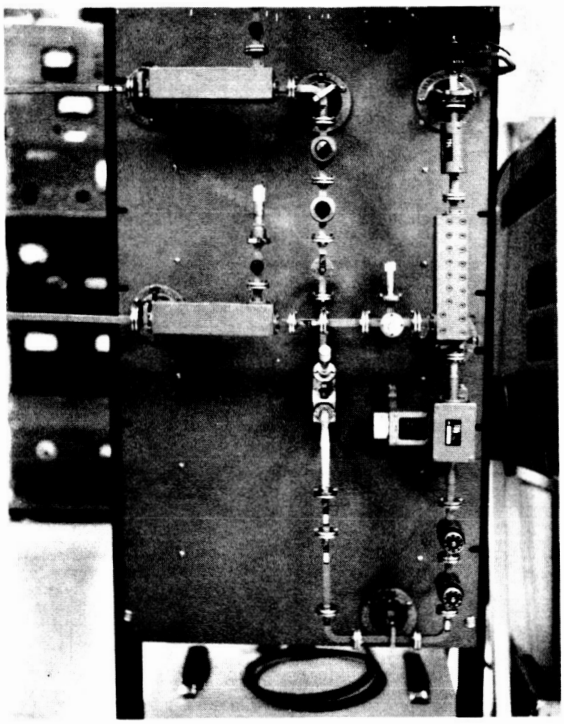

(a)

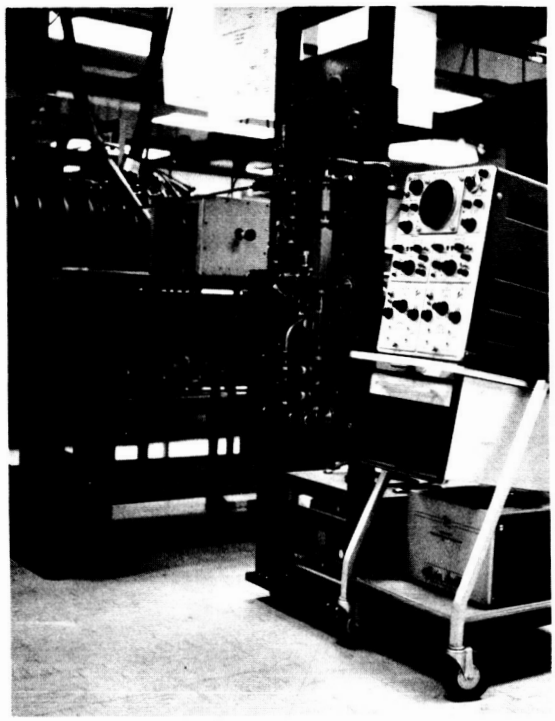

(b)

Fig. IV-4. Photographs of 8-mm Microwave Interferometer.

would provide a further improvement in the energy couplers. A design project was undertaken, and an improved coupler has been built. The resulting design is shown in Figs. IV-5, IV-6, and IV-7.

The basic shielding of the "squirrel-cage" shield is retained, with brass shorting plates taking the place of the copper braid shorting straps. A copper "can" is attached to the outer edges of the plates and attached directly to the shield of the coaxial input cable. The outer ends of the center-fed stix coil are grounded directly to the cover. Thus the E_z field is eliminated, since the entire outer can and the end plates are rf grounded.

Preliminary tests have been made on this coupler using the plotter designed for the original coupler tests.[10] The plotter has been modified somewhat to increase the efficiency of the testing procedure, and a schematic of this modified plotter is shown in Fig. IV-8. Previously, the magnetic probe signal was fed through rf amplifiers and plotted directly versus position on an x-y recorder.[4,10] However, the dipole probe used for measuring the E_z magnitude required a differential amplifier and was therefore connected directly to an oscilloscope containing a differential amplifier plug-in unit.

With a power supply now available which allows the operation of any oscilloscope plug-in unit as a separate amplifier, the differential plug-in unit is used separately without the need for oscilloscope display. The output from the differential amplifier is fed into the rf VTVM and E_z field plots are made on the x-y recorder in a method identical with magnetic probe measurements. The more tedious and time-consuming photographic methods required for preserving data with the oscilloscope, and the subsequent hand plotting required, are eliminated.

The parameters of the "can" coupler described above were measured in preliminary tests, and the results show marked improvement in coil performance. Although it was thought that the Q of the "can" shielded coil might be too low for effective use, the measured Q at 5.8 MHz is 150, comparable to shielded coils previously studied. The shape of the accelerating or energy coupling field component (E_θ) is actually superior to previous coils, with a maximum E_θ amplitude variation of about $\pm$ 1/4% between sections of the coil.

Fig. IV-5. New Energy Coupler with outer "can" cover and axial conductors removed.

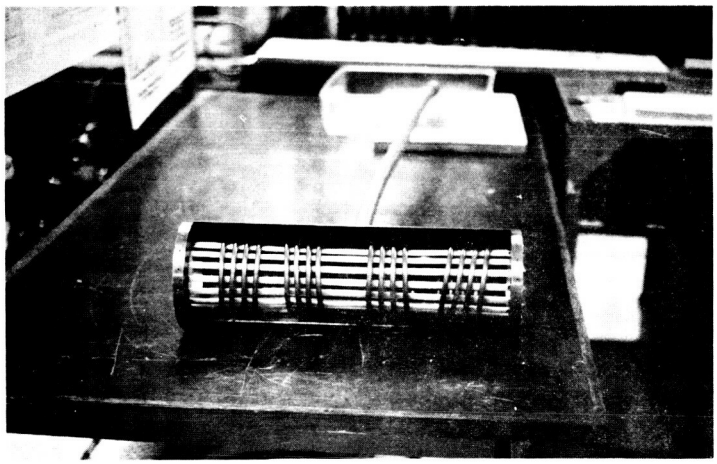

Fig. IV-6. New Energy Coupler with outer "can" cover removed and axial conductors in place.

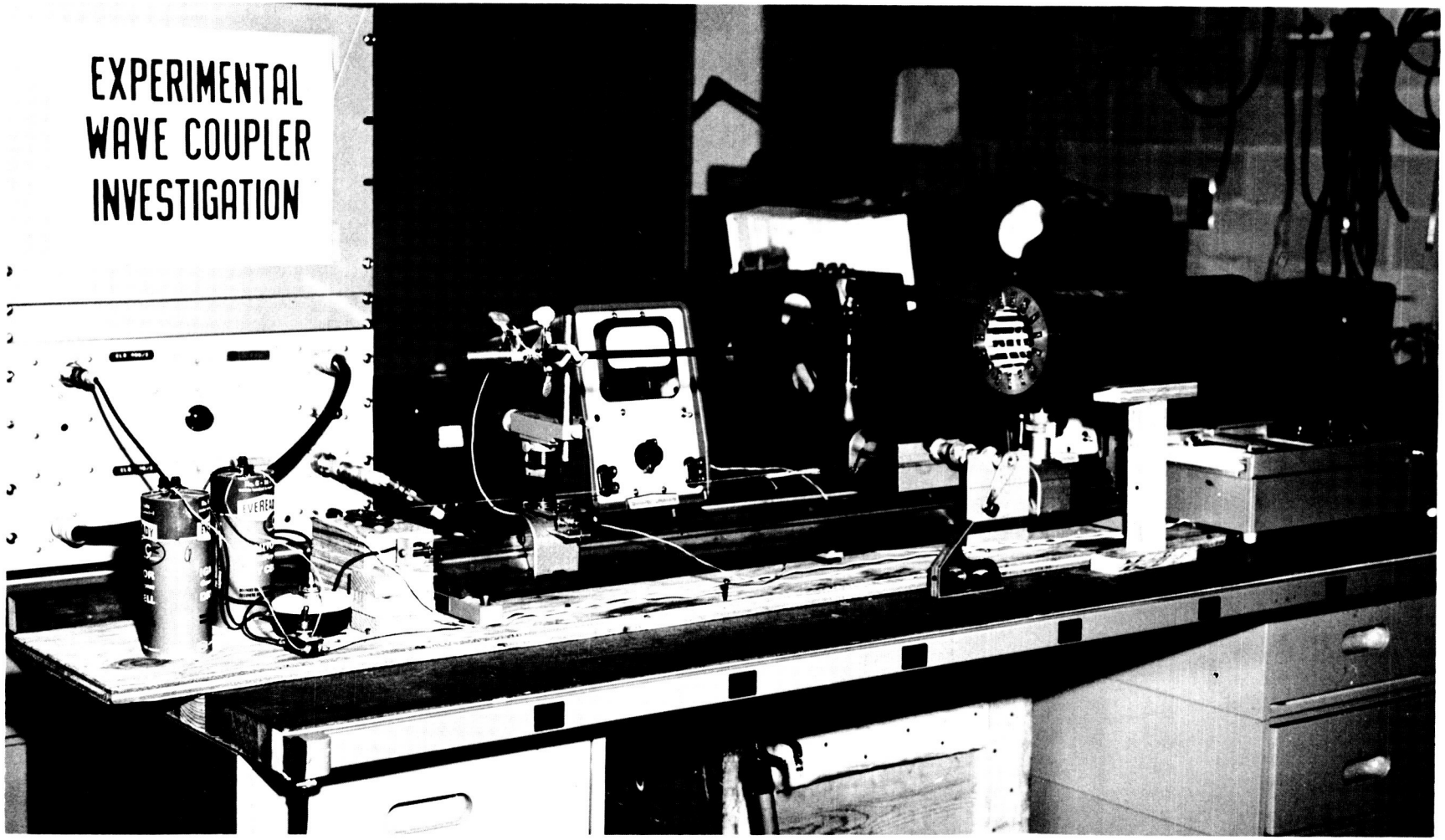

Fig. IV-7. Assembled Wave Coupler and Test Facilities.

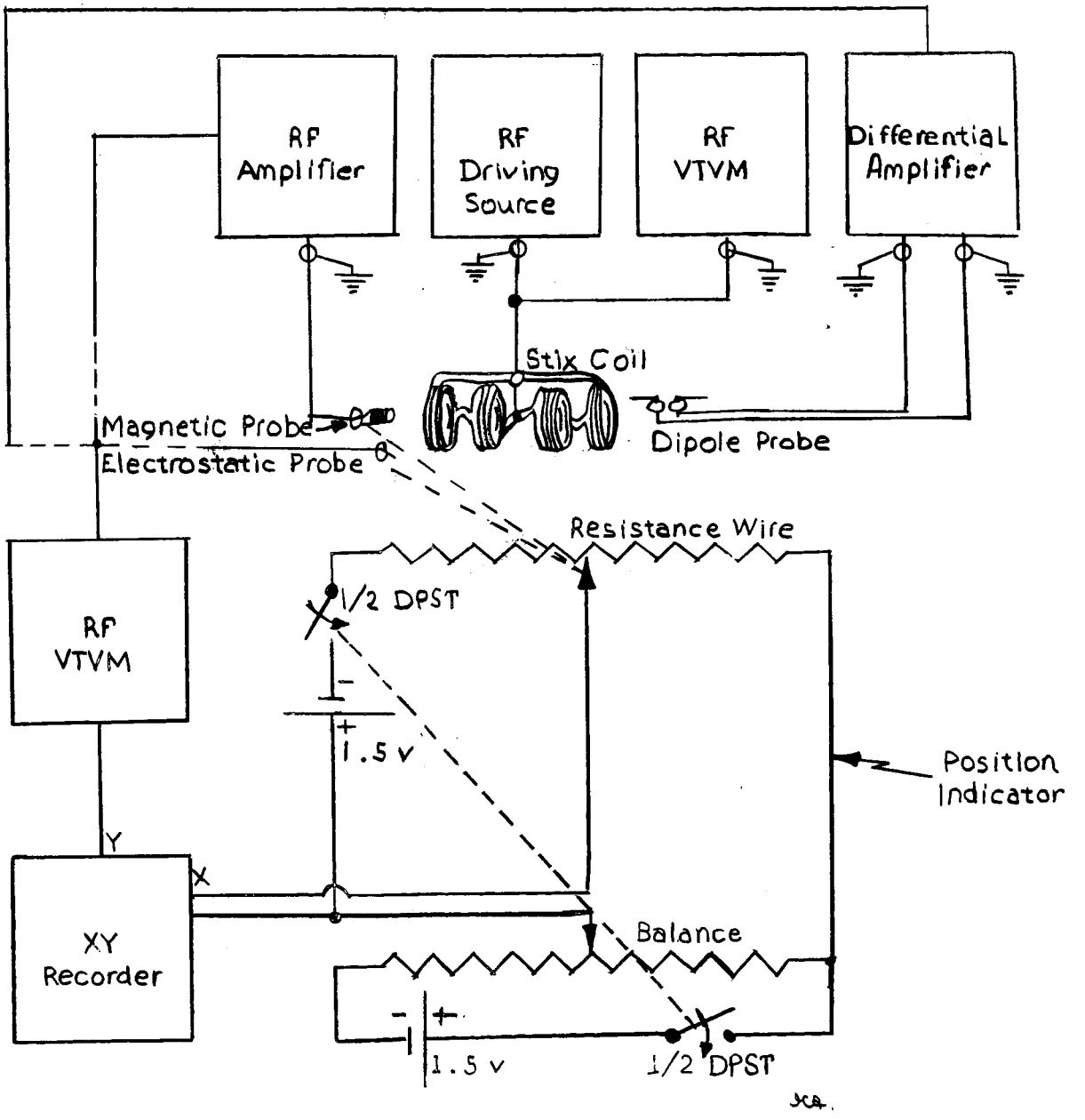

Fig. IV-8. Schematic Diagram of Probe Position Indicator and Block Diagram of Equipment.

Of greatest interest is the E_z shielding of the new coupler. Dipole probe measurements, plotted directly by the X-Y recorder indicate the shielding of the new arrangement is around 75% or better, comparable to previous configurations, and that the fringing E_z field near the shorting plate is reduced by about 90%. Present plans call for installation on the main experiment before the end of the next report period.

C. Probe Drive, Remote Control, and Screen Room

1. Probe Drive

Field measurements with magnetic probes, as well as wavelength measurements, are greatly facilitated by the mechanical probe drive which was discussed and illustrated in the previous report. This probe drive, which was fabricated at the conclusion of the last report period, is now installed on the main experiment. Three re-entry tubes of lengths differing by two foot increments provide access to the entire length of the plasma. Probes designed to measure the various wave components of interest are inserted, then positioned either axially by a worm gear and crank arrangement, or radially by tilting the plane of the attachment plate of the re-entry tubes. (Fig. IV-9)

Although the probe drive has greatly reduced the tedious and time-consuming adjustments required for axial measurements, the addition of a screen room complicated measurement procedures. Since it is conventional for a single operator to operate measuring equipment in the screen room while positioning the various probes, a remote-controlled device was designed and fabricated. This device allows for gradual axial adjustment of the probe along the entire range of bellows travel, while providing for rapid manual adjustment, when necessary. Radial adjustments, which are made much less frequently, are still made manually.

The axial adjustment system consists of a reversible AC motor coupled directly through reduction gears to the worm gear shaft of the probe drive. Limit switches mounted on the frame of the bellows support rods limit the probe transversal to 24 inches, the allowable travel of the bellows itself. The probe adjustment is controlled either at the probe drive or from a console in the screen room. There is a master off switch on the console as an added safety feature. A

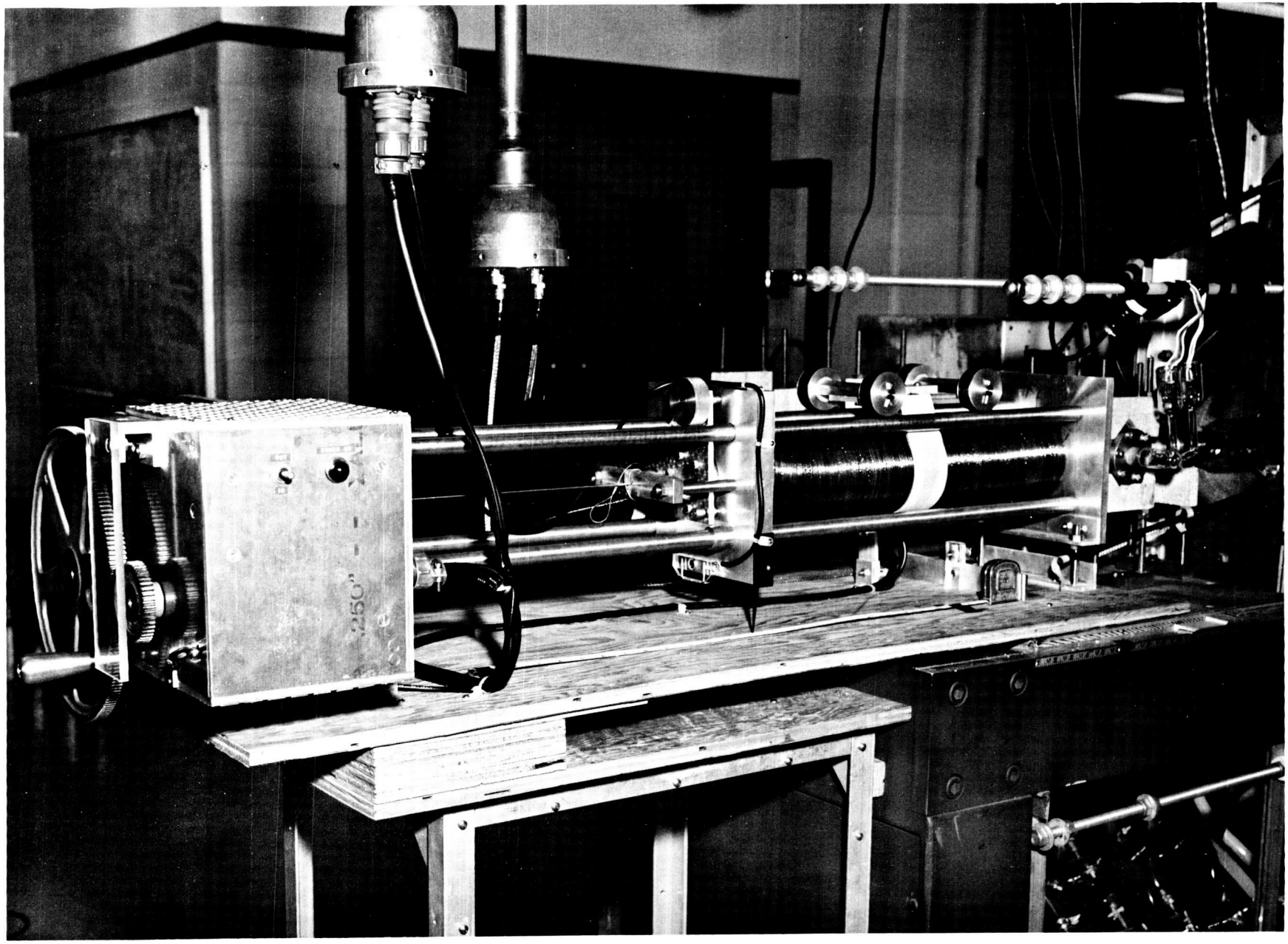

Fig. IV-9. Photograph of Probe Carriage showing signal and control connections to signal headers.

Wheatstone bridge circuit provides measurement of position, which is displayed on a calibrated microammeter on the control console.

2. Screen Room

In the past, reliable results were obtained from the experiment only through the use of extensive shielding of signal cables and oscilloscopes to prevent pick-up of stray rf signals. To shield the oscilloscope, a "cage" was used, made from copper screen wire and which was large enough for only one oscilloscope. Signal cables were shielded by the outer braid from RG-8/U coaxial cable, which was then carefully grounded.

A commerical screen room was installed to further reduce the pick-up of the large levels of stray rf power. The screen room has a floor area of 6 x 8 feet^2, allowing operation of as many as four oscilloscopes simultaneously in a shielded environment. Power enters the screen room through two 50 ampere line filters. Signal cables are shielded by 1-1/4 inch copper pipe conduits. The conduits have four input headers located near the experimental equipment. (Fig. IV-10)

The screen room installation has resulted in improved signal-to-noise ratios. It has also provided greater ease of operation of the experiment, eliminating the time-consuming procedure of shielding all signal cables individually and careful grounding of the shields to minimize noise pick-up.

3. Remote Control for Magnet Power Supply

To enable adjustment of the magnetic field from inside the screen room a remote control unit was designed and installed. The unit consists of a reversible AC motor gear-coupled to the shaft of the powerstat on the magnet power supply. Limit switches provide protection from mechanical overtravel. A 50 millivolt $\pm$ 1/2% accuracy meter is used to indicate the magnetic field strength by monitoring magnet current, and is located in the same control console occupied by the remote controls for the probe drive.

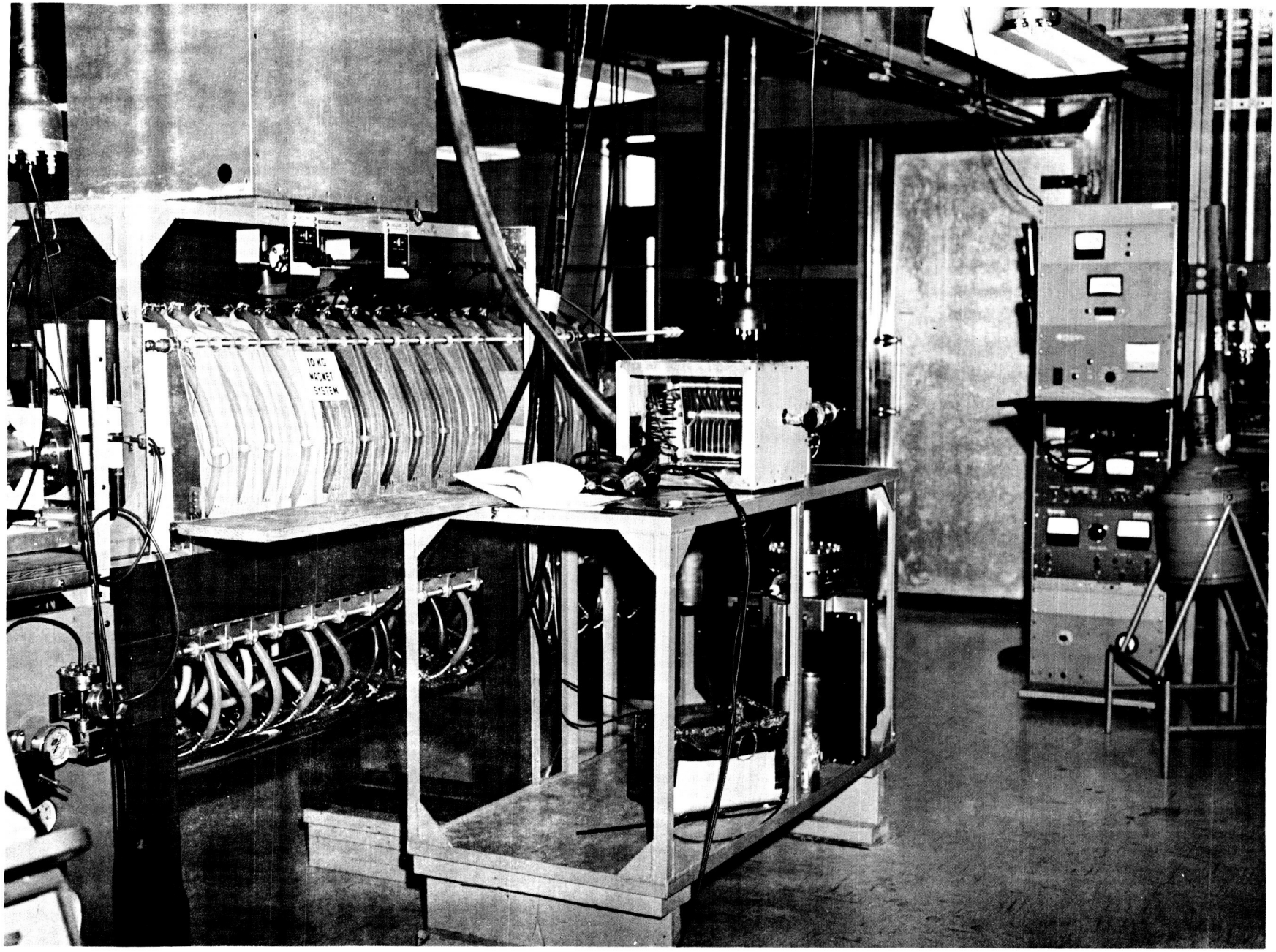

Fig. IV-10. Photograph of Experimental Facilities showing screen room and copper signal conduits.

V. EXPERIMENTAL INVESTIGATION OF NON-LINEAR PLASMA PHENOMENA

Nathan B. Dodge and Jimmy G. Melton (Professor Arwin A. Dougal)

The experimental observation and discussion of three new and unique non-linear plasma phenomena are presented here. They are:

1. Frequency mixing of one wave at or near the ion cyclotron frequency and a second wave of a higher frequency producing fields in the plasma at sum and difference frequencies.
2. Harmonic frequency wave generation from the driving frequency propagating wave undergoing harmonic ion cyclotron resonance absorption in the magnetic beach.
3. Fields generated at many frequencies distinct from harmonics of the driving frequency and distinct from the sum and difference frequencies characteristic of frequency mixing.

Note that the division of the subject into three classes is to some extent artificial, since the phenomena recorded are in all probability related, and may stem, in fact, from related non-linear plasma interactions.

A. Discussion of Non-Linear Plasma Wave Phenomena

Previously the consideration of non-linear wave phenomena was not emphasized in this work. Although the existence of these phenomena was not discounted, the investigations of plasma waves undertaken up to the present were not primarily concerned with higher-order wave mechanisms. Studies were directed more toward the mechanisms of first-order energy coupling and wave propagation.

In the detailed study of wave damping and energy conversion via ion cyclotron resonance heating, however, it is important to consider those loss mechanisms which might limit the coupling of energy. Non-linear effects become important in the high-amplitude region where the plasma undergoes substantial heating. The resonant wave phenomena and damping that occur here are expected to produce non-linear effects in the plasma. Due to non-linearities, second order (and higher) effects in plasma and plasma-wave interactions become important.

1. Frequency Mixing Phenomena

Experimental and theoretical work has appeared in the literature involving frequency mixing in a plasma. Although little of the work is immediately applicable here, certain points of general agreement may be noted. First, the frequency mixing is very likely due to wave interactions which result in a scattering of energy in wave-number space, i.e. $\vec{k}$ -space. Interactions of two waves, for example, result in a third, new wave. Secondly, such an interaction is a second-order, non-linear effect. Thirdly, such interactions can convert wave energy into thermal particle motion by exchanging energy from a non-resonant frequency to a damping frequency.

Thus, the inclusion of non-linear considerations leads to opposing possibilities. The first may lead to losses, by wave interactions which produce a wave that propagates undamped. The second is that further frequency mixing restores the energy to frequencies which can interact with the plasma particles. To determine if either of these predominates in the laboratory plasma requires detailed theoretical and experimental investigation, which is reported here.

The analysis of the problem has only progressed to the early stages. A general discussion of the approach to the non-linear problems is given here together with the most important factors involved.

In the laboratory plasma under consideration, ion-wave interactions are predominant. The waves present are at least partially transverse, and a finite magnetic field, with an axial linear gradient in one region exists. Heating energy is coupled to the plasma at a single radio frequency, although, as discussed more fully below, weak harmonics of this frequency exist in the rf oscillator. The plasma is first produced from neutral gas by a radio-frequency preionizer, which itself is capable of generating wave phenomena in the plasma (see part V-B).

The plasma itself is bounded in a cylindrical geometry and is inhomogeneous to the extent that radial density variations exist in the plasma column. The problem is thus three-dimensional, and is characterized by finite-dimension boundary conditions and gradients in both magnetic field and particle density.

If two waves at frequencies ω_1 and ω_2 are assumed to propagate approximately parallel to the axis of the plasma column, the electric field varies as:

$$\vec{E}_t = \vec{E}_{\omega_1}(r,\phi)\, e^{i(k_1 z - \omega_1 t)} + \vec{E}_{\omega_2}(r,\phi)\, e^{i(k_2 z - \omega_2 t)} + \vec{E}_{\omega_1-\omega_2}(r,\phi)\, e^{i[k_{\omega_1-\omega_2} z - (|\omega_1-\omega_2|)t]}$$

$$+ \vec{E}_{\omega_1+\omega_2}(r,\phi)\, e^{i[k_{\omega_1+\omega_2} z - (|\omega_1+\omega_2|)t]} \quad , \qquad \text{(assuming transverse waves)}$$

where the last two terms are the second-order frequency-mixing terms (higher order terms are neglected). The second order terms are of the form:

$$\vec{E}_{\omega_1 \pm \omega_2}(r,\phi) = \vec{E}_{\omega_1}(r,\phi) \cdot \overleftrightarrow{M}_{\omega_1 \pm \omega_2} \cdot \vec{E}_{\omega_2}(r,\phi)$$

In the above relations, ω_1 and ω_2 are the driving frequencies of the rf heating unit and preionizer, respectively, and $\overleftrightarrow{M}_{\omega_1 \pm \omega_2}$ are frequency-mixing matrices which are calculated from dynamic plasma equations and from boundary conditions imposed by the cylindrical containment geometry.

The above is a somewhat simplified picture, in that numerous "beat" terms, would result in the laboratory plasma from even higher-order interactions among the fundamental waves and the second-order frequencies. Thus the total electric field is expressed as:

$$\vec{E}_{\omega_k}(r,\phi) = \sum_{\text{all } i,j} \vec{E}_{\omega_i}(r,\phi) \cdot \overleftrightarrow{M}_{\omega_i \pm \omega_j} \cdot \vec{E}_{\omega_j}(r,\phi) \, .$$

Note also that the assumption that $k_{\parallel} \gg k_{\perp}$ is an oversimplification. In fact, it has been shown[5] that $k_{\perp} \gg k_{\parallel}$ in all probability.

3. Wave Generation

Kristiansen and Dougal[1,2,3,4,5] have reported measurements of wave attenuating at harmonics of the ion cyclotron frequency. It is also known that emission of electron cyclotron harmonics occur, and that ion cyclotron harmonic emission is observed from some of the larger fusion plasma machines, such as Ogra.[17] Very little

is reported, however, of such phenomena involving ions and ion resonance interactions.

Experimental observations reported here and discussed in the next section suggest that harmonics of the main rf signal are generated during damping of the cyclotron wave either at the fundamental, or near one of the cyclotron harmonics. Such generation is related to non-linear cyclotron resonance phenomena discussed previously.

Further observations reported here indicate that generation of signals occurs over certain bands of frequencies. Such observed behavior of the plasma confirms the non-linear nature of the plasma-wave interactions. Theoretical investigations are now planned along with further experimental studies to more fully define the nature of the generation mechanisms.

B. Observation of Non-Linear Plasma Phenomena

1. Equipment:

A Pentrix Spectrum Analyzer plug-in amplifier unit was used in conjunction with a Tektronix Model 555 dual-beam oscilloscope to investigate high-frequency signals in the plasma column. The method used to investigate signals received by the $\dot{b}_z$ magnetic probe was to display the $\dot{b}_z$ signal on one trace of the oscilloscope and through the use of the delayed trigger mode, to examine a portion of this signal with the spectrum analyzer, the resulting spectrum being displayed on the other trace as shown in Fig. V-1 . The center frequency of the spectrum analyzer was set at 30 MHz, with about a 50 MHz dispersion, so that frequencies from about 5 to 55 MHz were displayed. The frequency response of the analyzer extends down only to 10 MHz, but the roll-off below 10 MHz is gradual, so that the main rf excitation frequency, 5.8 MHz, was represented by a well defined spectral line, or "spike".

Utilizing the spectrum analyzer, a broad survey of the frequency content of $\dot{b}_z$ signals was made over neutral pressures of 0.2 to 10.0 millitorr and magnetic fields from 0.1 to 8.0 kilogauss. The results are described in the following subsections, which are divided according to the discussion in Section III-B.

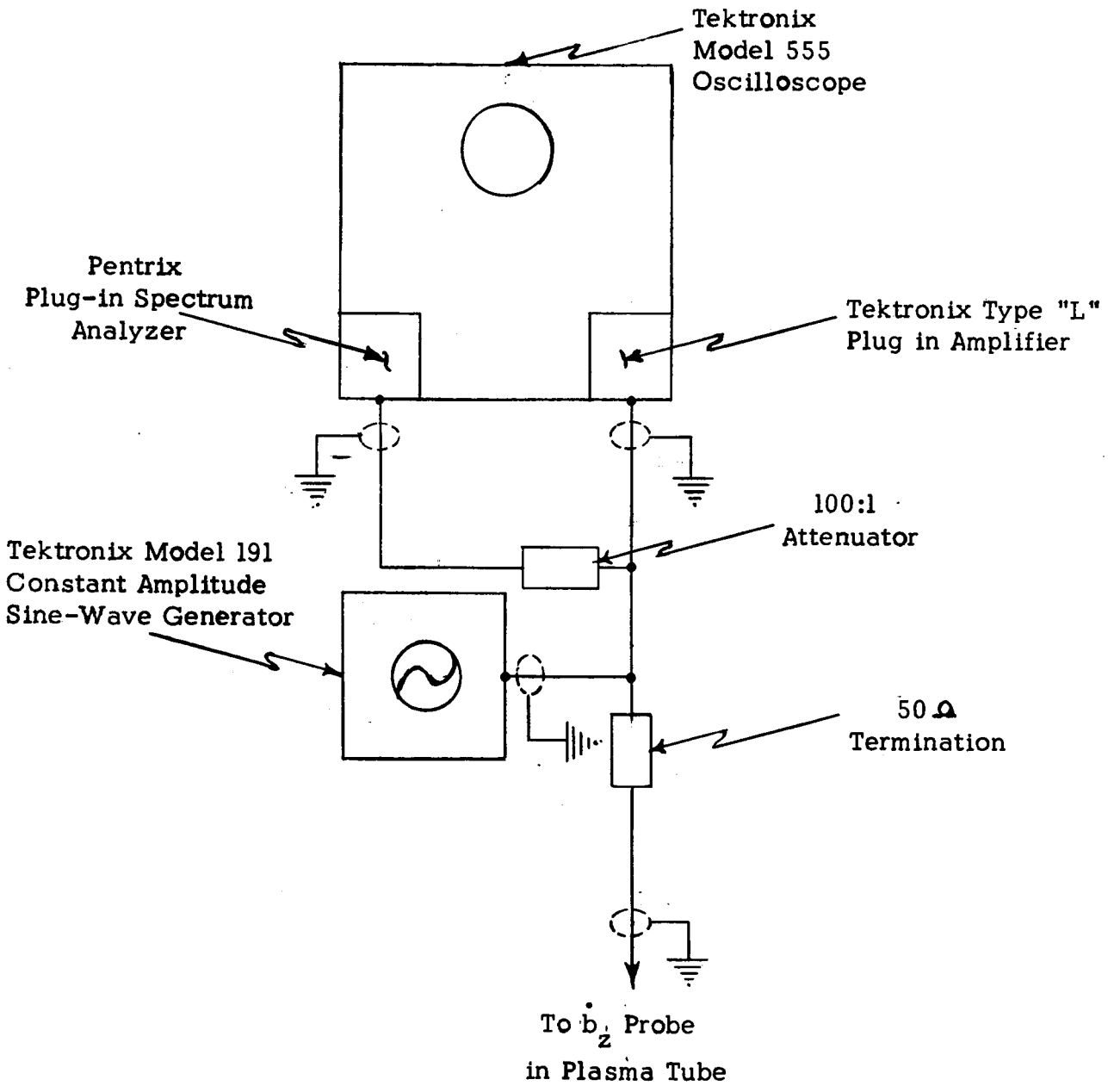

Fig. IV-1. Schematic of Spectrum Analysis Equipment

2. Observation of Frequency Mixing

It was observed that a strong 27.1 MHz signal was received by the $\dot{b}_z$ probe under a variety of plasma conditions when the 21.3 MHz preionizer pulse and the 5.8 MHz main rf pulse were overlapped in the timing sequence, as shown in Fig. V-2. In this experiment, the 40 Kw preionizer was not used. The 1 Kw preionizer pulse was approximately 3 msec long, and the main rf pulse was about 2 msec long and imbedded in the 3 msec preionizer pulse in time sequence, the preionizer pulse extending 500 μsec in time either side of the main rf pulse. The pulse durations were somewhat longer than normally used in order that the spectrum analyzer could complete its sweep of the entire 5-55 MHz frequency range during each pulse sequence.

The 27.1 MHz signal is the sum of the preionizer and main rf frequencies, and suggests non-linear interactions between the two driving frequencies in the plasma. This was further supported by altering the sequences of the pulses, or by turning off either the main or preionizer rf pulse. At sufficiently high densities such that the main r.f. pulse could cause both breakdown and heating, the 21.3 preionizer unit was turned off. The 27.1 MHz and 21.3 signals were observed to disappear. When the main rf unit was turned off and only the 21.3 preionizer was pulsed, the 5.8 and 27.1 MHz "spikes" disappeared. Furthermore, when the 21.3 and 5.8 MHz transmitters were pulsed in time sequence such that the pulses did <u>not</u> overlap, only the 21.3 MHz and 5.8 MHz "spike" were evident. It might also be noted that in all cases, breakdown occurred, so that a plasma column was present in the plasma tube.

As a further check, the 5.8 and 21.3 MHz pulses were operated simultaneously, but at reduced power levels so that breakdown did not normally occur except at higher pressures ($\approx$ 5 m Torr). In all cases when breakdown did <u>not</u> occur, "spikes" were still displayed at 21.3 and 5.8 MHz, although at lower amplitude, but the 27.1 MHz signal was absent. The same result was also true when pulsing the rf units at high power levels with the plasma tube pumped to the system base pressure, and no gas being leaked into the system, as shown in Fig. V-3.

The 27.1 MHz signal was observed both in deuterium and hydrogen gas, although the occurrence seemed more regular and a good deal stronger in deuterium.

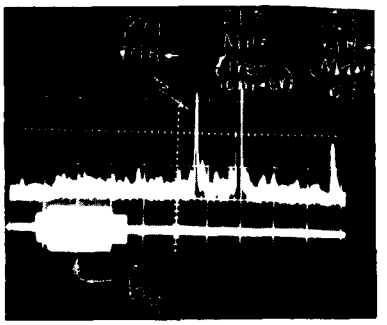

Fig. V-2. Frequency Spectrum of $\dot{b}_z$, showing 27.1 MHz "beat" signal. Spectral lines are also present at 21.3 MHz (preionizer frequency) and 5.8 MHz (main heater frequency). Note that the 5.8 MHz rf pulse occurs during the preionizer pulse.

H_2 gas
P = 3.0 mT
B = 0.5 Kg

Preionizer Pulse - 3 msec
Main rf Pulse - 2 msec

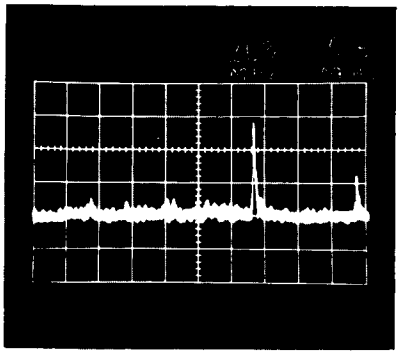

Fig. V-3. Frequency Spectrum of far-field $\dot{b}_z$ of Stix coil with no gas being leaked into system.

P = Base Pressure of System

B = 0

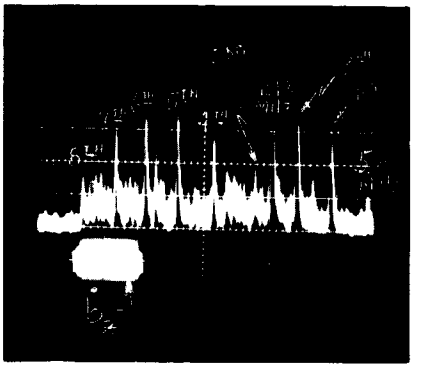

Fig. V-4. Spectrum of $\dot{b}_z$ Showing Harmonics of the 5.8 MHz Main rf Frequency.

H_2 gas

P = 0.45 mT

B = 0.25 Kg

A signal was also observed occasionally in both gases at 15.5 MHz, the difference frequency. However, this signal was always of much lower amplitude and was considerably more sporadic in occurrence.

From the rather qualitative observations made thus far, the amplitude of the 27.1 MHz signal (as well as the 15.5 MHz signal) seems to have some slight inverse dependence on neutral gas pressure. This may be due more to the increase in ion-neutral collisions at higher pressures, however, than to any qualitative relation between plasma density and signal, since at the higher neutral pressures, the relative ionization is quite low and the ion-neutral collision frequency should be very high. Also, there seems to be some dependence on magnetic fields, with the more prominent 27.1 MHz signals occurring at low magnetic fields, except at low gas pressures. This would indicate a correlation between the 27.1 MHz signal and the wave damping phenomena, since except at very low gas pressures, damping occurs at relatively low magnetic fields, due to cyclotron harmonic effects mentioned previously. This is a reasonable result, in that the greatest non-linearities would be expected near resonance, where electric fields are highest.

The frequency mixing which is suggested by the spectrum analysis leads to a further observation. For frequency mixing to exist, the preionizing rf pulse must be exciting a plasma wave in addition to instituting breakdown of the neutral gas. Speculation about such a wave led to the examination of the 21.3 MHz rf pulse alone. The magnetic field was varied at a number of neutral pressures, and the $\dot{b}_z$ signal was recorded. A slight but definite peak in the $\dot{b}_z$ signal was observed, and slight damping effects were also seen. A further step would be to examine the diamagnetic signal, to see if energy coupling to the plasma actually results during wave damping. Although this has not yet been verified, it appears that a wave-producing mechanism is a property of the preionizer arrangement, which at present couples energy through an axial rf discharge into the plasma. Thus the plausibility of two waves in the plasma, as well as the frequency mixing, is verified.

In the present case, the exact nature of all the plasma waves is unknown. The ion cyclotron, or left-handed wave has been assumed to be the wave "seen" by the magnetic probe, and undoubtedly exists at the lower neutral pressures. However,

at the higher neutral pressures, where wave damping occurs at harmonics of the cyclotron field, Swanson[7] has shown that quasi-static ion cyclotron waves may propagate. These waves are essentially longitudinal waves ($\vec{k} \parallel \vec{E}$), whereas the normal ion cyclotron wave is a transverse mode. Further, at very low fields ($B \lesssim 600g$), the "fast" or right-handed magnetohydrodynamic wave was observed to propagate, which is also transverse.

It might be noted that the electrode arrangement for the preionizer discharge (essentially, an axial arrangement) suggests that a longitudinal mode, such as the ion acoustic wave, might be produced, but a small transverse wave component is a distinct possibility. Both theoretical and experimental approaches are planned in order that the actual type of wave that is present may be verified.

The preceding paragraphs suggest an interaction which involves the mixing of two longitudinal waves, two transverse waves, one wave of each species, or waves with both transverse and longitudinal components. Such possibilities add further ramifications to the theoretical problem discussed earlier, and point to the importance of determining accurately the types of waves which exist in the plasma.

A further question arises as to the relative occurrence of the sum and difference signals, and their relative magnitude. It would seem that equal signal amplitudes would consistently occur at both frequencies; however, the 27.1 MHz signal predominates, while the 15.5 MHz signal is much weaker and a good deal more intermittent. In all probability, more of the same non-linearities become important to explain this effect, and a more rigorous and satisfactory explanation must await further experimental and theoretical research.

3. Wave Generation

A further and possibly related non-linear phenomena has been observed. In certain areas of plasma parameters, normally during resonance and damping phenomena, strong spectral lines were exhibited by the analyzer as seen in Figs. V-4, V-5a, and V-5b. In Fig. V-4 the fundamental frequency (5.8 MHz) is represented by the spectral line at the far right, and the line or "spike" coinciding with the second from center right vertical graticule line is the preionizer frequency, 21.3 MHz.

a.

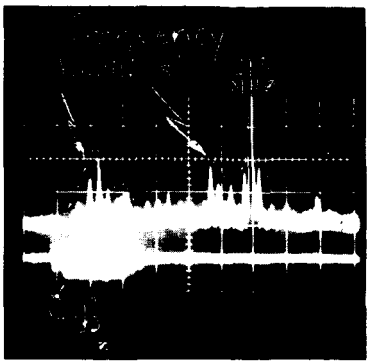

b.

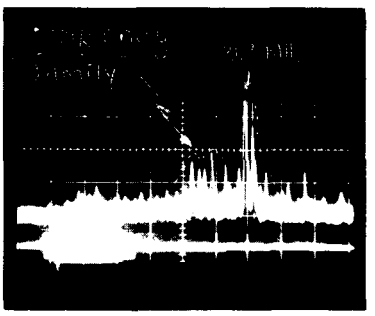

Fig. V-5. a. Spectrum of $\dot{b}_z$ Showing "Families" of Frequencies which Appear to be Generated in Bands

H_2 gas B = 2.0 Kg

p = 2.2 mT

b. Spectrum of $\dot{b}_z$ Showing "Families" of Generated Frequencies and Harmonics

H_2 gas B = 0.12 Kg

p = 2.2 mT

A number of other spectral lines are seen, spaced at approximately equal intervals across the display from 5.8 MHz. These lines were verified though the use of a Tektronix Constant Amplitude Signal Generator to fall at the harmonics of the 5.8 MHz fundamental.

Figures V-5a and V-5b depict the second, related wave phenomena. A number of spectral lines are grouped in two locations in Fig. V-5a. In Fig. V-5b spikes at both harmonics of 5.8 MHz, and in the configuration of Fig. V-5a are in evidence.

In the figures shown, the main and preionizing rf sequences overlapped, so that the mode-coupling frequencies may also be seen in the figures. However, the various harmonic lines shown existed whether or not the two signals overlapped. A good deal of shot-to-shot variation also existed.

Since the spectral lines in Fig. V-4 fall exactly at harmonics of the 5.8 MHz driving frequency, the spectrum of the main rf unit was examined by positioning the $\dot{b}_z$ probe in the near field of the Stix coil (i.e., actually in the section of the plasma tube around which the coil is wrapped). In this region, the signals are a factor of 50 higher than in the beach region. As shown in Fig. V-6, the spectrum analyzer reveals a harmonic content in the main rf unit. There was no plasma (or neutral gas) present in the tube except the residual gases present at the base pressure of the vacuum pump. The 5.8 MHz signal is quite large, even though the response of the spectrum analyzer (see next section) is much lower at 5.8 MHz. Thus the harmonic lines shown in the figure represent signals at much lower levels, only a few percent of the magnitude of the signal at the fundamental frequency.

Due to the harmonic content of the rf driver, it is accordingly seen that a distorted waveform is imposed on the plasma by the Stix coil, so that the wave which propagates along the plasma column also contains distorted fields. Through the convenient technique of Fourier Analysis, this wave may be regarded as a sum of waves of different frequencies propagating into the beach region. The harmonic waves are of very low amplitude, so the 5.8 MHz signal predominates, as mentioned above.

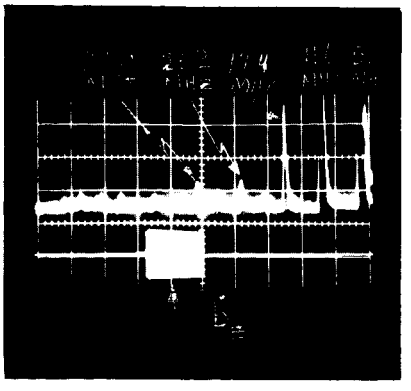

Fig. V-6. Spectrum of $\dot{b}_z$ in Near Field of Stix Coil, with No Gas Being Leaked into System.

P = Base Pressure of System

B = 0

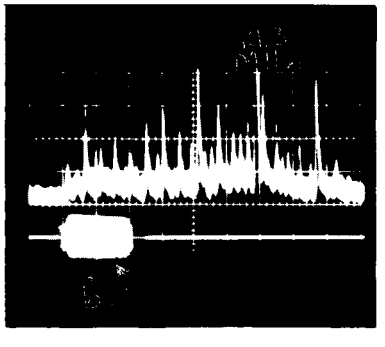

Fig. V-7. Spectrum of $\dot{b}_z$, Showing Dense Spectral Display which is sometimes present.

H_2 gas

P = 0.9 mT

B = 0.25 Kg

The very large increase in harmonic frequency amplitudes, as shown in Fig. V-4, suggests an energy conversion mechanism in the beach region resulting from the 5.8 MHz wave undergoing harmonic ion cyclotron resonance absorption. This may be seen from the following considerations.

First, the harmonic frequencies, although sometimes evident during the propagation of the wave, before cyclotron resonance and damping, are normally at low levels compared to the 5.8 MHz signal. Secondly, as cyclotron wave damping occurs in the magnetic "beach", the harmonic lines increase appreciably, often from below the spectrum analyzer noise level. Further, moving the $\dot{b}_z$ probe in the beach region while damping is taking place reveals that the amplification takes place in a relatively small region of the beach very near the physical region where wave damping occurs. Such evidence indicates that the frequency generation is due to non-linear effects in the magnetic beach during wave damping similar to those discussed for frequency mixing.

The second effect of the generation of "bands" of frequencies is more difficult to define, since as noted above, a great deal of shot-to-shot variation exists. This signal generation is probably due to the nonlinear effects discussed above, which could actually further distort the propagating waves thereby creating additional frequencies, or to the frequency-mixing discussed in the previous sub-section. The latter effect could cause very wide band frequency generation, since the various harmonics and the fundamental frequencies could all interact to produce "families" of waves, which could themselves interact. It is thus possible that an extremely dense spectral display could occur, and such a display is, in fact, occasionally present, as shown in Fig. V-7.

3. Summary

Sections 2 and 3 reveal that a very extensive amount of non-linear plasma interactions occur in the laboratory experiment. These interactions are tentatively categorized as (1) frequency mixing, (2) harmonic wave generation, (3) wave generation at frequencies unrelated to (1) and (2). All three phenomena have been observed in the laboratory, and a preliminary discussion of their nature has been given. Since only certain frequencies will heat the plasma through ion cyclotron

damping, the interactions present in the plasma may indicate the transfer of large amounts of energy into waves at frequencies which do not damp, but carry energy out of the experimental environment.

Much work needs to be done in the further investigation of these non-linear effects. Some plans for further work in this area are discussed in Section D.

C. Diagnostic Equipment

As described in Sec. V-B, the equipment used for diagnostics of the frequency mixing and wave generation consists of (1) a Tektronix type 555 dual-beam oscilloscope with a Type L plug-in, to display the actual $\dot{b}_z$ signal waveform, (2) the Pentrix spectrum analyzer used as the other oscilloscope plug-in, (3) a new Tektronix Type 191 Constant Amplitude Sine-Wave Generator in factory calibration, as a frequency standard, and (4) the $\dot{b}_z$ pickup coil located in the Pyrex re-entry tube of the probe drive.

One question which arises from the observation of the non-linear plasma and wave interaction is that of the realiability of the diagnostic equipment. It is particularly important to note whether any signal mixing or beating occurs in the spectrum analyzer, and whether harmonic effects are seen.

The spectrum analyzer exhibited a very poor frequency response in the 5-50 MHz range, so that data pertaining to the non-linear frequency effects must be considered only qualitative, and in no way quantiative measures of the amplitudes involved. However, the analyzer was never seen to exhibit harmonic signals, or signal beating, when specific frequencies were fed into the unit, as with the Tektronix signal generator. In particular, the unit was over-driven purposely to determine if beats would occur, and none were in evidence. Attention was also given to the problem of frequency images, which are relatively easy to distinguish, and none were found.

The $\dot{b}_z$ magnetic probe has been described previously, with a report on a calibration given at that time. The coil was rechecked and was found to have three resonant peaks between 2 and 55 MHz. Two peaks are slight, and occur at 9 and 18 MHz. The third, at 36 MHz, is pronounced. It is significant that these

frequencies do not coincide with the frequencies of interest, except in the case of 18 MHz, which is near the 3rd harmonic of the main rf unit.

With the preceding verification, it can be assumed that the harmonic and beat frequencies, which were observed represent actual plasma phenomena, and that the data, although qualitative, is meaningful.

D. Plans for the Next Period

A large amount of definitive work must be accomplished in order to understand the non-linear phenomena which have been discussed. Most importantly, the various plasma waves which are present must be investigated and defined in order that a proper approach to the theoretical aspect of the problem might be realized. During the next period, electric and magnetic probe data will be taken in an effort to accomplish these ends.

Further study of the plasma spectrum and non-linear effects are also planned. Tentative plans call for obtaining a spectrum analyzer capable of more linear frequency display between 5 and 55 MHz. Probe design will be reexamined to determine if the present configuration is optimum for the data now required on non-linear interactions.

The frequency mixing will be examined in terms of discovering particular dependence on various plasma parameters, such as magnetic field. Use of the microwave interferometer will enable the discovery of any relation between electron density and the non-linear interactions. Experimental data will be examined in relation to present theoretical information, and a correlation will be attempted, if pertinent.

References

1. M. Kristiansen and A. A. Dougal, "High Power RF Plasma Heating and Wave Propagation Near the Ion Cyclotron Frequency," 7th Annual Meeting of the Plasma Physics Division, American Physical Society, San Francisco, California, Nov. 8-11, 1965.

2. M. Kristiansen, J. G. Melton, F. C. Harris, N. B. Dodge, and A. A. Dougal, S.S.R. No. 6 on NASA Research Grant NsG-353, Plasma Dynamics Research Laboratory, The University of Texas, Austin, 1-73, January 15, 1966.

3. M. Kristiansen, J. G. Melton, N. B. Dodge, F. C. Harris, and A. A. Dougal, S.S.R. No. 7 on NASA Research Grant NsG-353, Plasma Dynamics Research Laboratory, The University of Texas, Austin, July 15, 1966.

4. M. Kristiansen and A. A. Dougal, "Waves Propagating Above the Ion Cyclotron Frequency (f_c) and Attenuating Near Harmonics of f_c," Bull. Am. Phys. Soc., Ser. II, 11, 716 (1966).

5. M. Kristiansen and A. A. Dougal, "An Experimental Investigation of Harmonic Ion Cyclotron Wave Propagation and Attenuation," To be published in Phys. Fluids, March, 1967.

6. S. Yoshikawa, R. M. Sinclair, and M. A. Rothman, "Ion Heating in the Model C Stellarator," CN-21/121, International Atomic Energy Agency Conference on Plasma Physics and Controlled Nuclear Fusion Research, Culham, U.K., September 6-10, 1965.

7. D. G. Swanson, A. W. Baird, III, and W. D. Echols, "Propagation of Ion Cyclotron Waves Above Ω_c," Texas Biannual of Electronics Research No. 4, pp. 152-156, November 15, 1966.

8. D. G. Swanson, Quasistatic Ion Cyclotron Waves," To be published in Phys. Fluids.

9. T. H. Stix and R. W. Palladino, Phys. Fluids 1, 446, (1958).

10. N. B. Dodge, M. Kristiansen, and A. A. Dougal, Rev. Sci. Inst., 37, 1455, 1966.

11. W. M. Hooke, M. A. Rothman, J. Sinnis, and J. Adam, Phys. Fluids 8, 1146, (1965).

12. T. H. Stix, Theory of Plasma Waves, (McGraw-Hill Book Company, Inc., New York, 1962).

13. R. R. Woollett, NASA TN D-2982, (1965).

14. G. Landauer, Bull. Am. Phys. Soc., Ser. II, 9, 312, (1964).

15. G. Bekefi, J. D. Coccoli, E. B. Hooper, and S. J. Buchsbaum, Phys. Rev. Letters 9, 6, (1962).

16. F. W. Crawford, G. S. Kino, and H. H. Weiss, Phys. Rev. Letters 13, 229, (1964).

17. A. E. Bazhanova, J. T. Karpukhin, and A. N. Karkhov, Nuclear Fusion, 1962 Supplement, Part 1, 227.

18. S. Yoshikawa, M. A. Rothman, and R. M. Sinclair, Bull. Am. Phys. Soc., Ser. II, 10, 207, (1965).

19. T. H. Stix, Bull. Am. Phys. Soc., Ser. II, 11, 577, (1966).

20. G. H. Watson, A Treatise on the Theory of Bessel Functions, (Cambridge University Press, New York, 1922).

21. C. C. Swett and R. Krawec, Bull. Am. Phys. Soc., Ser. II, 10, 509, (1965).

22. A. Erdélyi, W. Magnus, F. Oberhettinger, and F. C. Tricomi, Higher Transcendental Functions, Bateman Manuscript Project, (McGraw-Hill Book Company, Inc., New York, 1953), VII, p. 7.

23. B. D. Fried and S. D. Conte, "The Plasma Dispersion Function," Academic Press, Inc., New York, 1961.

24. I. R. Bernstein, "Waves in a Plasma in a Magnetic Field," Phys. Rev. 109, 10 (1958).

25. T. H. Stix, op. cit. Ch. 3.

26. W. P. Allis, S. J. Buchsbaum, and A. Bers, "Waves in Anisotropic Plasmas," M.I.T. Press, Cambridge, Mass., 1963.

27. R. Geller and D. Pigache, "Mecanisme d'Equilibre d'une Decharge P.I.G. Reflex et Determination Experimentale de $D_\perp$ dans un Plasma," J. Nucl, En. Part C, 4, 229 (1962).